Table of content

1 Jury members

Promotor: Prof. Christophe Pierreux

President: Prof. Jean-Baptiste Demoulin

UCL member: Prof. Stefan Constantinescu

UCL member: Prof. Patrick Jacquemin

UCL member: Prof. em. Pierre J. Courtoy

Non-UCL member: Prof. Sabine Costagliola (IRIBHM, ULB, Brussels)

International member: Dr. Cecilia Lässer (Krefting research center, Sahlgrenska Academy, University of Gothenburg, Sweden)

2 Acknowledgments

Ce travail est le fruit d'un peu plus de quatre années au sein de l'Institut de Duve, auxquelles il faut ajouter deux années de mémoire. Six ans au total, jalonnés de rencontres, de joies, d'éclats de rire, de soirées, de weekends, de moments plus difficiles aussi (et oui de temps en temps il faut travailler) mais le tout dans une ambiance fantastique et en étant entouré de personnes exceptionnelles. Je tiens donc à remercier toute les personnes qui, de près ou de loin, ont contribué à l'aboutissement de ce travail.

First, I would like to thanks all my Jury members; Pr. Demoulin, Pr. Constantinescu, Pr. Jacquemin and Pr. Courtoy. You have been following this work since its beginning and I thank you very much for your time and the excellent discussions that we had each year as well as the excellent remarks and suggestions that you made. Many thanks to Pr. Sabine Costagliola for the critical comments that she made and the stimulating discussions that we had during the private defense. I also would like to thank Dr. Cecilia Lässer for her involvement in this Jury. Thank you for the thorough analysis of the manuscript, for the numerous comments that you made (especially for the paper), for the great discussions that we had about the exciting EV field and for your presence at my private defense. It was an honor to have you all as Jury members.

Je remercie spécialement le Pr. Pierre Courtoy, directeur de l'unité CELL à mon arrivée au laboratoire. Merci pour votre temps et votre implication dans mon projet et plus particulièrement dans la rédaction de l'article et de cette thèse. Merci pour vos idées, votre esprit critique, votre perfectionnisme, vos conseils et votre enthousiasme qui ont grandement contribué à l'amélioration du papier et de la thèse.

Je tiens ensuite à remercier l'instigateur de toute cette aventure. Oui, Christophe, tout cela c'est à cause de toi (ou grâce à toi, c'est selon), tout ça pour un choix malheureux que tu as fait il y a un peu plus de six ans ! Alors merci ! Merci d'avoir été un promoteur d'une disponibilité et d'une pédagogie exemplaire. Merci d'avoir cru en moi et de m'avoir donné l'opportunité de réaliser cet important chapitre de ma vie. Merci de m'avoir transmis ta passion pour la recherche, ta rigueur

expérimentale (je ne parle pas du cahier, on est bien d'accord), ton esprit critique, ton optimisme ainsi qu'une partie de ton savoir et de ton impressionnante capacité à mémoriser tous les articles que tu lis (oui oui, plus je m'entraine, plus je retiens). Enfin, merci de m'avoir appris ce que cela fait de subir un échec et de devoir rebondir. C'était sans doute la leçon la plus difficile à apprendre mais c'est aussi celle qui me servira le plus dans ma vie professionnelle comme privée.

Un énorme MERCI à mes génialissimes collègues de bureau (devrais-je dire amis de bureau ?) ; Léolo, Catherine et Charlotte. Chacun à une échelle différente vous avez contribué à embellir les journées au labo et à rendre toutes ces années inoubliables. Il n'y a sans doute pas assez de mots (et je ne peux pas doubler le volume de ma thèse) pour vous dire à quel point votre présence était essentielle et à quel point vous allez me manquer. Donc, du fond du cœur (oui Charly ça m'arrive d'en avoir un) merci pour tout. Si mes prochains collègues vous arrivent ne serait-ce qu'à la cheville, je serai le plus heureux du monde !

Merci aux autres membres de l'équipe epithelial-diff, actuels et anciens, avec une pensée toute particulière pour Ophélie. Je suis très fier de ton parcours, c'était un plaisir de pouvoir te former et de te voir évoluer au quotidien. Je te souhaite tout le meilleur pour la suite, continue d'exploiter tes capacités au maximum et surtout, même si les EVs sont toutes petites, n'aies pas peur de voir les choses en grand, tu iras très loin !

Merci à toute l'unité CELL, PI, post-doc, doc, techniciens, animaliers que j'ai eu le privilège de côtoyer durant ces six années. Nous avons la chance d'évoluer dans un environnement de travail collaboratif et de pouvoir maintenir une belle ambiance au sein du plateau grâce à l'organisation d'activités extra-professionnelles. Je compte sur vous pour maintenir cette bonne ambiance essentielle à une vie commune agréable pour tous ! Un grand merci à Pat' pour son dévouement à la résolution de tous les petits problèmes du labo et pour ses innombrables et interminables digressions qui animent notre quotidien. Un merci particulier à Dona, pour sa joie de vivre, sa disponibilité, pour les discussions scientifiques ou non que nous avons pu avoir. Merci de m'avoir conseillé et soutenu dans les moments plus compliqués. Je te souhaite le meilleur pour ta carrière et dans le privé avec tes trois monstres et ton mari.

Merci aux anciens et tout particulièrement à Gigi et Tony, vous n'êtes plus parmi nous depuis longtemps mais je me remémore encore souvent la « belle époque ». Merci Gigi de m'avoir fait découvrir les joies de la microdissection et surtout merci de m'avoir accueilli à bras ouverts au sein de l'équipe. Souvent copiée mais jamais égalée, tu as été un modèle pour moi tout au long de mon parcours au labo. Merci Tony pour tous ces bons moments passés dans le labo, tu es le grand artisan de l'ambiance de l'époque, Joe Dassin en était vert de jalousie. Ce fût un réel plaisir de vous côtoyer, de travailler et de festoyer à vos côtés ! Merci aussi à Ludo et Hélo. Ludo, ta soirée de thèse a été le point de départ de mon aventure au labo, une soirée que je n'oublierai jamais ! Et merci pour le coup de main sur le reviewing du papier. Hélo, merci de m'avoir ébloui pendant toutes ces années. Promis, ma reconversion dans le jardinage ne va pas tarder ;-). Sabine (sorry je te case dans les anciens mais tu peux voir que tu es bien entourée), simplement un grand merci pour tout ce que tu as fait pour moi, j'espère de tout cœur que tous tes souhaits se réaliseront.

Merci aux BIOMED et particulièrement à Cédric, Benoit, Lucie, Marion² et Aline. Ça fait maintenant dix ans qu'on a commencé ce cursus en Sciences Biomédicales à Namur ensemble (oui Ced nous ça fait 11 ans mais chuuuut… et on pourrait encore remonter plus loin !), il nous a fallu un peu de temps pour nous apprivoiser mais quel beau résultat ! La légende dit qu'une amitié qui dure plus de sept ans durera toute la vie, maintenant vous savez à quoi vous attendre ;-). Merci pour tous ces bons moments, ces weekends à la mer ou ailleurs, ces tequilab… et tout ce que la bienséance m'empêche d'écrire ici ! Je vous aime !

Merci aux SBIM de l'UCL ; Edith (présidente !!!), Thomas, Matias, … de nous avoir accueillis (nous petits namurois) plus que chaleureusement pour le Master. Merci pour toutes ces soirées et les amitiés qui en ont découlé. Merci de m'avoir permis de rencontrer un tas de gens géniaux ; Marc, Manu, Melissa, Carmelo, Camille, Eva, Chico, … qui sont devenus des personnes importantes de ma vie. Faites attention, les sept ans approchent à grands pas ;-).

Merci aux Docs de l'Institut, aux anciens pour avoir intronisé les weekends Doc (Tony, Gigi, Fab, KD, …) qui ont permis de créer une ambiance unique entre les différents groupes de recherches. Merci à mes contemporains ; Manu, Marc, Mati, Max, Thomas, Melissa, Sara, Marine, Eli, Carole, … d'avoir contribué à pérenniser

ces weekends mémorables et qui ont vraiment fait de l'Institut de Duve un endroit unique pour réaliser une thèse. Merci pour toutes les soirées passées et celles à venir. Un merci particulier à l'ICP futsal team, Manu, Marc, Mati, Max, Alex, Léolo, Joao, Claude et aux anciens pour toutes ces deuxièmes places et ces innombrables Mounier le vendredi midi (j'en profite pour remercier Jess, Math et Ol pour leur accueil et leur bonne humeur presque perpétuelle tout au long de ces années).

Merci à l'équipe du Good Morning ; Carmelo, Cédric, Marc, Manu, Mati, Thom, Chico et Leo pour nos weekends, nos soirées foot, nos soirées tout court et tous ces bons moments passés avec vous.

Merci à l'Oxygène Rixensart ; Gégé, Babar, Pilou, Fabi, Arnaud, Quentin pour ces quelques saisons passées avec vous et toutes celles à venir ! Merci aussi aux membres de la MTM pour leur accueil cette année et pour leur soutien dans mon projet de rénovation des ronds-points de la région. Vivement la saison prochaine !

Merci Pauline pour ces trois années et demi à tes cotés. À l'heure où j'écris ces lignes nous avons décidé de nous séparer mais tu restes une part importante de ma vie et de cette thèse. Merci pour ta présence et pour tous les beaux souvenirs que je garderai de notre relation. Merci aussi à toute ta famille ; Alexis, Jean-Pierre, Marianne, Laurence, Bruno, Paul, Yvette et tous les autres pour leur accueil plus que chaleureux au sein de la famille et leur soutien pendant les périodes plus compliquées de ma thèse.

Merci Rosine d'avoir ensoleillé la toute fin de cette grande étape de ma vie, je t'en suis immensément reconnaissant. Nous ne sommes qu'au tout début de notre histoire mais je suis convaincu qu'elle sera remplie de bonheur.

Un énorme merci à mes deux frères d'adoption, Marc et Manu. Je ne vais pas pouvoir faire le détail de toutes les choses qu'on a faites, qu'on fait et qu'on fera encore et qui me font dire que vous êtes les plus précieux des amis, donc tout simplement merci d'être là, merci d'être vous ! On a passé six années exceptionnelles à l'Institut, très souvent collés l'un à l'autre. On a vécu tout un tas de choses qui n'ont fait que renforcer notre amitié et rares étaient les jours où l'on ne se voyait pas. Même si aujourd'hui nos chemins s'éloignent légèrement, je suis certain qu'ils ne se sépareront jamais et que nous serons toujours là l'un pour l'autre ! Un merci tout particulier à Marc, tu m'as fait l'honneur de me faire

confiance pour être parrain d'Éric, sache que ça me comble de joie, qu'il me comble de bonheur à chaque fois que je le vois et que je suis le plus heureux des parrains quand j'ai la chance de pouvoir m'occuper de lui.

Enfin, un tout grand merci à ma famille ; mes grands-parents, mes tontons (et tatas :D), mes cousins, ma cousine, mon parrain et ma marraine. Merci pour votre soutien et votre intérêt pour le charabia incompréhensible que je vous racontais (j'espère qu'après la défense publique vous y verrez plus clair). Merci d'être là quoi qu'il arrive ! Il parait qu'on ne choisit pas sa famille mais si j'avais eu le choix je n'aurais pas voulu que vous soyez autrement. Last but not least, Maman, Papa, MERCI. Merci de m'avoir toujours poussé pour réussir ce que j'entreprenais. Merci de m'avoir soutenu dans les moments plus difficiles. Merci de m'avoir donné les outils nécessaires pour avancer sereinement dans la vie. Je ne suis surement pas assez reconnaissant envers vous, pour tout ce que j'ai eu l'opportunité de faire et pour la situation dans laquelle je suis à présent, mais sachez que je suis tout à fait conscient de la chance que j'ai eue et de la chance que j'ai de vous avoir comme parents. Je vous aime très fort !

3 Abbreviation list

ALIX: ALG-2-interacting protein X

ARF: ADP-ribosylation factor

ATC: anaplastic thyroid carcinoma

ATP: adenosine tri-phosphate

BMPs: bone morphogenetic proteins

BRAF: b-type Raf kinase

CaCo: human epithelial colorectal adenocarcinoma cells

CM: conditioned medium

Cnx: connexin

DIT: di-iodotyronin

DNA: desoxyribonucleic acid

DUOX2: dual oxidase 2

DUOXA2: dual oxidase maturation factor 2

DEHAL1: iodotyrosine dehalogenase 1

E.: embryonic day

EDTA: Ethylenediaminetetraacetic acid

EGF: epidermal growth factor

EGF-R: epidermal growth factor receptor

EM: electron microscopy

EPCs: embryonic endothelial progenitor cells

EphA4: ephrin receptor A4

ERK: extracellular-signal regulated kinase

ESCRT: endosomal sorting complex required for transport

EVs: extracellular vesicles

FGFs: fibroblast growth factors

Foxe1: forkhead box E1

FTC: follicular thyroid carcinoma

GEMM: genetically engineered mouse model

GTP: guanosine tri-phosphate

Hhex: hematopoietically-expressed homeobox protein

HUVEC: human umbilical vein endothelial cells

I^-: iodide

I_2: iodine

ILV: intraluminal vesicle

ISEV: International Society of Extracellular Vesicles

i-Tg: iodinated thyroglobulin

KD: knock-down

KO: knock-out

lta: lateral thyroid anlage

MAPK: mitogen-associated protein kinase

MCT8: monocarboxylate transporter 8

MDCK: Madin-Darby canine kidney cells

MHC: major histocompatibility complex

miRNA: micro ribonucleic acid

MIT: mono-iodotyronin

MLCK: myosin light-chain kinase

MNG: multinodular goiter

mRNA: messenger ribonucleic acid

mta: median thyroid anlage

MTC: medullary thyroid carcinoma

MVE: multivesicular endosome

NIS: sodium/iodide symporter

Nkx2-1: NK2 homeobox 1

paa: pharyngeal arch arteries

Pax8: paired box gene 8

PKC: protein kinase C

PTC: papillary thyroid carcinoma

PTEN: phosphatase and tensin homolog

RNA: ribonucleic acid

SEM: scanning electron microscopy

Shh: sonic hedgehog

SNARE: soluble NSF attachment protein receptor

T3: triiodothyronin

T4: tetraiodothyronin

Tbx1: T-box transcription factor 1

TEM: transmission electron microscopy

Tg: thyroglobulin

TH: thyroid hormones

TH-R: thyroid hormones receptor

TPO: thyroperoxidase

TRE: thyroid hormones response element

TSAb: thyroid stimulating antibodies

TSBAb: TSH-stimulation blocking antibodies

TSH: thyroid stimulating hormone

TSH-R: TSH-receptor

TTFs: thyroid transcription factors

UBBs: ultimobranchial bodies

VEGF: vascular endothelial growth factor

VEGFR2: vascular endothelial growth factor receptor 2

VPS: vacuolar protein sorting

ZO: zonula occludens

ZONAB: ZO-1-associated nucleic acid binding protein

4 Summary

Intercellular communications are essential for organ development, tissue homeostasis, and disease progression. In addition to conventional communication modes by soluble factor secretion or cell-cell contact, most cells can release vesicles to transfer information to their microenvironment or to distant sites, through proteins and RNA cargoes loaded in the vesicles. Communications mediated by extracellular vesicles (EVs) are intensively studied in the field of cancer, but their role in embryonic development is poorly understood.

Since a few years, our lab is interested in epithelial:endothelial communication during thyroid gland ontogenesis and oncogenesis. In this context, the aim of my thesis was to determine if extracellular vesicles could be involved in thyroid organogenesis and thyroid cancer.

I first demonstrated that embryonic endothelial progenitor cells (EPCs) produce extracellular vesicles (EVs) with exosomal characteristics. Using an *ex vivo* culture system of thyroid lobes, I was able to show that EPC-EVs stimulated thyroid follicle expansion. Analysis of the protein cargo of EPC-EVs by mass spectrometry revealed the presence of EV-associated lamininα1β1γ1. As this latter was already known to promote folliculogenesis, two experiments were designed to test whether EVs depleted of laminins can promote folliculogenesis. Firstly, knockdown of lamininα1 in EPCs caused a change in EV production, associated with loss of folliculogenic potential of the remaining EVs. Secondly, separation of EVs from the laminins by floatation gradient generated two fractions, EV-rich and laminin-rich, both endowed with folliculogenic activity. My data thus suggest that endothelial cells can produce extracellular vesicles favoring thyrocyte organization in follicles, a mechanism promoted by lamininα1.

In the final year of my thesis, I initiated a project to evaluate the implication of extracellular vesicles during papillary thyroid carcinoma development in a mouse model. We developed a protocol to isolate EVs from dissociated thyroid lobes and demonstrated that following oncogenic $BRAF^{V600E}$ induction, EVs with exosomal characteristics are released in the tumor microenvironment.

5 Introduction

Intercellular communication is a key process not only in embryogenesis and tissue homeostasis but also in cancer progression. Communication from one cell to another can be mediated by direct contact or by production of factors released in the extracellular environment and able to travel over short or long distances. Two types of factors are produced by cells: (i) soluble factors such as vascular endothelial growth factor (VEGF) and hormones (i.e. thyroid hormones T3 and T4); and (ii) sedimentable factors or extracellular vesicles that carry and protect a complex cargo. Both soluble factors and sedimentable factors may act close to the producing cell, whereas only hormones and sedimentable factors act at long distances via transportation through the blood flow.

During my thesis, I focused on intercellular communications regulating thyroid organogenesis and initiated the study of their implications in papillary thyroid cancer progression. Our laboratory has indeed demonstrated that thyroid gland development involves reciprocal communication between thyroid progenitors and endothelial cells. Reciprocal communication allows thyroid progenitors to differentiate and organize into a multitude of epithelial monolayers (i.e. thyroid follicles). This work identified the pro-angiogenic factor VEGFa as a factor abundantly produced by thyroid progenitors. This factor was shown to promote endothelial cell recruitment around the thyroid progenitor cells, and disruption of this recruitment impaired thyroid follicle formation. This observation suggested that endothelial cells instruct thyroid progenitors to self-organize in follicle.

To understand thyroid organogenesis, and in particular follicle formation, the lab is using an *ex vivo* culture system of mouse embryonic thyroid. This original 3 dimensional (3D) culture system has been developed in the laboratory and reproduces the essential steps of thyroid gland development. Our lab showed that it is possible to mimic the effect of endothelial cells on folliculogenesis by using medium conditioned by embryonic endothelial progenitor cells (EPCs) in this *ex vivo* culture system. Folliculogenesis could be induced by both a soluble and a sedimentable component from this medium. Our lab demonstrated the role of laminins as potent soluble folliculogenic factors. I focused on the sedimentable

material, and tested the hypothesis that it contained instructive extracellular vesicles (EVs).

Extracellular vesicles are small membrane vesicles produced by almost all types of cells. They have been demonstrated to act as powerful vehicles for intercellular communication as they can carry, while protecting, messages such as mRNA and miRNA, to a broad range of distances. Most of the studies on extracellular vesicles are performed *in vitro* using cultured cells, and their implication *in vivo* and in organ morphogenesis have been poorly studied.

In the following sections, I will present the thyroid gland, its function and development, and the diseases affecting adult thyroid and in particular thyroid cancer. Finally, I will discuss intercellular communications and focus on extracellular vesicles.

5.1 The thyroid gland

5.1.1 Histological characteristics and hormones production

The thyroid gland is an endocrine gland that produces thyroid hormones (triiodothyronine, thyroxine and calcitonin) involved in organ development and homeostasis, body growth and energy expenses. In mammals, the thyroid is located at the base of the neck in front of the trachea and is composed of two lobes, on each side of the trachea, linked by an isthmus (**Fig. 1A**) (Maenhaut *et al.*, 2015). The tissue is composed of three main types of cells, thyrocytes, endothelial cells and C cells, surrounded by the stroma (**Fig. 1B**). Thyrocytes are polarized epithelial cells organized in monolayers and forming a hollow sphere, the follicle (**Fig. 1B**).

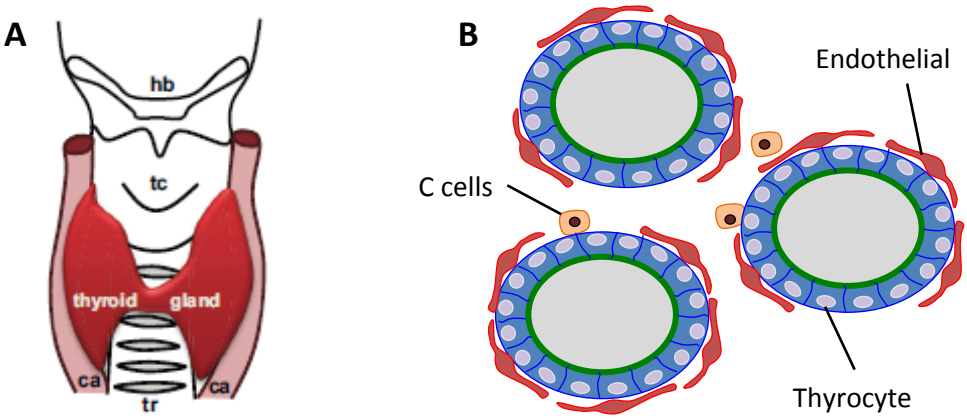

Figure 1: Anatomy and histology of the thyroid gland. A, the thyroid gland consists of two lobes, on each side of the trachea, linked by an isthmus. hb, hyoid bone; tc, thyroid cartilage; tr, trachea; ca, carotid artery (Nilsson and Fagman, 2017). B, angiofollicular units are the functional units of the thyroid gland. They are composed of polarized thyrocytes (blue), organized in follicles with their apical pole (green) facing the colloid (grey) and closely surrounded by a dense capillary network (red). C cells (orange) are located under the basal pole of thyrocytes.

Thyrocytes produce the thyroglobulin-derived hormones, triiodothyronine and thyroxine (T3 and T4), by incorporating oxidized iodide in thyroglobulin (Tg), a 660kDa homodimeric glycoprotein synthetized by the thyrocytes and secreted in the lumen of the follicles (i.e. the colloid). Thyrocytes first capture iodide (I^-) from the pericapillar space through the sodium-iodide symporter (NIS) present at their basal pole (**Fig. 2**). Iodide reaches the apical pole of the thyrocyte by an unknown mechanism and is transferred into the colloidal space, through the apical membrane, via pendrin and other transporter such as the channel anoctamin (Twyffels *et al.*, 2014). In the colloidal space, iodide is oxidized by thyroperoxidase (TPO), in presence of H_2O_2 (generated as described below), and incorporated onto one (MIT) or two (DIT) tyrosine residue of Tg. MIT and DIT are further coupled by TPO to form T3 and T4 and the resulting iodinated-Tg (i-Tg) is stored in the colloid. The production of H_2O_2 levels is ensured by dual oxidase 2 (DUOX2) present at the apical membrane of the thyrocytes (**Fig. 2**). DUOX2 is an enzyme that produces H_2O_2 by catalyzing the oxidation of NADPH. DUOX maturation factor 2 (DUOXA2) is essential for H_2O_2 production as a chaperone by ensuring the correct localization of DUOX2. When T3 and T4 blood levels are low, the pituitary gland produces thyroid-stimulating hormone (TSH) that will bind its receptor (TSH-R) at the basal pole of thyrocytes. Binding of TSH on its receptor stimulates the capture of i-Tg by micro-pinocytosis at the apical pole of the thyrocytes. Endosomes, filled with i-Tg, are targeted to lysosomes where T3 and T4 are excised by lysosomal enzymes. T3 and T4 are released from the lysosomes and transported (by unknown mechanisms) to the basal pole of the thyrocytes to be released in the blood flow via the basal transporter monocarboxylate transporter 8 (MCT8). Unused MIT and DIT are dehalogenated by the NADPH-dependent specific iodotyrosine dehalogenase 1 (DEHAL1) and the resulting Iodide is recycled into thyroid hormone synthesis pathway. When T3 and T4 blood levels are restored, the hypothalamo-hypophyseal feedback loop will decrease the production of TSH and consequently the release of T3 and T4 (**Fig. 2**). It is important to note that, upon binding to its receptor, TSH control the overall production of i-Tg by stimulating thyroglobulin synthesis as well as the expression of NIS and TPO, and the activation of TPO and DUOX2. TSH also indirectly regulates the expansion of the microvasculature surrounding the follicle (Colin *et al.*, 2013; Nilsson and Fagman, 2013; Rousset *et al.*, 2015).

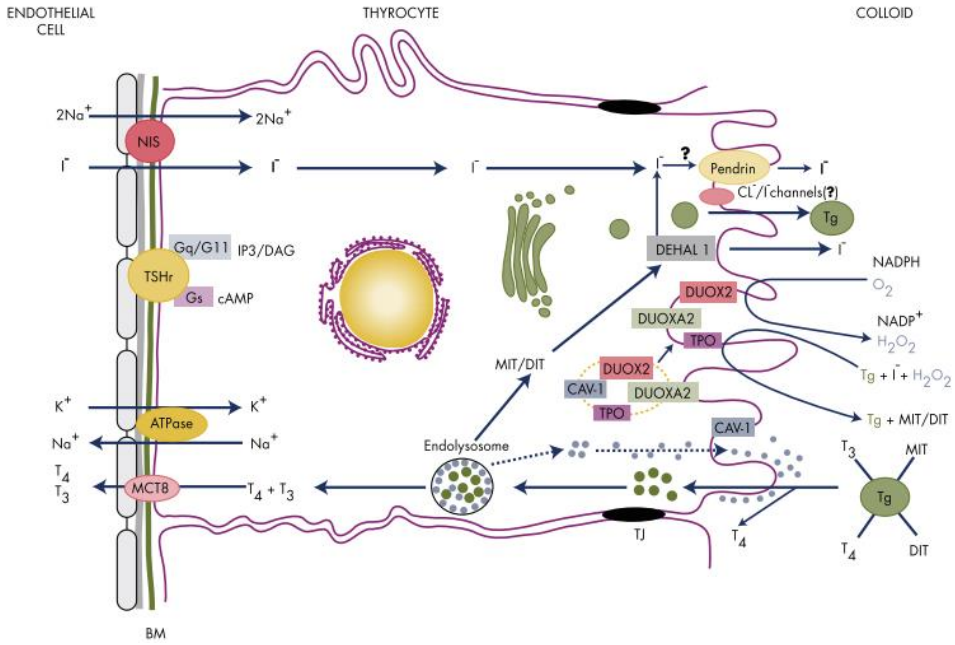

Figure 2: Thyroid hormone synthesis, from iodide uptake to release of T3 and T4. Iodide (I^-) readily crosses the fenestrated endothelium and enters the thyrocyte via NIS. At the apical pole of the thyrocyte, I^- is transferred into the colloid space via pendrin or other ion transporters, readily oxidized by TPO and incorporated on tyrosine residues of thyroglobulin (Tg) to form MIT and DIT which are reorganized into T3 and T4. Iodinated-Tg is stored in the colloid. To release T3 and T4 in the bloodstream, iodinated-Tg is first endocytosed by the thyrocyte and digested by lysosomal proteases. Free T3 and T4 are then exported into the blood flow through the basolateral transporter MCT8 (Colin *et al.*, 2013).

Thyrocyte function thus requires the close proximity of blood vessels, from which iodide is captured, and into which T3/T4 are released. This association between blood vessels and follicles is called the angio-follicular unit, which is considered as the functional unit of the thyroid (**Fig. 1B**). Besides their classical role of oxygen and nutrient supplier, the microvasculature around the follicles is also essential for thyroid homeostasis as well as for maintaining the morphology and the functional state of the angio-follicular units. For example, upon iodide deficiency during goiter formation, it was demonstrated that angiogenesis is stimulated in two phases. The first phase is TSH-independent and occurs before thyrocyte proliferation. During this phase, endothelial cells proliferation and microvascular activation occur in order to restore iodide levels in thyrocytes by an increase in blood flow around the follicle. The second angiogenic phase occurs after prolonged iodide deficiency, is TSH-dependent and promotes thyrocytes proliferation. These observations indicate that angiogenesis is essential for thyrocyte adaptation to iodide deficiency (Gerard *et al.*, 2008).

The second thyroid epithelial cell type is named C cell. C cells are found associated with follicles, either as single cell or as small clusters of cells, but not participating to the follicular structure. They are inserted in-between thyrocytes at their basal pole, within the basal lamina, and thus belong to the angio-follicular unit. C cells produce calcitonin, a hypocalcemic hormone that favors calcium release in urine, and decreases bone calcium release in the blood by inhibiting osteoclast activity. (Colin *et al.*, 2013).

5.1.2 Embryogenesis

In mammals, both thyroid endocrine cell types, thyrocytes and C cells, originate from the endoderm. Thyrocyte progenitors bud from the median thyroid anlage (mta) in the pharyngeal floor (anterior), whereas C cells derive from the ultimobranchial bodies (UBBs) that originate from the lateral thyroid anlage (lta) at the most caudal part of the fourth pharyngeal pouches (**Fig. 3**) (Nilsson and Fagman, 2017).

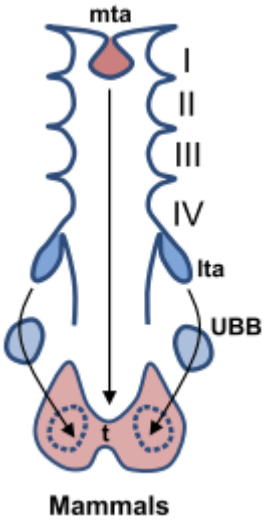

Figure 3: Embryologic origins of thyroid epithelial cells. The median thyroid anlage (mta) arises from the pharyngeal floor and will give rise to thyrocytes. Ultimobranchial bodies derive from the lateral thyroid anlages (lta) that arise from the fourth (IV) pharyngeal pouch. Cells from both mta and lta will later fuse and form the bilobated thyroid (Nilsson and Fagman, 2017).

5.1.2.1 Specification, budding, migration and folliculogenesis

Specification

Thus, the thyroid gland, like the pancreas and the lungs, originates from the endoderm. In the most anterior part of the endoderm, in the pharyngeal floor, a group of polarized cells, located close to the aortic sac (**Fig. 4.1**), will co-express a set of four transcription factors: Hhex, Nkx2-1, Pax8 and Foxe1. The presence of these four thyroid transcription factors (TTFs) will specify the fate of endodermal cells to the thyroid lineage. This happens around embryonic day 8.5 (E8.5) and will lead to the formation of the thyroid placode (**Fig. 4.1**) (De Felice and Di Lauro, 2011). *In vitro* experiments have demonstrated that fibroblast growth factors (FGFs) and bone morphogenetic proteins (BMPs) can trigger the specification of thyroid cells from endodermal stem cells. However, the cellular origin of FGFs and BMPs *in vivo* remains unknown (Longmire *et al.*, 2012; Teshima *et al.*, 2016; Wendl *et al.*, 2007).

Budding and migration

As the number of polarized and specified cells in the thyroid placode increases, cells progressively lose their polarity. At E9.5, the thyroid primordium buds ventrally towards the aortic sac (**Fig. 4.2**) and the mass of thyrocyte progenitors migrates caudally towards the third pharyngeal arch arteries (paa3, **Fig. 4.3**). Around E11, the first endothelial cells are found close to the thyroid epithelium. At E12.5, the thyroid epithelium extends laterally and dorsally along the paa3 (**Fig. 4.4**) and fuses with the descending UBBs. The UBB spherical masses express Nkx2-1 but not Pax8. Upon fusion, around E13.5 the thyroid gland has reached its final position and thus consists of two lobes, on each side of the trachea, linked by an isthmus (**Fig. 4.5**). Despite the fusion of the thyroid anlage with the UBBs, the two cell types will not mix directly.

Folliculogenesis

Follicle formation, i.e. folliculogenesis, is the final step of thyroid morphogenesis and starts at E14.5. The non-polarized thyrocyte progenitors first organize in cord-like structures surrounding small masses of cells originating from the UBBs (**Fig. 4.6**, left).

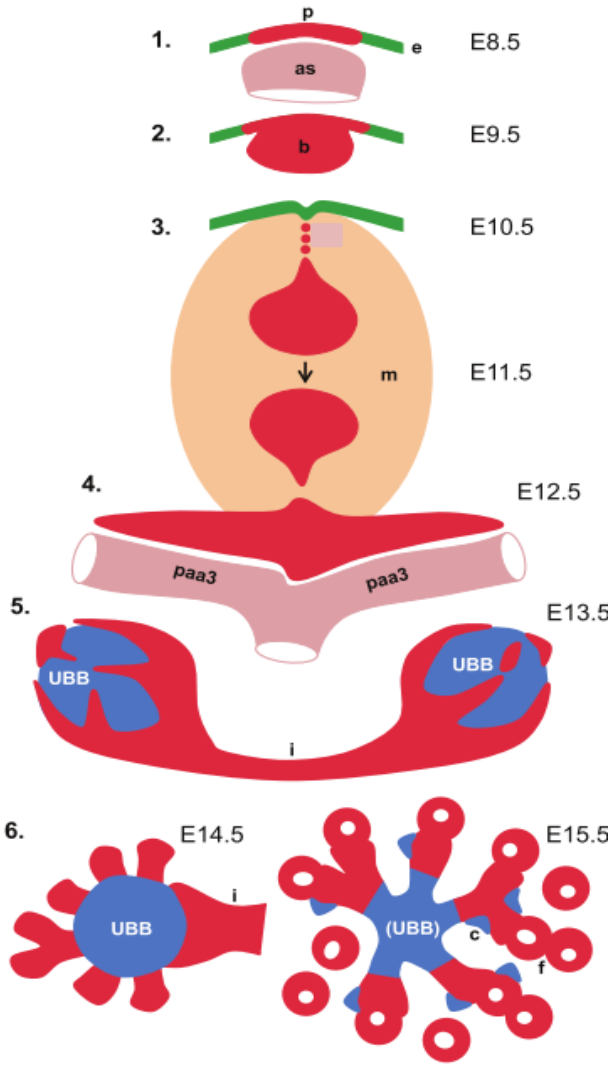

Figure 4: Developmental steps of the thyroid gland. **1**, specification of thyrocyte precursors (red) in the pharyngeal floor (p) of the endoderm (e), close to the aortic sac (as). **2**, budding of the thyroid primordium. **3**, migration of the thyroid primordium, in the mesoderm (m), and apposition close to the third pharyngeal arch arteries (paa3). **4**, elongation of the thyroid primordium along the paa3. **5**, bilobation, formation of the isthmus (i) and fusion with the ultimo-branchial bodies (UBB). **6**, expansion, organization of the thyrocytes in follicles (f) and mixing of the C cells (c). Adapted from (Nilsson and Fagman, 2017).

Thyrocyte progenitors will progressively polarize, form small lumens within clusters of thyrocytes, and initiate their differentiation program (e.g. expression of Tg). Central cells of the UBBs give rise to calcitonin-expressing C cells that will spread and mix within the gland (**Fig. 4.6**, right). Although associated with mature follicular structure, C cells are probably not involved in follicle formation. Indeed, in zebrafish, follicles form despite the absence of C cell, demonstrating that these cells are not required for follicle formation. At E15.5, the thyroid gland starts to display its final architecture, with follicular structures delineating small follicular lumens, which will then expand in size by proliferation of thyrocytes.

Polarization of epithelial cells and organization in monolayers delineating a lumen are processes also observed in other organs. Monolayers can form simple tube (e.g. in the intestine), highly branched tubes (e.g. in the lung and pancreas) or closed independent spheres like in the thyroid. This organization in monolayers surrounding a lumen is essential for organ function. The molecular mechanisms of lumen formation have been largely studied using epithelial cell lines such as MDCK and involve fusion of multiple intracellular vesicles with the nascent apical pole of adjacent cells (**Fig.5**) (Chou *et al.*, 2016). During my thesis, folliculogenesis will be monitored by evaluating luminal expansion.

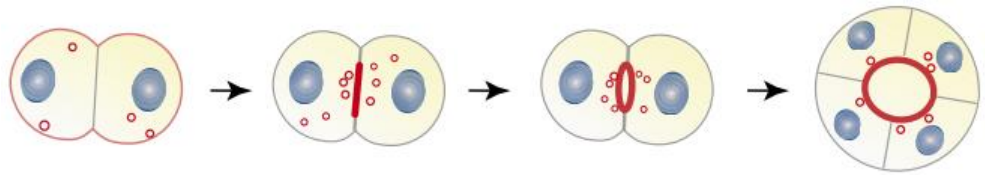

Figure 5: Schematic representation of *de novo* lumen formation in MDCK cells. After cell division, apical proteins (red) localize on cellular membrane facing the extracellular matrix. Apical proteins are then progressively internalized on intracellular vesicles, which fuse at the cell-cell junction, thereby creating a lumen between the two cells and defining their apical pole. Lumen size increases by continuous and concerted fusion of intracellular vesicles from the different cells with the developing apical pole. Note that the baso-lateral membranes, in grey, are separated from the apical membranes by tight junctions (not represented). Adapted from (Chou *et al.*, 2016).

At E17.5, follicular lumina are clearly visible, even though they continue to increase in size after birth, and the genes involved in thyroid hormones synthesis (*Tsh-r*, *Tg*, *Nis*, *Tpo*, *Duox*…) are strongly induced (Fagman *et al.*, 2006; Nilsson and Fagman, 2017).

The four TTFs, expressed from the early stage of thyroid development through adult life, are thought to regulate all these developmental steps (De Felice and Di Lauro, 2011). However, whereas their roles in the earliest developmental steps (specification, budding and migration) of thyroid development have been well documented, their subsequent functions are poorly understood.

5.1.2.2 Roles of the key thyroid transcription factors

The four TTFs, Nkx2-1, Pax8, Hhex and Foxe1, are expressed during all the developmental processes but also in the adult thyroid. Evidences point towards transcriptional cross-regulation between these factors (**Fig. 6**) (De Felice and Di Lauro, 2011). Indeed, even if at an early stage, the transcription factors Hhex, Nkx2-1 and Pax8 are independently expressed, the expression of Foxe1 depends on Pax8. During the budding process, Nkx2-1 regulates the expression of Hhex and Foxe1, while Pax8 and Hhex are inter-dependent and control Foxe1. Although Foxe1 does not seem to regulate any of the other TTFs, the above-mentioned regulatory loops give rise to a strong network (**Fig. 6**). In addition, the deletion of any one of the TTFs inevitably leads to athyreosis or severe thyroid hypoplasia, despite the fact that the three others remain expressed in the thyroid placode (Nilsson and Fagman, 2017; Parlato *et al.*, 2004).

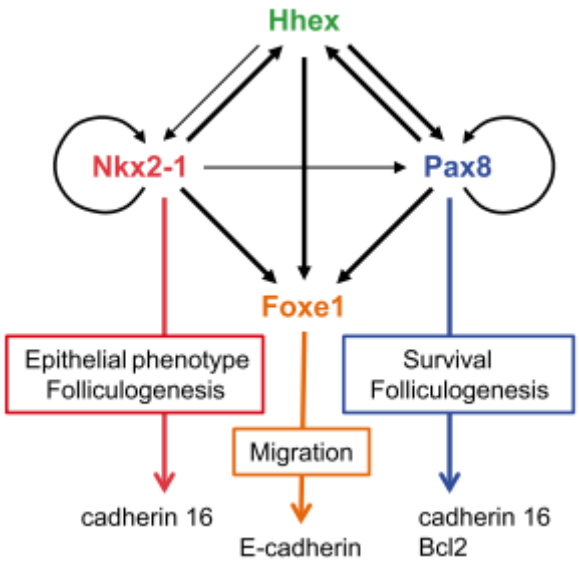

Figure 6: The interconnected transcription factor network in thyroid embryogenesis. See text for explanations. Adapted from (Nilsson and Fagman, 2017).

Hhex

Besides its important role in the transcriptional network that regulates thyroid development, the specific role of Hhex in the early stages of this process is still unknown. However, its role appears to be different than in other endoderm-derived organs where it is expressed. Hhex has been demonstrated to be important for the specification of the ventral pancreas; it determines the appropriate location of pancreatic progenitors in the endoderm (Bort *et al.*, 2004). In addition, it was demonstrated that Hhex is important for liver bud formation through the repression of sonic hedgehog (Shh) signaling pathway (Bort *et al.*, 2006). Even though, *Hhex*$^{-/-}$ thyroid primordium is hypoplastic, it displays an appropriate central location and correct budding. Furthermore, unlike in other endoderm-derived organs, Shh levels are not restored in *Hhex*$^{-/-}$ thyroid primordium, suggesting that Hhex is neither involved in thyroid primordium specification nor in its budding (Parlato *et al.*, 2004).

Nkx2-1

Absence of *Nkx2-1* causes athyreosis (i.e. absence of thyroid gland), as well as lung development arrest (Minoo *et al.*, 1999). On the other hand, in *Nkx2-1* null mutants, UBBs are present but will eventually regress (Kusakabe *et al.*, 2006), suggesting that Nkx2-1 is involved in early morphogenesis rather than in cell specification. It is interesting to note that Nkx2-1 can be phosphorylated. It has been shown that transgenic mice expressing a mutant form of Nkx2.1 that cannot be phosphorylated display disorganized follicles and gene expression changes. This suggests that Nkx2.1 also controls thyroid differentiation and follicle formation (**Fig. 6**) (Silberschmidt *et al.*, 2011).

Pax8

In *Pax8* null mutant, placode formation and budding are not impaired (Parlato *et al.*, 2004). However, the anti-apoptotic factor Bcl2, which is strongly expressed in wild-type thyroid progenitors, is weakly expressed in *Pax8*$^{-/-}$ mice and zebrafish, resulting in increased apoptosis. This indicates that Pax8 might regulate thyroid progenitor survival through the regulation of Bcl2 expression (**Fig. 5**) (Fagman *et al.*, 2011; Porreca *et al.*, 2012). Surprisingly enough, no thyroid defect is observed in *Bcl2* KO mice (Roset *et al.*, 2007).

Maintenance of cohesion in the developing thyroid depends on the expression of cadherins (Fagman *et al.*, 2003). *Pax8* has been shown to be essential for cadherin 16 expression in thyroid cells (de Cristofaro *et al.*, 2012). Moreover, using *in vitro* culture of Fisher rat thyroid cells or murine primary thyrocytes, the group of Santisteban recently demonstrated that Pax8 controls expression of cadherin 16 and that this promoted apical polarization and folliculogenesis (**Fig. 6**) (Koumarianou *et al.*, 2017).

Foxe1

The observation that the expression of Foxe1 decreases when thyroid bud ceases its migration suggest that Foxe1 is implicated in thyroid bud migration (**Fig. 6**) (De Felice *et al.*, 1998). However, the mechanisms by which Foxe1 regulates thyroid bud migrations are still unknown. Furthermore, the role of Foxe1 in thyroid bud migration is controversial because of the inconsistent phenotype of *Foxe1* KO mice, displaying ectopic thyroid or agenesis.

5.1.2.3 Extrinsic factors involved in thyroid morphogenesis

Due to the migration into different microenvironments during embryonic development, the thyroid tissue will come sequentially in contact with different cell types or tissues. Hence, extrinsic factors produced by these various microenvironments might influence thyroid development.

Cell:Cell communication

T-box family transcription factor 1 (Tbx1) deletion is associated with many defects in endoderm-derived organs, including in the thyroid gland (Fagman *et al.*, 2007). Indeed, in *Tbx*$^{-/-}$ mice, the thyroid bud is formed but does not develop, resulting in a hypoplastic thyroid (Fagman *et al.*, 2007). It was reported that Tbx1 is expressed in the subpharyngeal mesoderm and controls the generation of Nkx2-1^{+} progenitors in the thyroid placode as demonstrated by the reduced number of Nkx2-1^{+} cells in the thyroid placode of *Tbx*$^{-/-}$ mice. Furthermore, mesoderm specific deletion of *Tbx1* results in a size reduction of the thyroid. The effect of mesodermal Tbx1 on thyroid development is mediated by FGF8, also produced by the mesoderm. Indeed, deletion of *Fgf8* in Tbx1 expressing cells reproduces the *Tbx*$^{-/-}$ phenotype, and expression of FGF8 in *Tbx*$^{-/-}$ cells rescues the *Tbx*$^{-/-}$ phenotype (Lania *et al.*, 2009). A similar mechanism has been described during thyroid specification in zebrafish (Wendl *et al.*, 2007). This suggests that, in mammals, the Tbx1-FGF8 pathway promotes proliferation of thyroid progenitors rather than their specification. Recent findings show that a FGF10-Sox9 pathway, reminiscent to what has been described in the pancreas and lungs, might be involved in thyroid development and thyrocyte progenitors proliferation during folliculogenesis (Liang *et al.*, 2018). However, the relation between FGF10 and Sox9 in the thyroid remains ill defined.

Blood vessels are important not only for thyroid function but also for its embryonic development. Indeed, several human blood vessels malformations are associated with thyroid developmental defects. This was first demonstrated for embryonic large vessels in *Shh*$^{-/-}$ mice in which the thyroid is hypoplastic and only forms one lobe in late embryos (Fagman *et al.*, 2004). *Shh*$^{-/-}$ mice display abnormal paa development along which, in wild-type embryos, the mass of thyroid progenitors elongate to form the two lateral lobes. This suggests that paa are

important for thyroid positioning and bilobation, even if this process is primarily Shh-dependent (Alt *et al.*, 2006; Fagman *et al.*, 2006). At later stages, our group has showed that newly formed microvessels are essential for follicle formation. Indeed, deletion of *Vegfa* in thyroid progenitors results in reduced endothelial cell recruitment and folliculogenesis defects (**Fig. 7**).

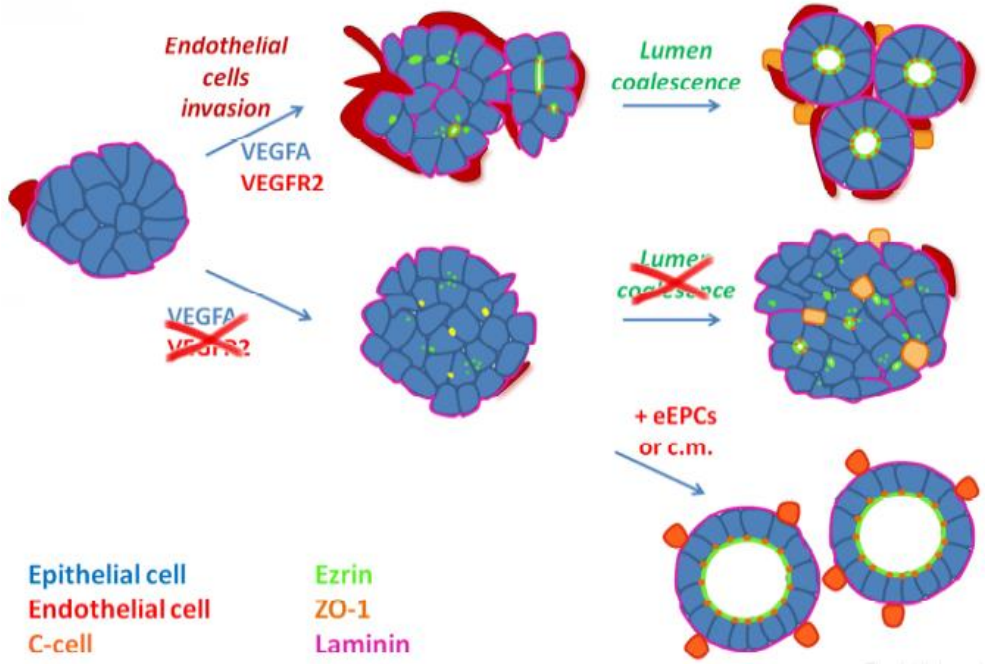

Figure 7: Role of endothelial cells in thyroid follicle formation. In wild-type thyroid, thyrocyte progenitors (blue) produce VEGFa to recruit endothelial cells (red). Subsequently, thyrocyte progenitors start to form intracellular pre-luminal vescicles (green) that fuse with the apical pole of the cell to form the central lumen surrounded by polarized thyrocytes. Upon deletion of *Vegfa* in thyrocyte progenitors, endothelial cells recruitment is impaired and follicles do not form (persistence of intracellular pre-luminal vesicles). This defect can be reproduced *ex vivo* upon treatment of thyroid explant with VEGFR2 inhibitor. However, follicle formation is rescued by culturing thyroid explants with either endothelial progenitor cells or with medium conditioned by these cells (Hick *et al.*, 2013).

Similarly, culture of thyroid anlages in the presence of a VEGFR2 inhibitor caused rapid endothelial apoptosis and a complete depletion of this cell type in the cultured tissue. This was associated with defective follicle formation. Adding EPC cells or medium conditioned (CM) by EPCs on explants depleted from endothelial cells rescued follicle formation, indicating that endothelial cells produce a factor involved in thyroid folliculogenesis (**Fig. 7**) (Hick *et al.*, 2013). In zebrafish, Opitz *et al.* nicely illustrated the coordination between thyroid and cardiovascular development using fluorescent protein. However, they also demonstrated that, although important for thyroid morphogenesis, embryonic vessels do not trigger thyroid development (Opitz *et al.*, 2012).

Ephrin signaling has been shown to control the organization of epithelial cells in pancreas and thyroid. Signalization through Ephrins and their tyrosine kinase receptors (Eph) is contact-dependent which differs from the classical soluble ligand/transmembrane receptor signalization. Upon Ephrin/Eph binding, a classical forward signaling and a reverse signaling are generated by Ephs and Ephrins respectively. At E9.5, the receptor EphA4 (Ephrin receptor A4) is ubiquitously expressed in the foregut endoderm, and its expression is maintained in thyrocytes during thyroid development and throughout adult life, suggesting a role for Ephrin signalization in the thyroid gland. Surprisingly, thyroid development in *EphA4*$^{-/-}$ embryos appears normal. However, *EphA4*$^{-/-}$ adult thyrocytes are flat and follicles are smaller, arguing for a role of forward and reverse Ephrin signaling between thyrocytes at the follicle maturation stage rather than in early development (Fig 7A). EphA4 is also expressed by UBBs at early stages, until the fusion with the thyroid anlage. Furthermore, knock-in expression of EphA4 at later stages results in reduced number of C cells remaining as a cluster at the center of the lobes. Altogether, these observations suggest that reverse Ephrin signaling is involved in C cell generation at early stages of thyroid development, while controlling C cell proliferation and migration (**Fig. 8**) at later stages (Andersson *et al.*, 2011).

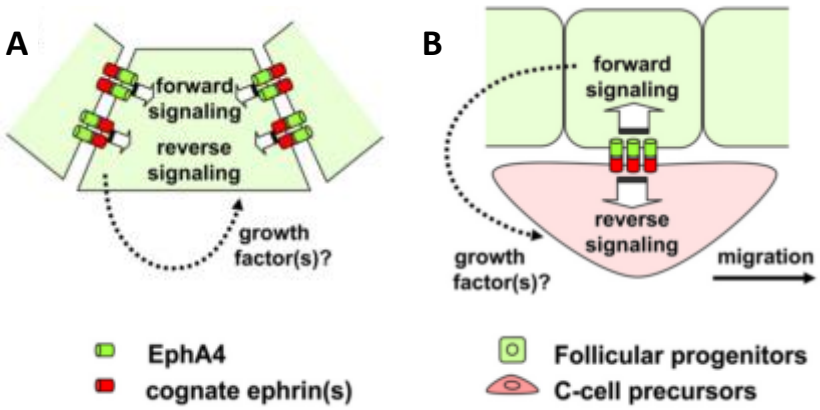

Figure 8: Ephrin signaling in thyroid morphogenesis. A, concomitant expression of Eph receptors and cognate ephrins by each of two adjacent cells results in intracellular forward and reverse signaling in both cells. B, independent expression of Eph receptors or cognate ephrins in two adjacent cells results in intracellular reverse and forward signaling respectively (Andersson *et al.*, 2011).

Cell:matrix interactions

Beyond cell-cell communication, interaction of epithelial cells with the extracellular matrix (ECM) is crucial for organ morphogenesis and function. The ECM can be divided in two parts: the interstitial matrix and the basement membrane or basal lamina. This latter correspond to a 50-100nm thick sheet of ECM separating epithelial or endothelial cells from the surrounding stroma. The composition of ECM varies between organs but also according to the developmental stage and the physiological state of the tissue. ECM components fulfill three important roles: structure (collagens, elastins), adhesion (laminins, fibronectin) and resiliency (glycosaminoglycans and proteoglycans). Below, I focus on collagens and laminins, the latter being the main component of the basal lamina.

The most abundant collagen is type I collagen, a fibrous protein composed of three polypeptidic α-chains (115kDa/chain) organized in a super helix. Type I collagen is found in the interstitial matrix of many organs. In the basal lamina, we find a non-fibrous collagen, type IV collagen. There are six isoforms, α1 to α6, which

form a triple helix with globular domains at the N- and C-terminal part of the helix. After secretion, type IV collagen trimers will be able to interact via their globular domains to form a network-like scaffold that gives the structure to the basal lamina.

The second very abundant protein found in the basal lamina is called the laminin. Laminins are heterotrimers composed of one α, one β and one γ chains, assembled in a central coiled coil domain and held together by disulfide bonds. Five different α chains (from 200 to 400kDa), four different β chains and three different γ chains (from 120 to 200kDa) have been described; hence laminin trimers are large protein complexes with a size between 440 and 800kDa. Laminin nomenclature is based on the chain composition of the trimers; for example, laminin111, which is ubiquitously expressed in developing organs, is composed of α1, β1 and γ1 chains. The three chains are synthetized in the cytoplasm and secreted in the extracellular space as a trimer; the lack of any of the chains will block secretion. Upon secretion, laminins will interact with the type IV collagen network, but also with other extracellular matrix proteins and cell surface receptors such as integrins.

Although mostly studied *in vitro*, several evidences point to a critical role of ECM during thyroid development. As demonstrated for several epithelial cell lines such as kidney-derived MDCK or intestinal-derived Caco-2 cells, thyroid porcine cells cultured in suspension form cyst-like structures with the apical pole of the cells facing the culture medium. They thus display an inverted polarity. Upon transfer in type I collagen, these inverted cysts reverse their polarity so that the apical poles now face the central lumen of the cystic/follicular structure (Mauchamp *et al.*, 1998). Fragments of adult thyroid tissue will also maintain a 3D follicular structure with well-defined apico-basal polarity only if cultured in type I collagen (Toda *et al.*, 2011). Finally, the group of Costagliola nicely demonstrated that thyrocyte progenitors, obtained by transient but concomitant expression of Pax8 and Nkx2-1 in embryonic stem cells, and cultured in extracellular matrix (Matrigel), organize in 3D follicles that can rescue thyroid function *in vivo* (Antonica *et al.*, 2012). More recently, combining *in vivo* and *ex vivo* studies, our group was able to demonstrate that the trimeric protein laminin111 is involved in thyroid folliculogenesis (Villacorte *et al.*, 2016). Indeed, in both *Vegfa KO* thyroid and *Smad1/5* double KO thyroid, follicles do not form correctly and both models present impaired basal lamina assembly. Furthermore, EPC-CM, containing abundant laminin111, is able to rescue follicle formation in *Vegfa* KO and *Smad1/5* KO thyroid explants.

Interestingly, knockdown of lamininα1 in EPCs prevents the pro-folliculogenic effect of EPC-CM, suggesting an important role of laminin111 in thyroid folliculogenesis. Our *in vivo* work and conclusion are supported by *in vitro* evidences obtained by the group of Keith Mostov in MDCK cells (O'Brien *et al.*, 2001). Using dominant negative N17Rac1 MDCK cells, they observed defective laminin assembly and inverted apico-basal polarity, despite the presence of a collagen type I-rich microenvironment. Exogenous laminins restored correct apico-basal polarity and lumen formation in N17Rac1 MDCK cysts, demonstrating the essential role of laminin assembly in epithelial orientation and apico-basal polarization (O'Brien *et al.*, 2001).

5.1.3 Thyroid diseases

A variety of diseases such as multinodular goiter, Hashimoto's thyroiditis, Graves' disease and cancer can affect the thyroid gland. Here, I will briefly present these diseases and focus on thyroid cancers.

Goitrogen diseases

The most common thyroid disease is the goiter. It is due to iodine deficiency that results in enhanced TSH-mediated growth of the thyroid gland. If several nodules cause thyroid abnormal growth, the disease is called multinodular goiter (MNG). MNG is characterized by enlarged follicles, delimited by flat thyrocytes, and the appearance of necrotic area infiltrated by macrophages. MNG presents two types of follicles, hyper-functional (hot) follicles and hypo-functional (cold follicles) (Studer *et al.*, 1989). Development of nodules is favored by DNA mutation in genes involved in thyroid homeostasis and thyroid hormone synthesis, goitrogen dietary (i.e. diet that limits iodide uptake), smoking and stress (Colin *et al.*, 2013; Knobel and Medeiros-Neto, 2003; Studer *et al.*, 1989).

Another well-known disease is Hashimoto's thyroiditis. It is an autoimmune disease mediated by cellular and humoral immunity, which results in progressive thyroid destruction leading to hypothyroidism. The decrease in thyroid hormone is detected by the pituitary, which will produce TSH to stimulate thyroid hormones synthesis. This hyper-stimulation can also lead to goiter development (McGrogan *et al.*, 2008).

Finally, Graves' disease is another pathology leading to thyroid enlargement. It is also an autoimmune disease in which TSH-R is recognized by autoantibodies. There are two types of autoantibodies, TSH-stimulation blocking antibodies (TSBAb) and thyroid stimulating antibodies (TSAb). The latter stimulates thyroid hormones production and expansion of the thyroid gland (Maheshwari and Weis, 2012).

Thyroid cancers

Thyroid cancers represent 2% of the cancer diagnosed worldwide. They are the most frequent endocrine cancers, with a three times higher incidence in women than in men. The reported incidence of thyroid cancer has been increasing regularly for decades. This is mainly explained by improvement of diagnostic techniques and the increasing usage of ionizing radiation for medical purposes (Kitahara and Sosa, 2016). There are four types of thyroid cancers: anaplastic thyroid carcinoma (ATC), medullary thyroid carcinoma (MTC), follicular thyroid carcinoma (FTC) and papillary thyroid carcinoma (PTC). They are distinguished by the differentiation state, the cell of origin, tissue histology and causal mutations. (Fagin and Wells, 2016).

ATC is a dedifferentiated cancer deriving from follicular cells; it is one of two rare forms (2%) but it is the most aggressive (10% survival after ten years) form of thyroid cancer. Most of the time, ATC is the consequence of non-diagnosed FTC or PTC. MTC is a differentiated cancer deriving from C cells while FTC and PTC are differentiated cancer deriving from follicular cells. Both are less aggressive and have a slow development rate. FTC, representing only 2% of thyroid cancers, are characterized by small and closed follicles that breach the conjunctive tissue surrounding the cancerous nodule. PTC are by far the most frequent thyroid cancers, with more than 80% of the cases. They develop from follicular cells, which exhibit an eosinophil cytoplasm with elongated nucleus, and are characterized by papillary-like projections in the lumen of the follicles; the latter lose their round shape. Although PTC present a high survival rate with more than 95% survival after ten years, persistence of the disease can lead to a more aggressive and infiltrating form of cancer. Those highly metastatic forms are resistant to radioiodine treatment and their poor prognostic has recently been linked to a particular mutational profile (Durante *et al.*, 2013; Fagin and Wells, 2016).

In PTC, the most frequently affected proto-oncogene is the *BRAF* (B-type Raf kinase) gene, which is associated with poor prognosis. This gene codes for the BRAF protein, a serine/threonine kinase that is activated upon phosphorylation of threonine 599 (T599) and serine 602 (S602) residues (**Fig. 9**), which results in the activation of the mitogen-activated protein kinase (MAPK)/extracellular signal-regulated kinase (ERK) pathway, controlling cellular proliferation. 60% of PTCs display the transversion T1799A in the *BRAF* proto-oncogene that causes the substitution of a valine at position 600 into a glutamate in the protein sequence (noted V600E). The V600E substitution thus occurs on a residue located between T599 and S602 (**Fig. 9**). The presence of the negatively charged glutamate residue in position 600 mimics the phosphorylation of both T599 and S602 residues and causes a constitutive activation of the kinase, leading to MAPK pathway activation (Fagin and Wells, 2016; Kimura *et al.*, 2003). In 10-30% of PTC, the increase in MAPK activity results from the RET/PTC re-arrangement in the *RET* gene, which codes for a tyrosine kinase receptor. Occurrence of this re-arrangement is favored by ionizing radiation.

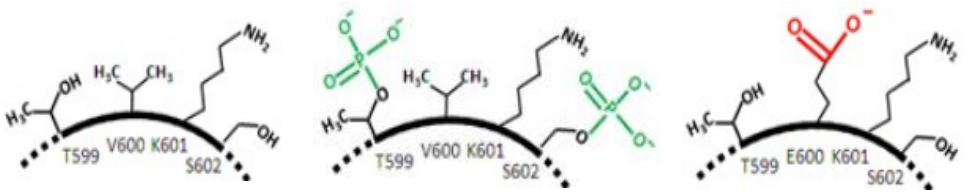

Figure 9: Molecular impact of the V600E substitution in BRAF protein. On the left side, the inactive wild-type BRAF. On the center, the doubly phosphorylated (green) and active wild-type BRAF. On the right side, the constitutively active mutated $BRAF^{V600E}$.

A genetic mutation in a cell is often the first step of tumorigenesis. This mutation will transform the initiator cell that will develop particular characteristics allowing to: proliferate extensively, dedifferentiate, be insensitive to external regulators, escape apoptosis, recruit blood vessels, invade the neighboring tissue, modify its metabolism and escape the immune system (Hanahan and Weinberg, 2011). All these characteristics are essential for tumor growth and most of these involve intercellular communication.

5.2 Principles of intercellular communication

Intercellular communication is an essential process for multicellular organisms and is mediated by signals of electrical (i.e. transfer of ions) and molecular (i.e. biological molecules) nature. Those signals can be used in four different ways: (i) via communicating or gap junctions, which are cytoplasmic bridges that connect the cytoplasm of two adjacent cells and allow exchange of electrical signals and small molecules; (ii) via direct contact (i.e. Delta/Notch), allowing a molecule expressed at the surface of one cell (ligand) to interact with another molecule (receptor) expressed at the surface of the neighboring cell; (iii) via local release of soluble molecules (ligands) in their environment (i.e. VEGF) that will bind their receptor on the target cells; and (iv) via long distance communication, either through electrical signals transported along nerves or through hormones and cytokines transported in the blood flow (Silverthorn, 2007). Recently, a new way of intercellular communication using membrane vesicles produced by the cells and effective on both short and long distances was proposed. This new type of communication is the subject of my thesis and will be detailed in section 4.3.

5.2.1 Cytoplasmic bridges

The simplest form of intercellular communication consists in the transfer of electrical and chemical signals from one cell to another through communicating or gap junctions. There is a vast diversity of communicating junctions but they are all composed of proteins called connexins that are the structural units of the junction (**Fig. 10A**). Six connexins associate to form a hemi-channel, or connexon, at the cell membrane (**Fig. 10B**) (Donahue *et al.*, 2017). A single hemi-channel transfers molecules from the cytoplasm to the extracellular space (**Fig. 10C**) (Genetos *et al.*, 2007). The association of two hemi-channels from neighboring cells forms a cytoplasmic bridge, or gap junction, that allows direct transfer of ions and small molecules such as amino-acids or ATP between both cytoplasm (**Fig. 10D**) (Thi *et al.*, 2012). Communication via gap junction is an important process in developmental biology but also in cancer progression. Indeed, gap junction-incompetent (i.e. $Cnx43^{-/-}$ and $Cnx45^{-/-}$) embryonic stem cells fail to form a primitive endoderm in embryonic body culture (Worsdorfer *et al.*, 2017). In the thyroid,

thyrocytes are all equipped with communicating junctions and thus all thyrocytes forming a follicle must be considered as a unit as they will all respond similarly to extracellular signals (Munari-Silem *et al.*, 1994). Conversely, two adjacent follicles are independent and may behave differently (Munari-Silem *et al.*, 1991).

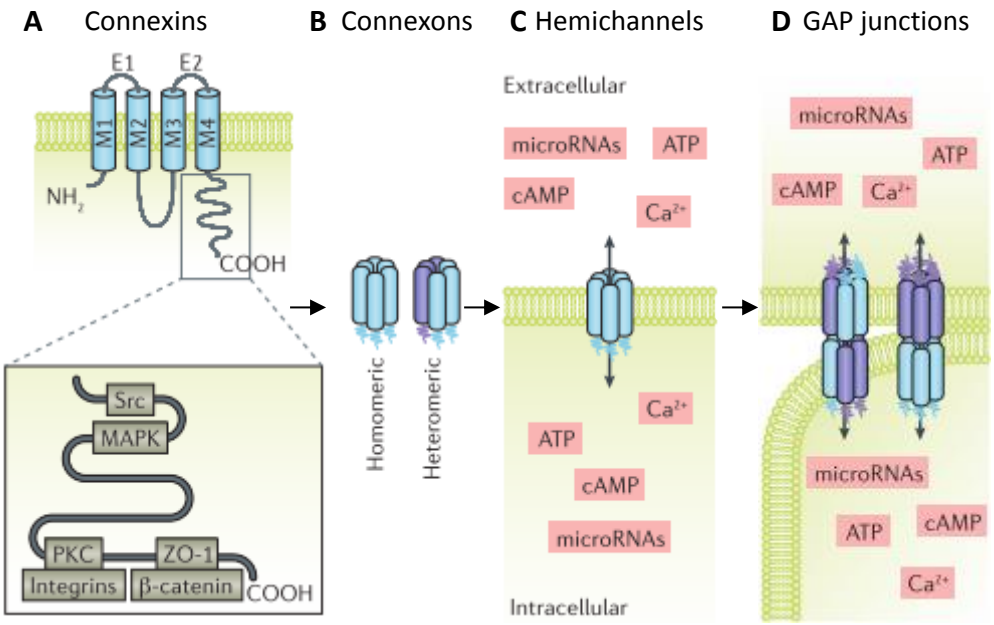

Figure 10: From Connexin to gap junction. **A**, a connexin is a transmembrane protein with four transmembrane domains (M1 to M4) and two extracellular loops (E1 and E2). Its intracellular C terminal tail can interact with several regulatory cytoplasmic proteins (SRC, MAPK, PKC, ZO-1, β-cathenin and integrins). **B**, a connexon is formed by the association of six connexins. **C**, a connexon is called a hemichannel when it transfer small molecule from the cytoplasm of the cell to the extracellular space. **D**, the association of two connexons on adjacent cells forms a cytoplasmic bridge or gap junction. The gap junction allows the passage of small molecules (up to 1kDa) from one cytoplasm to another. Slightly adapted from (Donahue *et al.*, 2017).

5.2.2 Communication by direct contact (juxtacrine)

Three other cellular junctions are involved in intercellular communication: adherent junctions, desmosomes and tight junctions. Adherent junctions and desmosomes are involved in the cohesion of tissues (Steed *et al.*, 2010). They are

composed of proteins of the cadherin superfamily of adhesion molecules that interact with the cytoskeleton. β-catenin mediates the interaction of adherent junction with α-catenin and the actin cytoskeleton (Yamada *et al.*, 2005). In addition, β-catenin is involved in the regulation of intracellular signaling of the Wnt pathways (Kikuchi, 2000). It is generally admitted that adherent junctions affect intracellular signaling by regulating the junctional/cytosolic ratio of β-catenin. Indeed, cancer cells lose their contact with their neighboring cells, and deregulation of the β-catenin pathway is observed in many cancers (Morin, 1999). Similar mechanisms are proposed for desmosomes, and are mediated by plakoglobin rather than β-catenin (Maeda *et al.*, 2004; Thomason *et al.*, 2010). Finally, tight junctions were originally known as barrier junctions between outer and inner body, as well as actors in the establishment and maintenance of cellular polarity (Steed *et al.*, 2010). Several studies have revealed that they also act as sensor by impacting on various signaling pathways and controlling gene expression, cell proliferation and differentiation (Matter *et al.*, 2005). They are composed of transmembrane proteins (i.e. occludin, claudins), adaptor proteins (ZO-1, ZO-2, ZO-3), signaling proteins (aPKC, PTEN) and transcriptional regulators (ZONAB) (Martin *et al.*, 2011).

Besides junctional proteins that can also function as sensors and thus mediate intercellular communication, other molecules are primarily involved in communication. This is best exemplified by the Delta/Notch ligand-receptor interaction in which one cell exposes the ligand Delta at its surface, and this ligand can bind the Notch receptor, exposed at the surface of an adjacent cell (i.e. the target cell). The interaction between the ligand and its receptor triggers a signaling cascade in the target cell. The Delta/Notch signaling pathway is mainly involved in cell fate determination (Kidd and Lieber, 2016). Upon binding of Delta to the Notch receptor, the intracellular domain of Notch is cleaved and translocates to the nucleus where it will influence the expression of target genes (Bray and Gomez-Lamarca, 2017). During embryonic development, it was proposed that Notch signaling is involved in tip and trunk cell specification in the pancreas by promoting the expression of Nkx6-1 in trunk cells (Afelik and Jensen, 2013). Although there is no report of Delta/Notch-mediated communication in thyroid development, it was reported that Delta/Notch signaling could play a role in thyroid cancer establishment and in angiogenesis since expression of Notch1, Notch4 and Delta-like 4 was found in tumors and healthy tissues (Geers *et al.*, 2011). Communication by direct contact does occur in the thyroid via the Ephrin/Eph signaling. Interaction

between EphrinA4 receptor and its cognate ephrin(s) ligand, modulate follicle formation and C cell dispersion (Andersson *et al.*, 2011).

5.2.3 Local communication: autocrine and paracrine signaling

The best-studied communication way is via production of *soluble* molecules that will interact with their receptor on the target cells. For example, epidermal growth factor (EGF) binding to its tyrosine kinase receptor (EGF-R) triggers the activation of RAS, which self-activate the MAPK/ERK signaling pathway, resulting in cell proliferation. When the released soluble factor acts on the producing cell, we refer to autocrine signaling. Paracrine communication is defined by the action of a molecule on cells nearby the producing cell. As previously said, paracrine communication is essential for the development of the thyroid gland. For example, FGF8 produced by the mesoderm surrounding the thyroid primordium is essential for its development at early stages. FGF8 will trigger proliferation of thyrocytes (Lania *et al.*, 2009) probably by binding to its receptor, FGFR2, on the surface of thyrocytes (De Felice and Di Lauro, 2004). At later stages, thyrocyte progenitors secrete VEGFa that promotes endothelial cell recruitment into the thyroid primordium (Hick *et al.*, 2013). This ligand is detected by the tyrosine kinase receptor VEGFR2 on endothelial cells. Binding of VEGFa to VEGFR2 can induce several signaling cascades resulting in endothelial cell proliferation, migration and survival (Koch *et al.*, 2011).

5.2.4 Long distance communication: hormones, cytokines and neural influx

Hormones are long-distance chemical signals secreted in the blood flow, and produced by a tissue called an endocrine tissue. Once in the blood flow, hormones can act everywhere in the body depending on the expression of their specific receptors at the surface or inside the target cells. Insulin, a crucial hormone produced by the pancreatic islets of Langerhans, binds to its membrane receptor, the insulin receptor, expressed at the surface of several tissues such as adipose tissue or muscles in order to decrease blood sugar concentration. Thyroid hormones (TH) act on the skeletal, neurological and cardiovascular system by binding to the cytoplasmic thyroid hormone receptor (TH-R) (Boelaert and

Franklyn, 2005). This receptor belongs to the nuclear receptor family and binds, together with a co-repressor, to thyroid hormone response element (TRE) in genomic DNA. Upon binding of TH on TH-R, the co-repressor is replaced by a co-activator that promotes the transcription of genes downstream of the TRE (Harvey and Williams, 2002). Another example of hormonal action in the thyroid is the action of TSH, released by the pituitary, on its receptor (TSH-R). TSH-R is a G protein-coupled receptor that can activate different G protein subtypes, subsequently regulating thyroid growth and function as mentioned previously (Kleinau *et al.*, 2013).

Cytokines are chemical signals mainly known for their role in modulation of the immune response. Recent evidences indicate however that they play essential roles in development and cell differentiation (Ulrich *et al.*, 2015).

Lastly, a third situation of long-distance communication is observed in neurons, where an electrical signal travels along the cell and is transformed in a chemical signal (neurotransmitter) that is released to transfer the information to the following neuron.

Until recently, those three types of long-range communication were the only known ways by which cells were able to transmit messages to distant cells or location. In the last decade, numerous groups have shown, in different contexts and cell types that vesicles, produced by most cells in the body and released in the extracellular environment and circulation, are also able to transmit long distance signals and thus mediate intercellular communication.

5.3 Extracellular vesicles: new vehicles for intercellular communication

Extracellular vesicles (EVs) are membrane vesicles produced by every cell types in the body. They are delimited by a lipid bilayer and contain a molecular cargo composed of soluble proteins, transmembrane proteins and nucleic acids. This cargo will vary according to the producing cell type and the physiological or pathological status of the cell (van Niel *et al.*, 2018; Yanez-Mo *et al.*, 2015). A peculiar characteristic of EVs, as compared with the other communication ways, is the encapsulation of the molecular messenger or signal. This allows the protection of the transported miRNA and mRNA, particularly sensitive to degradation. Despite the tremendous enthusiasm around EVs, it is important to keep in mind that most of the studies on EVs were performed with *in vitro*-produced EVs. Moreover, proofs for the physiological relevance of EVs as true communication vehicles *in vivo* are still a matter of debate.

5.3.1 Discovery of extracellular vesicles

The first report on extracellular vesicles (EVs) dates back to the late 1960's. Platelet-free plasma was shown to contain lipid-rich particles ("platelet dust") able to promote coagulation (Wolf, 1967). The observation that EVs are loaded with a cargo was reported in 1983 by the group of Rose Johnstone and the group of Philip Stahl, both working on reticulocyte maturation. During this process, reticulocytes need to get rid of transferrin receptors. Using electron microscopy -which is still the only technique allowing visualization of EVs- they were able to see that reticulocytes secreted membrane vesicles covered with transferrin receptors (**Fig. 11**) At that time, they postulated that those vesicles were "garbage bags" used by the cell to discard molecules that were not further needed (Harding *et al.*, 1983; Pan and Johnstone, 1983).

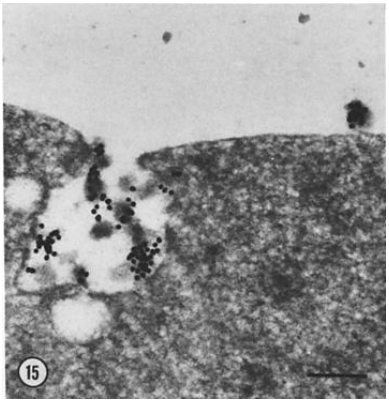

Figure 11: Reticulocytes use extracellular vesicles to discard transferrin receptors during the maturation process. Electronic micrograph of rat reticulocytes discarding transferrin receptors through release of extracellular vesicles. Black dots represent colloidal gold particles bearing (i.e. covered by) transferrin antibodies used to localize transferrin attached to its receptor. (Harding *et al.*, 1983).

More than ten years later, in 1996, the group of Hans Geuze was the first to propose that EVs were not garbage bags but tools for communication. They demonstrated that B-lymphocytes produce MHC-II bearing vesicles and that these vesicles were able to induce T-lymphocyte response *in vitro (Raposo et al., 1996)*. Nevertheless, it is only a decade later that the interest for EVs started to explode. Jan Lötvall's group demonstrated that EVs were carrying mRNA and miRNA and that those nucleic acids were functional after delivery in a recipient cells. They showed that, after incubation of human mast cells with EVs from mouse mast cell, thus containing mouse mRNA, the human mast cell expressed mouse proteins (Valadi *et al.*, 2007).

5.3.2 Types of extracellular vesicles

EVs can be classified in two categories : (i) vesicles budding from the plasma membrane such as apoptotic bodies, oncosomes and microvesicles, and (ii) vesicles produced by the endosomal machinery of the cell and called exosomes (van Niel *et al.*, 2018).

Although apoptotic bodies are presented as giant microvesicles (>1µm) produced by dying cells, it turns out that they might be involved in human EPCs proliferation and differentiation upon injury (Hristov *et al.*, 2004). Hence, these fragments of dying cells are considered as a communication vehicle or signal, informing the neighborhood about its situation. Microvesicles are smaller (50 nm to 1 µm) budding vesicles produced by healthy cells (**Fig. 12**), while oncosomes can be much bigger (up to 10 µm) and are produced by tumor cells. With a size comprised between 50 nm and 150 nm, exosomes are the smallest EVs. They are first produced as intraluminal vesicles (ILVs) within multivesicular endosomes (MVEs), before their release in the extracellular milieu upon fusion of the MVEs with the plasma membrane (**Fig. 12**). More than their size, it is their way of production, via the endosomal machinery, that defines exosomes (Colombo *et al.*, 2014; Meehan *et al.*, 2016; Raposo and Stoorvogel, 2013; Yanez-Mo *et al.*, 2015).

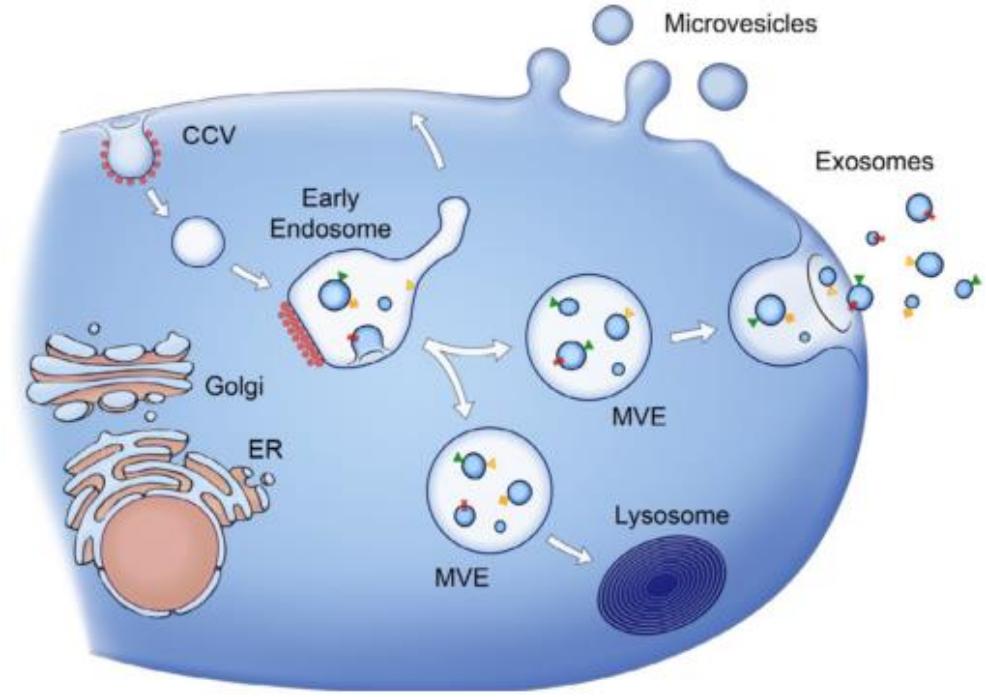

Figure 12: Extracellular vesicles produced by healthy cells. Microvesicles are produced by plasma membrane sprouting whereas exosomes are produced by the recycling endosomal machinery of the cell that starts with the formation of endocytic vesicles (i.e. clathrin coated vesicles, CCV). Then, early endosomes will produce new intraluminal vesicles (i.e. they are now called multivesicular endosomes, MVE) and enter either the degradation or secretion pathway being target to the lysosomes or the plasma membrane respectively (Raposo and Stoorvogel, 2013).

It is important to note that small microvesicles and exosomes bear the same biophysical characteristics (van Niel *et al.*, 2018). Moreover, despite intensive work to improve isolation methods, it is currently very complicated to obtain pure population of a single type of vesicle (Kowal *et al.*, 2016; Willms *et al.*, 2016).

5.3.3 Biogenesis and release of extracellular vesicles

As previously mentioned, biogenesis of microvesicles and exosomes is different but both processes involve membrane reorganization events. Microvesicles arise from an outward budding of the plasma membrane, whereas exosomes are produced as ILVs by inward budding within MVEs and are later released upon fusion of MVEs with the plasma membrane. Although the production of microvesicles and exosomes do not occur at the same location, there are similarities in the sorting machineries and the cellular mechanisms involved in both processes (Colombo *et al.*, 2014; Kowal *et al.*, 2014). The first step of EVs biogenesis is the accumulation of a specific cargo at the cytosolic face of the plasma membrane (microvesicles) or recycling endosomes (exosomes). Then, those cargoes are enriched in the developing vesicle by clustering mechanisms followed by budding and fission of the membrane, which result in the release of the vesicle, either directly outside the cell or inside the MVE, prior secondary extracellular release. Thus, EV biogenesis resembles the budding of viruses at the plasma membrane (e.g. influenza) or multivesicular bodies (e.g. HIV-1).

5.3.3.1 Targeting of cargoes to extracellular vesicles

Cargoes are the first regulators of EVs formation. Their abundance and nature vary between cell types and depend on the physiological or pathological state of the producing cells (Kalra *et al.*, 2016). ILVs' cargo can come either from the Golgi apparatus or from the maturation of endosomes after internalization of molecule at the plasma membrane (**Fig. 13**, upper left) (Klumperman and Raposo, 2014). The mechanisms of preferential loading of cargoes (i.e. proteins or RNA) to forming ILVs could result from specific interaction with proteins and lipids. For example, it was reported that ESCRT (e.g. ESCRT-0 and ESCRT-I) components can cluster ubiquitylated proteins that will be loaded into the forming ILVs (Colombo *et al.*, 2013). Tetraspanins are involved in transmembrane protein clustering and

loading into ILVs (van Niel *et al.*, 2011), and ceramide are involved in the loading of phospho-lipoproteins into ILVs (Trajkovic *et al.*, 2008). It was also proposed that lipid raft could be involved in protein loading into ILVs (de Gassart *et al.*, 2003). Finally, it was reported that ESCRT-II is involved in bicoid mRNA loading into ILVs (Irion and St Johnston, 2007), and that the heterogeneous nuclear ribonucleoprotein A2B1, once sumoylated, is able to bind specific exosomal miRNA motifs and helps their loading into ILVs (Villarroya-Beltri *et al.*, 2013).

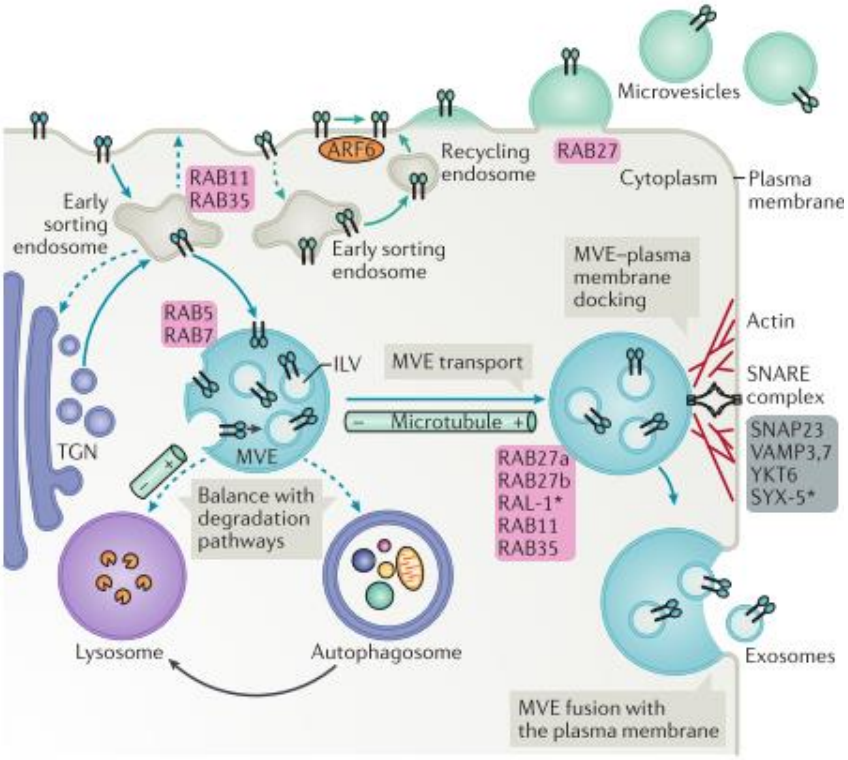

Figure 13: Sorting of cargoes and release of extracellular vesicles. Upper left: Sorting of cargoes from the Golgi apparatus or the plasma membrane to early endosomes and loading into forming ILVs. Microvesicles' cargoes come from recycling endosomes. At right: Transport of a MVE to the plasma membrane on the microtubule network, docking and fusion with the plasma membrane. Small GTPases (pink) are involved in endosome trafficking and docking with the plasma membrane. SNARE-associated proteins (grey) are involved in the fusion process. (van Niel *et al.*, 2018)

Targeting of cargoes to the plasma membrane for sorting into microvesicles is also regulated by endosomal recycling and endocytosis (Muralidharan-Chari *et al.*, 2009). Although similar ways are used by microvesicles and exosomes (**Fig 13**, upper left), it seems that targeting of cargoes to a particular type of vesicles is relatively specific since cargoes preferentially sent to the plasma membrane are not likely to be found in exosomes (van Niel *et al.*, 2018).

5.3.3.2 Mechanisms of exosome biogenesis

The first breakthrough in understanding the mechanisms of ILVs and MVEs formation was the discovery of the endosomal-sorting complex required for transport (ESCRT) machinery. It is composed of four elements acting sequentially during the process. First, ESCRT-0 and ESCRT-I cluster ubiquitylated cargoes at the membrane of the MVEs (**Fig. 14**), and then recruit ESCRT-III via ESCRT-II (not illustrated in fig. 13). The ESCRT-III subunit performs the budding and fission of the membrane (**Fig. 14**). Depletion of ESCRT components has revealed the existence of ESCRT-independent pathways. The ESCRT-independent pathway requires interacting proteins such as syntenin, a PDZ adaptator, and ALIX, known as linker between cargoes and VPS32, a subunit of ESCRT-III (**Fig. 14**) (Baietti *et al.*, 2012; Colombo *et al.*, 2013).

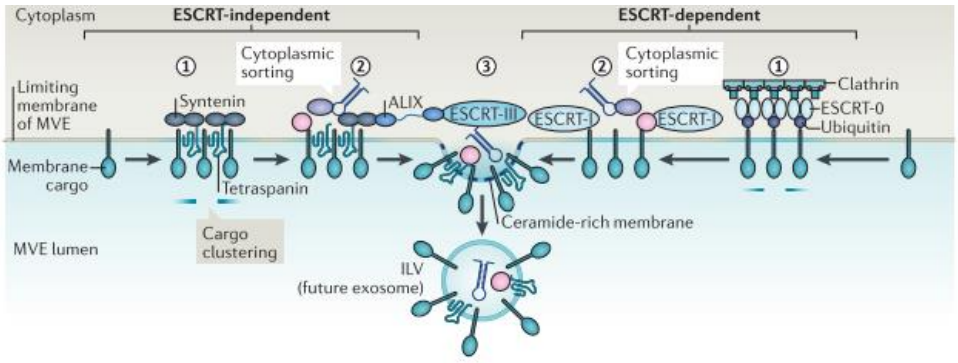

Figure 14: Mechanisms of intraluminal vesicle biogenesis. ESCRT-dependent and ESCRT-independent mechanisms require: 1) Clustering of lipids and membrane-associated proteins; 2) recruitment of cytosolic proteins and RNA; 3) budding and fission of the endosomal membrane. Adapted from (van Niel *et al.*, 2018)

Another ESCRT-independent, lipid-based mechanism, involves the local generation of ceramide by hydrolysis of sphingomyelin (Trajkovic *et al.*, 2008). Ceramide microdomains create spontaneous negative curve on the membrane. Moreover, ESCRT-independent endosomal sorting can be regulated by members of the tetraspanin family (**Fig 14**). Tetraspanins are small glycosylated membrane proteins composed of four transmembrane domains, two extracellular loops and three short intracellular loops that can be post-translationnally modified by addition of palmitate moieties. Tetraspanins cluster with one another (i.e. forming tetraspanin-enriched microdomains) and can interact with a large variety of other transmembrane proteins, such as integrins, as well as with growth factor and cytokine receptors. Therefore, tetraspanins were proposed to have a role in cell and membrane compartmentalization (Charrin *et al.*, 2014). The tetrasapanin CD63, which is particularly enriched in exosomes, but also CD81 and CD9 have been shown to regulate endosomal sorting and various cargo targeting in exosomes. Tetraspanins are indeed prone to cluster with one another, with other transmembrane proteins and with cytosolic proteins (Andreu and Yanez-Mo, 2014; MacDonald *et al.*, 2015; van Niel *et al.*, 2011). The generated membrane microdomains will bud, probably because of the cone-like structure recently demonstrated for CD81, and undoubtedly shared by the other members of the familly (Zimmerman *et al.*, 2016).

5.3.3.3 Mechanisms of microvesicle biogenesis

Beside the shared ceramide microdomains and the ESCRT-dependent mechanisms of cargo clustering and membrane fission (**Fig. 15**), microvesicle biogenesis requires several changes in the plasma membrane, including a rearrangement in lipid composition driven by a Ca^{2+}-dependent enzymatic machinery (Minciacchi *et al.*, 2015). The exposition of phosphatidylserine in the outer leaflet will cause bending of the plasma membrane and restructuration of the underlying actin cytoskeleton, resulting in membrane budding and microvesicle formation (**Fig. 15**). Another important lipid involved in this process might be cholesterol since its depletion in activated neutrophils impairs microvesicle formation (Del Conde *et al.*, 2005). Cytoskeletal components and regulators such

as RHO family of small GTPases (RhoA) and their associated protein kinase (ROCK) are associated with microvesicle biogenesis in tumor cells (Li *et al.*, 2012).

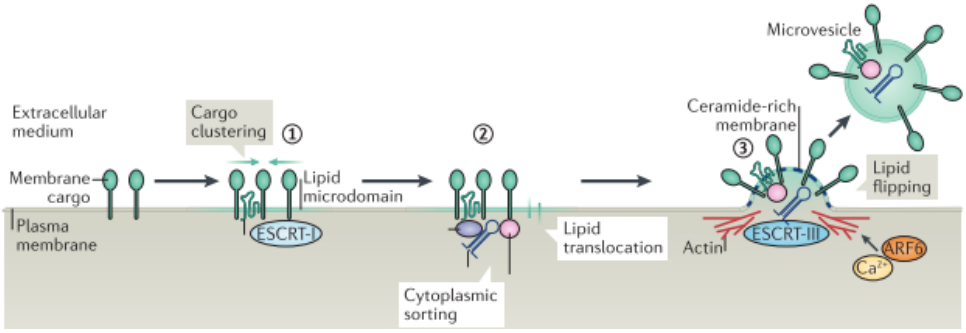

Figure 15: Mechanisms of microvesicle biogenesis. 1) Clustering of lipids and membrane-associated proteins; 2) recruitment of cytosolic proteins and RNA; 3) budding and fission of the plasma membrane. Adapted from (van Niel *et al.*, 2018)

5.3.3.4 Release of extracellular vesicles

The release of microvesicles is likely to occur straight after packaging of the cargo, through membrane fission (**Fig 13** pg. 40). On the contrary, the release of exosomes require two additional steps : MVEs targeting to, and fusion with, the plasma membrane (**Fig. 13** pg. 40) (van Niel *et al.*, 2018).

The mechanism involved in microvesicles release is ATP-dependent and requires an interaction between actin and myosin (McConnell *et al.*, 2009). In cancer cells, the ARF6/ARF1 (small GTP-binding proteins)-dependent phosphorylation of myosin, via phospholipase D, ERK and MLCK, results in acto-myosin contraction and release of microvesicles (**Fig. 15**) (Muralidharan-Chari *et al.*, 2009). The release of microvesicles is very likely to involve extracellular sensing, and thus intercellular communication, since serum deprivation, and therefore changes in the interaction between growth factors and their receptors, decrease the release of microvesicles (Taverna *et al.*, 2003).

Exosomes' release first requires the transport of MVEs to the plasma membrane. Intracellular transport of organelles involves interactions of MVEs with the microtubule cytoskeleton and its associated motors kinesin (anterograde

transport) and dynein (retrograde transport) (**Fig. 13** pg. 40) (Bonifacino and Glick, 2004). In contrast to the transport of MVEs to lysosomes and autophagosomes for degradation, the transport of MVEs to the plasma membrane is an anterograde transport along microtubules (from the minus end to the plus end). Rab-GTPase 27B regulates the motility of the MVEs along microtubules while Rab27A is involved in the docking of the MVEs with the plasma membrane (**Fig. 13** pg. 40) (Ostrowski *et al.*, 2010). As Rab27 isoforms are not expressed in all cell types, this implies that each cell type must have its own secretory machinery. The fusion of the MVEs with the plasma membrane is probably mediated by SNARE proteins such as the synaptosomal-associated protein 23 (SNAP23) and syntaxins (SYX) (**Fig. 13** pg. 40) (Colombo *et al.*, 2014). Once again, this mechanisms can vary depending on the cell type and different mechanisms can be operational in the same cell (van Niel *et al.*, 2018).

5.3.4 Targeting extracellular vesicles to recipient cells

Once released in the extracellular milieu, EVs need to interact with target cell to deliver their message. Message delivery requires either docking of the EVs with a surface receptor, internalization of the EVs through endocytosis, or fusion with the plasma membrane (**Fig.16**). However, these complex processes are not well described yet. Nevertheless, it is likely that the mode of interaction with the target cell depends on the main message and downstream effect of the EVs (Mulcahy *et al.*, 2014). One can postulate that, if a transmembrane protein mediates the message carried by the EV, the EV will interact with the target cell through a receptor that will trigger an intracellular signal. On the other hand, if the message is inside the EV (i.e. RNA or cytosolic protein) the EV will either fuse with the target cell or interact with a receptor and then be endocytosed (**Fig. 16**). Cell specificity is probably determined by specific interactions between proteins expressed at the surface of the target cell and cluster of enriched proteins at the surface of the EVs. Those interactions could be mediated by tetraspanins, integrins, lipids, heparan sulfate or extracellular matrix components (**Fig. 16**) (Colombo *et al.*, 2014; van Niel *et al.*, 2018). It has been reported that integrins at the surface of tumor exosomes may guide EVs to specific organs (Hoshino *et al.*, 2015). For example, human breast cancer cell exosomes bearing integrins $\alpha 6\beta 4$ on their surface preferentially target the lung, which is known to be the main metastatic site

for breast cancer cells. Furthermore, the authors demonstrated that knock-down of integrin β4 in breast cancer cells (and consequently in exosomes produced by those cells) decreased exosome uptake and metastasis in the lung (Hoshino *et al.*, 2015).

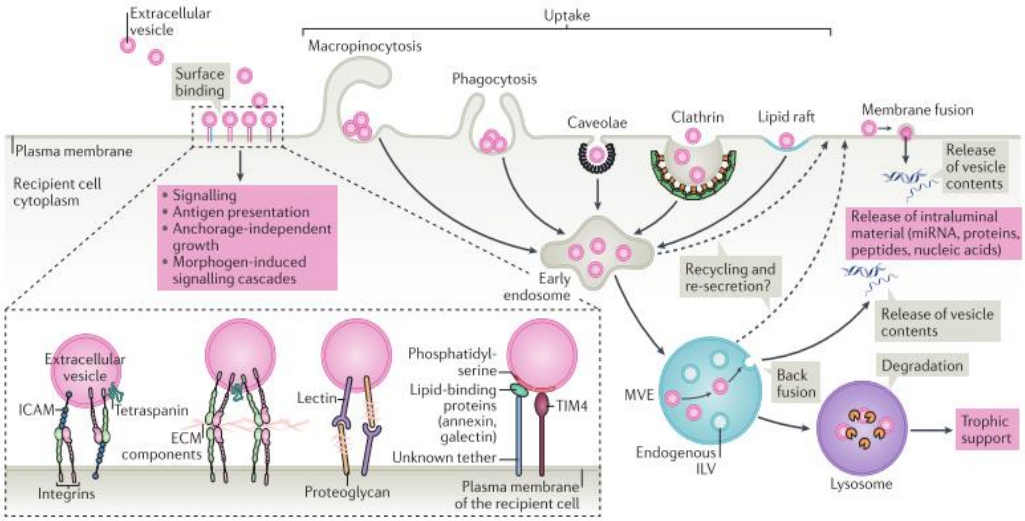

Figure 16: Cellular interaction, fate and message delivery of extracellular vesicles. At left: Ligands expressed in the membrane of EVs can interact with receptors expressed at the cell surface and trigger a cellular response. At right: EVs endocytosed by target cells can be both recycled and re-secreted, degraded or their cargo can be released in the cytoplasm upon fusion with MVE membrane. Lastly, fusion of EVs with the target cell results in a direct release of their cargo in the cytoplasm. Adapted from (van Niel *et al.*, 2018)

It is important to mention that, to reach cells within a tissue, a vesicle must travel through the extracellular matrix and cross the dense basal lamina. This might be a challenge in adult tissue with a thick basement membrane, like the thyroid or the kidneys. However it was reported that EVs bear matrix metalloproteases at their surface, and can thus degrade ECM proteins (Yue *et al.*, 2015). Also, it cannot be excluded that EVs use holes created in the basal lamina by invadopodia from infiltrating macrophages, as described in a pathological model of cystinotic kidney (Naphade *et al.*, 2015) or in cancer cells (Hoshino *et al.*, 2013).

5.3.5 Roles of extracellular vesicles

Since a decade, an increasing number of functions have been attributed to extracellular vesicles (Tkach and Thery, 2016), from antigen presentation and immunomodulation (Raposo *et al.*, 1996) to maintenance of tumor micro-environment (**Fig. 17**, left) (Antonyak *et al.*, 2011) or modulation of cellular metabolism. In addition, tumor exosomes were shown to prepare metastatic niches to facilitate the invasion of metastatic cells (**Fig. 17**, right) (Hoshino *et al.*, 2015). Roles of EVs in the regulation of lipids at the plasma membrane of the recipient cell have also been reported (Record *et al.*, 2014).

The role of EVs in embryogenesis is poorly studied. Nevertheless, correlations can be made between important embryological processes and roles attributed to EVs. The group of Susan Eaton proposed that EVs (argosomes) were involved in the establishment of morphogen (e.g. Wnt and shh) gradients in *Drosophila* (Greco *et al.*, 2001; Panakova *et al.*, 2005). This role was later attributed to exosomes when Gross *et al.* revealed the presence of Wnt proteins on their surface (Gross *et al.*, 2012). Furthermore, establishment of the above-mentioned shh gradient was attributed to an ESCRT-dependent mechanism in another study (Matusek *et al.*, 2014). Finally, it was suggested that EVs may contribute to the regulation of cellular polarity (Lakkaraju and Rodriguez-Boulan, 2008), although lots of questions remain in this field.

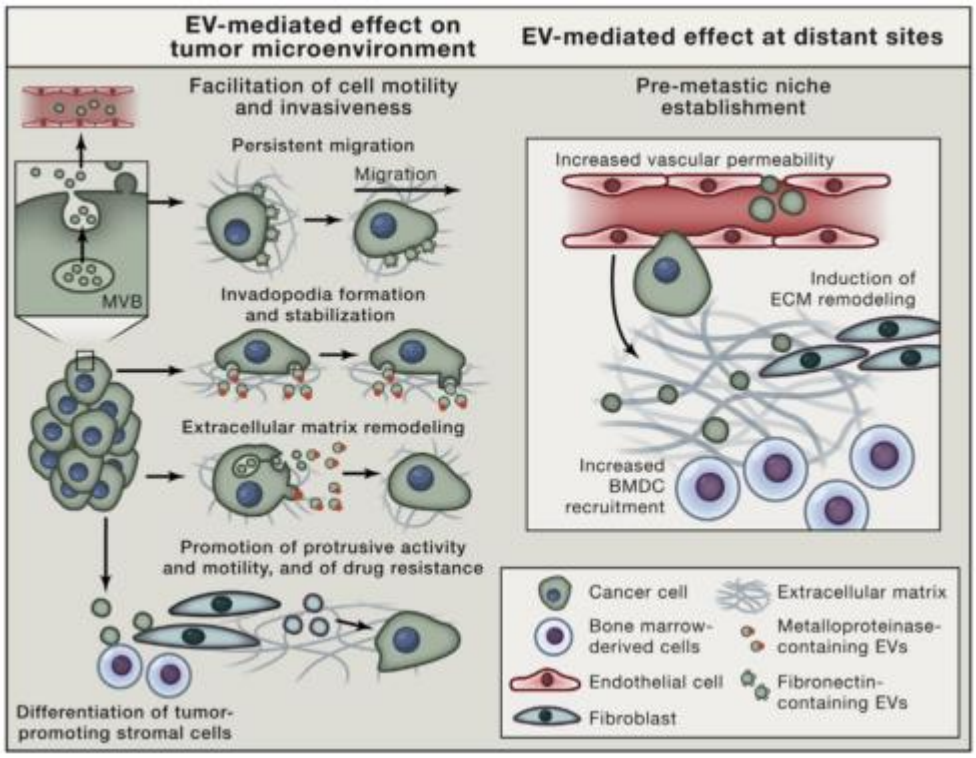

Figure 17: Cartoon summarizing of the effects mediated by tumor-derived extracellular vesicles. Representation of the various effects of tumor-derived extracellular vesicles on the tumor microenvironment (left side), facilitating cellular motility and invasion, and at distant sites (right side), by establishing pre-metastatic niches (Tkach and Thery, 2016).

To date, two studies report on the role of EVs in epithelial tissue, but not thyroid, organogenesis. Recently, mesenchyme-derived exosomes were reported to promote salivary gland progenitor expansion (Hayashi *et al.*, 2017). Using an original co-culture system of ceramide-fluorescent labelled-mesenchyme and salivary gland explants, the authors demonstrated that mesenchyme cells produce extracellular vesicles that target salivary gland epithelial cells. They further demonstrated that mesenchyme-derived exosomes were loaded with miR133b-3p, which decreases the expression of DIP2B, a protein implicated in DNA methylation, in salivary gland epithelial cells. The authors postulated that this process facilitates the expression of genes involved in epithelial cell proliferation (Hayashi *et al.*, 2017). In 2018, it was reported that exosomes, produced by primary embryonic

kidney ureteric bud cells, could act as secondary signal during kidney organogenesis (Krause *et al.*, 2018). However, the precise role of exosome in this process remains unclear since the authors reported an effect on the overall organization of the tissue but not on the organogenesis itself.

Several roles have been proposed for endothelial cell-derived EVs. Exosomes produced by human endothelial progenitor cells stimulate endothelial cells proliferation and migration, and promote the expression of pro-angiogenic molecules (Li *et al.*, 2016). These effects could be mediated by miR-214, as exosomes from miR-214-depleted endothelial cells do not promote angiogenesis and migration (van Balkom *et al.*, 2013). Furthermore, it was reported that EPC-derived exosomes could accelerate cutaneous wound healing by promoting angiogenesis through Erk signaling (Zhang *et al.*, 2016b). Endothelial cell-derived exosomes were also reported to be involved in extracellular matrix remodeling, via the presence of the collagen fibers cross-linking protein, lysyl oxidase-like 2, at the surface of exosomes (de Jong *et al.*, 2016). To date, no report on the role of endothelial-derived EVs in organogenesis have been published.

Finally, it is important to mention that more and more studies are presenting exosomes as non-invasive diagnostic tools, highlighting their potential as disease biomarkers (Fais *et al.*, 2016; Kourembanas, 2015; Lener *et al.*, 2015; Muralidharan-Chari *et al.*, 2010). In 2015, Lee et al. reported that exosomes produced by papillary thyroid cancer cells (TPC1) were enriched in miR-146b and miR-222 as compared with exosomes produced by normal thyroid follicular cells (NTHY) (Lee *et al.*, 2015). More recently, miR-31 was shown to be over-represented in exosomes from patients with papillary thyroid carcinoma (PTC) as compared with exosomes from patients with benign tumors. They also identified miR-21 to be over-expressed in exosomes from patients with follicular thyroid carcinoma (FTC) as compared with exosomes from patients with benign tumors. Lastly, they highlighted that miR-21 and miR-181a-5p were reciprocally expressed in exosomes from PTC and FTC patients. Altogether, their results could help distinguishing PTC from FTC in a non-invasive way (Samsonov *et al.*, 2016).

6 Aim of the work

Thyroid gland development and papillary thyroid cancer (PTC) are two opposite processes. During thyroid embryogenesis, a mass of proliferating thyroid progenitors reorganizes into a collection of spherical monolayers, composed of polarized differentiated cells, which synthesize thyroid hormones. Conversely, in papillary thyroid carcinogenesis, the functional and well-organized adult tissue reorganizes into a mass of proliferating and dedifferentiated cells. Our team wishes to understand how intercellular communications regulate thyroid ontology and oncology.

Since a decade, extracellular vesicles (EVs) are increasingly recognized as vehicles for intercellular communication, by transporting complex cargoes of proteins and nucleic acids between cells, protected by a lipid bilayer. Communication through EVs is predominantly studied in cancer cells where their role is intensively investigated, both as biomarker and pathogenic factor, but their relevance in developmental biology is still poorly understood. The goal of my thesis was to study intercellular communication via EVs in the thyroid, by comparing ontology and oncology. I mostly focused on their role during thyroid folliculogenesis and initiated a project on their implication in papillary thyroid carcinoma.

The host laboratory has demonstrated that thyroid folliculogenesis depends on the production of stimulating factor(s) by the follicular microenvironment, in particular by endothelial cells. The first and main objective of my thesis was to determine if EVs produced by endothelial cells play a role in controlling thyroid follicle formation. To test this hypothesis, I used EPCs-conditioned medium as EV source and resorted to an original *ex vivo* culture system of developing thyroid lobes to test the role(s) of EVs. A substantial amount of time was then spent on developing tools and methods to study of EVs in the lab. My results demonstrate that EPCs produce EVs that can stimulate folliculogenesis independently of co-sedimented proteins.

In the final year of my PhD, I extended my research to thyroid cancer by training and supervising an under-graduate student on the implication of EVs in thyroid cancer. The challenge here was to work *in vivo* using a mouse model of

thyroid cancer. The main objective was to isolate and characterize EVs from dissociated normal and cancerous tissue. Preliminary results are very interesting and open the door for a new PhD project aiming at elucidating the role of EVs in PTC establishment and highlighting their potential as biomarkers of PTC.

7 Results

7.1 Extracellular vesicles from endothelial progenitor cells promote thyroid follicle formation

Jonathan Degosserie, Charlotte Heymans, Catherine Spourquet, Mathias Halbout, Ludovic D'auria Patrick Van Der Smissen, Didier Vertommen, Pierre J. Courtoy, Donatienne Tyteca, Christophe E. Pierreux

The work presented in this manuscript is my main contribution. To achieve this, I had to learn and develop specific experimental procedures of EV research that were not mastered in the lab. I planned and performed the experiments and I wrote the manuscript.

This revised manuscript was resubmitted the Journal of Extracellular Vesicles.

Extracellular vesicles from endothelial progenitor cells promote thyroid follicle formation

Jonathan Degosserie[(1)], Charlotte Heymans[(1)], Catherine Spourquet[(1)], Mathias Halbout[(2)], Ludovic D'auria[(4)], Patrick Van Der Smissen[(1,3)], Didier Vertommen[(5)], Pierre J. Courtoy[(1)], Donatienne Tyteca[(1,3)], Christophe E. Pierreux[(1)]

(1) CELL Unit, de Duve Institute, Université Catholique de Louvain, Brussels, Belgium

(2) BCHM Unit, de Duve Institute, Université Catholique de Louvain, Brussels, Belgium

(3) PICT plateform, de Duve Institute, Université Catholique de Louvain, Brussels, Belgium

(4) Neurochemistry group, CEMO division, Institute of Neuroscience, Université Catholique de Louvain, Brussels, Belgium

(5) PHOS Unit, de Duve Institute, Université Catholique de Louvain, Brussels, Belgium

Corresponding author : Christophe E. Pierreux, de Duve Institute, avenue Hippocrate 75 B1.75.05 1200 Brussels, Belgium ; christophe.pierreux@uclouvain.be

Jonathan Degosserie : avenue Hippocrate 75 B1.75.05 1200 Brussels, Belgium ; 0032/2.764.7569 ; jonathan.degosserie@uclouvain.be

Charlotte Heymans : avenue Hippocrate 75 B1.75.05 1200 Brussels, Belgium ; 0032/2.764.7569 charlotte.f.heymans@uclouvain.be

Catherine Spourquet : avenue Hippocrate 75 B1.75.05 1200 Brussels, Belgium ; 0032/2.764.7569 ; catherine.spourquet@uclouvain.be

Mathias Halbout : avenue Hippocrate 75 B1.75.08 1200 Brussels, Belgium ; 0032/2.764.7539 ; mathias.halbout@uclouvain.be

Ludovic D'auria : avenue Mounier 53 B1.53.02 1200 Brussels, Belgium ; 0032/2.764.53.59 ; ludovic.dauria@uclouvain.be

Patrick Van Der Smissen : avenue Hippocrate 75 B1.75.05 1200 Brussels, Belgium ; 0032/2.764.7546 ; patrick.vandersmissen@uclouvain.be

Didier Vertommen : avenue Hippocrate 75 B1.75.02 1200 Brussels, Belgium ; 0032/2.764.7486 ; didier.vertommen@uclouvain.be

Pierre J. Courtoy : avenue Hippocrate 75 B1.75.05 1200 Brussels, Belgium ; pierre.courtoy@uclouvain.be

Donatienne Tyteca : avenue Hippocrate 75 B1.75.05 1200 Brussels, Belgium ; 0032/2.764.7591 ; donatienne.tyteca@uclouvain.be

Christophe Pierreux : cf. corresponding author ; 0032/2.764.6522

Extracellular vesicles from endothelial progenitor cells promote thyroid follicle formation

Organogenesis is a complex and dynamic process requiring reciprocal communication between different cell types. In the thyroid, thyrocyte progenitors secrete the angiocrine factor, VEGFA, to recruit endothelial cells. In return, endothelial cells promote thyrocyte organization into spherical follicular structures, which are responsible for thyroid hormone synthesis and storage. Medium conditioned by endothelial progenitor cells can promote follicle formation and lumen expansion (i.e. folliculogenesis) in an *ex vivo* culture system of thyroid lobes. Here, we postulated that endothelial cells instruct thyrocyte progenitors by producing extracellular vesicles. We found that medium conditioned by endothelial progenitor cells contain extracellular vesicles with exosomal characteristics and that these vesicles can be incorporated into thyrocyte progenitors. By mass spectrometry, laminin peptides were abundantly identified in the EV preparations, probably co-sedimenting with EVs. Laminin-α1 silencing in EPC abrogated the folliculogenic effect of EVs. However, density gradient separation of EVs from laminins revealed that both EV-rich and laminin-rich fractions exhibited folliculogenic activity. In conclusion, we suggest that endothelial cells can produce extracellular vesicles favouring thyrocyte organization into follicles and lumen expansion, a mechanism promoted by laminin-α1.

Keywords: thyroid; folliculogenesis; endothelial cells; extracellular vesicles; laminins

Introduction

The thyroid is an endocrine gland composed of three main cell types: thyrocytes, C cells and endothelial cells. Thyrocytes are polarized epithelial cells organized as monolayers into follicles enclosing packed iodothyroglobulin in the colloid, and responsible for the production of thyroglobulin-derived hormones, T3 and T4. C cells are epithelial cells, closely associated with follicles, which produce calcitonin. A dense network of endothelial cells surrounds each thyroid follicle. The close juxtaposition between follicles and blood capillaries is essential for bidirectional exchange supporting thyroid function. Iodide is captured from bloodstream into thyrocytes, and incorporated into thyroglobulin as T3 and T4 hormonogenic peptides. When T3 and T4 blood levels are low, thyrocytes capture iodothyroglobulin and release by proteolysis T3 and T4 hormones that are excreted into the blood flow. The functional couple between follicles and blood capillaries, often called the angio-follicular unit, forms during embryonic development [1,2].

During embryogenesis, thyrocyte progenitors derive from the endoderm upon expression of a combination of four transcription factors (Nkx2.1, Pax8, Foxe1 and Hhex), and first form a mass of non-polarized cells. The bud of thyrocyte progenitors migrates ventrally and then elongates laterally to form two lobes, on each side of the trachea, linked by the isthmus. By the end of gestation, thyroid progenitors differentiate and organize into a multitude of follicles associated with their blood capillaries [3]. We have demonstrated, by genetic inactivation of *Vegfa* in embryonic mouse thyroid, that endothelial cells are essential for the organization of thyrocyte progenitors in follicles [4]. Using an *ex vivo* culture system of thyroid lobes, we further showed that endothelial progenitor cells (EPCs) act on thyroid development independently of the blood flow, by secreting one or several instructive factors that promote the formation of spheroid structures delineated by a monolayer of differentiated thyrocytes and their luminal expansion (hereafter referred to as “folliculogenesis”). More recently, we reported that folliculogenesis is also controlled by BMP ligands. Indeed, thyroid-specific deletion of *Smad1* and *Smad5* display defective follicular organization and disrupted basement membrane assembly [5]. Furthermore, unpublished data from our group revealed that the folliculogenic activity could be retrieved not only from total medium conditioned by EPCs, but also from a crude sedimentation of this medium. Whether this

sedimentable activity corresponds to extracellular vesicles (EVs), and whether EVs could control thyroid follicle formation, is yet unknown.

EVs are small membrane-bound vesicles produced by almost every cell type and involved in intercellular communications [6]. EVs were first described in the early 80's as « garbage bags » used by maturing reticulocytes to dispose of transferrin receptor [7,8]. However, in the last decade, EVs have been shown to carry proteins and RNAs, and their potential as vehicles for intercellular communication was revealed [9,10]. EVs can be divided into three main populations: (i) large-size EVs include apoptotic bodies and oncosomes; (ii) microvesicles of medium size (~100-1000 nm) are produced by plasma membrane budding; and (iii) exosomes are small- size EVs (<150 nm) produced by the endosomal machinery [11,12]. Communication through EVs has been shown in a large variety of physiological and pathological processes [11,13]. Recently, exosomes isolated from developing submandibular glands have been shown to control expansion of epithelial progenitors during organogenesis [14]. Yet, the role of EVs in embryonic development is poorly known.

The goal of the present study was to examine whether endothelial cells can stimulate folliculogenesis via the release of EVs. We show that EPCs produce EVs with exosomal characteristics that stimulate folliculogenesis in thyroid lobes cultured *ex vivo*.

Materials and Methods

We have submitted all relevant data of our experiments to the EV-TRACK knowledgebase (EV-TRACK ID: EV170013) [15].

Animals

All mice were of CD1 strain. Mice were raised and treated according to the principles of laboratory animal care of the University Animal Welfare Committee. Females were mated and the day of the vaginal plug was considered as embryonic (E) day 0.5. At the indicated day of gestation, mice were sacrificed by cervical dislocation.

Dissection and culture of thyroid lobes

Thyroid lobes micro-dissected from E14.5 mouse embryos were cultured as described for 3 days [16]. Briefly, lobes were placed on microporous filters (Millipore) at the air:medium interface in M199 medium (Gibco) supplemented with 10% foetal bovine serum (FBS, Sigma), 100 U/mL penicillin, 100 µg/mL streptomycin, 0.25 µg/mL fungizone and 2 mM L-glutamine, supplemented by ~6 108 EVs (corresponding to 1.3 µg protein) for 104 cells or not (control condition). Supernatant from ultracentrifuged medium (EV-low EPC-CM) was concentrated 10-fold on Amicon Ultra-4, with a 50kDa nominal cut-off (as in [4]), before incubation with the thyroid lobes. To ensure optimal contact with explants, 10 µL from the culture medium (control, EPC-EVs, sh-EVs, GipZ-EVs, EV-rich, Laminin-rich or EV-low medium) was added on top of the filter, 3 times per day.

Immunolabeling on sections

Cultured thyroid explants were fixed in 4% formaldehyde for 1 hour and embedded in gelatin. Immunofluorescence was performed on 7-µm sections as described [17] using anti E-cadherin (1:1000, BD Bioscience) and anti-ezrin (1:200, Thermo Fisher Scientific) primary antibodies, followed by secondary antibodies coupled to Alexa-488 or Alexa-568 (Thermo Fisher Scientific). Alternatively, fixed explants were immunolabelled as whole mount [4]. Fluorescence was observed with a Zeiss Cell Observer Spinning Disk microscope (objective 40x, oil immersion).

Quantification of ezrin$^+$ follicles was performed at least on 5 sections spanning each lobe using a Zeiss Observer Z1 inverted fluorescence microscope. Open follicles were counted manually when lumen was > 10 µm. Values were normalized to untreated explants, considered as unity. Per condition, a minimum of 6 lobes, from 3 independent experiments, was used for quantifications.

Cell Culture

Embryonic endothelial progenitor cells (EPC) [18] were cultured on gelatin-coated dishes in DMEM (Westburg) supplemented with 20% FBS (Sigma), 100 U/mL penicillin, 100 µg/mL streptomycin and 100 µM non-essential amino acids. Cells were trypsinized using Tryple Express (Invitrogen). Conditioned medium (CM) was

prepared by incubating 80% confluent EPC in M199 without serum for 24 hours (7 mL / 78 cm² dish). Transduction of cells was performed with pGIPZ lentiviral vectors as described and validated in Villacorte *et al*. [5].

For primary cultures, E14.5 thyroid lobes were micro-dissected and washed in DPBS (Gibco) containing 0.2 mM EDTA. Thyroid lobes were gently dissociated in Accutase® (ThermoFisher Scientific) for 30 min at 37°C and the enzymatic reaction was stopped by adding M199 containing 10% FBS. Dissociated cells were counted and seeded in Ibidi® chambers suited for microscopy (Ibidi) at 50,000 cells per well (100 mm^2) in M199 containing 10% FBS. After overnight incubation at 37°C, dead or non-attached cells were discarded by medium replacement and culture was continued for an additional 3 hours before analysis.

EV isolation

EPC-CM was collected after 24 hours and submitted to differential ultracentrifugation: 1,000*g* for 10 min (GR 4.11, Jouan), 20,000*g* for 15 min (referred to as 20k pellet) in a Ti50 rotor (Beckman), and 150,000*g* for 90 min (first 150k pellet) in a Ti80 rotor (Beckman). The first 150k pellet was washed once by suspension in PBS and resedimentation at 150,000*g* for 90 min. This material is hereafter referred to as "150k pellet" and was finally collected in PBS or in appropriate medium, depending on further application.

Density gradient

Alternatively, the 150k pellets were further purified by floatation in iodixanol gradient as described [19]. Briefly, 1.3 mL of sample was mixed with 1.3 mL of 60% iodixanol stock solution (Axis-Shield) to obtain a 30% iodixanol layer, placed at the bottom of the tube. Then, 1.2 mL of 20% and 1.2 ml of 10% iodixanol, diluted from the stock solution, were sequentially added on the top of the 30% layer to obtain 3 layers in the gradient with a final volume of 5 mL. Gradients were centrifuged at 100,000*g* for 16 hours in a swinging bucket rotor (SW55 rotor, Beckman), and 8 fractions (denoted F1 to F8 from top to bottom) of 625 µL were collected by aspiration from top, diluted in PBS pelleted again at 150,000*g* for 90 min in a Ti80 rotor as above, and suspended in the appropriate medium. To test biological activity, we used 2/3 of EV-rich (F1-4) as buoyant fraction, 2/3 of laminin-rich (F5-

8) as dense fraction or 1/3 of F1-4 mixed with 1/3 of F5-8 as reconstituted 150k pellet. Density of each fraction was calculated, using an equilibrating gradient, as mass/volume (g/cm^3) by reference to water (1g/cm^3).

Nanoparticle Tracking analysis

Extracellular vesicles were counted in samples before and after separation by floatation in iodixanol gradient by the Zetaview (Particle Metrix, GmbH), which captures Brownian motion through a laser scattering microscope combined with a video camera to obtain size distribution (50-1000nm) and concentration. Dulbecco's phosphate buffer saline (DBPS without calcium and magnesium, ThermoFisher) pre-filtered on 100-nm nylon membrane or M199 medium (Gibco) was used to dilute samples. Samples were diluted 1:10-1:500 to reach 50-200 particle/frame corresponding to ~2 10^7-1 10^8 particles/ml. Sensitivity was set to 72.2 and camera shutter to 70 in order to detect less than 3 particles/frame as background when DBPS alone was injected. Measurements were performed with medium resolution for two cycles at 11 different positions (or frames) of the cell chamber containing the sample; measurements were reproduced 2-3 times. The Zetaview software was used to generate results in text files. Graphs for particle size and distribution were designed with Prism (GraphPad software).

EV fluorescent labelling

To label EPC-EVs, the suspended 150k pellet was incubated with the membrane dye PKH67 (Sigma) according to manufacturer's instructions. Free dye was then eliminated by the density gradient. The four first fractions, containing labelled EVs, were pooled, washed in PBS and collected by ultracentrifugation at 150,000*g* for 90 min.

EVs incorporation and immunofluorescence on cells

The equivalent of 10 µg protein of PKH67-stained EVs was incubated with a primary culture of embryonic thyroid cells. After 3 hours, cells were rinsed extensively with PBS to remove remaining particles, fixed with 4% formaldehyde pH 7.4 for 15 min, and then washed again extensively. Cells were further permeabilized with 0.05%

saponin pH 7.4 for 15 min and incubated for 30 min in blocking solution (1% BSA; 0.1% lysine; 0.01% saponin in PBS). Permeabilized cells were then incubated with anti-CD63 (1:150, Biolegend) primary antibody, diluted in blocking solution for 1 hour, washed with blocking solution, incubated with secondary antibody coupled with Alexa-568 (1:1.000, Invitrogen) together with Hoechst 33258 as nuclear dye (1:1.000, Sigma) in blocking solution for 1 hour. After final wash in blocking solution, cells were rinsed 3 times with PBS, post-fixed in 4% formaldehyde for 5 min and mounted in aqueous mounting medium (Dako). Preparations were observed with a Zeiss Cell Observer Spinning Disk microscope (objective 100x, oil immersion).

Western blotting

For western blotting, 150k pellets were lysed in RIPA buffer (150 mM NaCl; 1% Triton X-100; 0.5% sodium deoxycholate; 0.1% SDS; 50 mM Tris pH 8.0; 1X protease inhibitor cocktail (Roche)). Protein concentration was measured using bicinchoninic acid. Loads normalized to 4 mg protein were resolved on 10% homemade polyacrylamide gels or 4-15% pre-casted polyacrylamide gels (Biorad), then transferred onto PVDF membrane and processed as described [20]. Following primary antibodies were used: anti-calnexin (1:10.000, ADI-SPA-860D Enzo Life Science), anti-CD63 (1:300, 143902 Biolegend; in non-reducing environment), anti-CD9 (1:300, EPR2949 Abcam), anti-flotilin-1 (1:200, 610821 BD Transduction) and anti-laminin-α1 (1:1000, kind gift from T. Sasaki). Immuno-reactive bands were detected using chemiluminescence (Super Signal Chemiluminescent Substrate; Thermo Scientific) and images were acquired using Fusion Solo S (Vilber Lourmat).

Scanning electron microscopy

150k pellets were allowed to adhere onto poly-L-lysine-coated coverslips then fixed in 1% glutaraldehyde, washed and post-fixed with 1% OsO_4. Samples were dehydrated in ethanol, critical point-dried and coated with a 10-nm gold film. Specimens were observed with CM12 electron microscope (Philips, Netherlands) at 80 kV with the use of a secondary electron detector, as described [21].

Mass spectrometry

150k pellets were suspended in 50 µL of 50 mM NH_4HCO_3 pH 8.0, reduced and alkylated, and incubated overnight at 37°C with trypsin and 0.2% Rapigest® for enzymatic digestion. Detergent was hydrolysed with HCl and sedimented by centrifugation. Peptides were collected from the supernatant and analysed by liquid chromatographic tandem mass spectrometry (LC-MS/MS). The LC-MS/MS system consisted of an LTQ XL IonTrap mass spectrometer (ThermoScientific, San José, CA) equipped with a microflow ESI source and interfaced to an LCPackings Ultimate Plus Dual gradient pump, Switchos column switching device, and Famos Autosampler (Dionex, Amsterdam, Netherlands). Two RP peptide traps C18 Pepmap 100 Dionex (0.30 mm x 5 mm) were used in parallel with two analytical BioBasic-C18 columns from ThermoScientific (0.18 mm x 150 mm). Samples (6.5 µl) were injected and desalted on the peptide trap equilibrated with solvent A (3.5% ACN v/v, 0.1% TFA in water) at a flow rate of 30 µl/min. After valve switching, peptides were eluted in backflush mode from the trap onto the analytical column equilibrated in solvent B (5% ACN v/v, 0.05% v/v formic acid in water) and separated using a 100-min gradient from 0 to 70% solvent C (80% ACN v/v, 0.05% formic acid in water) at a flow rate of 1.5 µl/min. Peak lists were generated and searched using the bioinformatic software Proteome Discoverer 1.4.1 (Thermofischer scientific). In details, peak lists were generated using extract-msn (ThermofischerScientific) within Proteome Discoverer 1.4.1. From raw files, MS/MS spectra were exported with the following settings: peptide mass range 350–5000 Da, minimal total ion intensity 500. The resulting peak lists were searched using SequestHT against a target-decoy mouse or human protein database obtained from Uniprot. The following parameters were used: trypsin was selected with proteolytic cleavage only after arginine and lysine, number of internal cleavage sites was set to 1, mass tolerance for precursors and fragment ions was 1.0 Da, considered dynamic modifications were + 15.99 Da for oxidized methionine and +57.00 for carbamidomethyl cysteine. Peptide matches were filtered using the q-value and Posterior Error Probability calculated by the Percolator algorithm ensuring an estimated false positive rate below 5%. The filtered Sequest HT output files for each peptide were grouped according to the protein from which they were derived and their individual number of peptide spectral matches was taken as an indicator of protein abundance. Finally, identified proteins were manually validated.

Statistical analysis

Statistical analyses were performed with Prism software (GraphPad) using Kruskal-Wallis test with Dunn post-test for ezrin$^+$ follicles quantification. Student's t-test was performed for western blot quantification. Data are presented as means ±SD.

Results

Endothelial progenitor cells produce extracellular vesicles with exosomal characteristics

We have previously shown that endothelial cells are essential to promote thyroid folliculogenesis, and that medium conditioned (CM) by endothelial progenitor cells (EPC) can promote folliculogenesis in thyroid explants [4]. Furthermore, crude high-speed ultracentrifugation of the CM revealed that the sedimentable material was endowed with folliculogenic activity. Here, we first tested whether this activity could be ascribed to EV generated by EPCs. To this aim, medium conditioned by EPC was submitted to differential ultracentrifugation [22,23]. We focused on the 150k pellet, which was analysed with a nanotracking device and by scanning electron microscopy. For size distribution in the hydrated state, the 150k pellet was analysed using a particle analyser, which defined a main population with a mean size around 100 and 150 nm and quantified the amount of vesicles (Fig. 1A). In this range of size, approximately 3.6 10^8 particles were obtained per 10^6 producing cells. The electron microscope revealed round monomorphous objects of 100 nm as approximate size in the dried state, consistent with vesicles (Fig. 1B). Western blotting characterization of the 150k pellet in comparison with total lysate from the parental EPC cell line showed enrichment in CD63, flotilin-1 and CD9, three well-known EV markers (Fig. 1C). Conversely, calnexin, a protein of the endoplasmic reticulum, was not detected in the 150k pellet, arguing against significant contamination by intracellular membrane compartments. These biochemical data were confirmed by mass spectrometry analysis (see below, green lines in Table 1). Finally, equilibration of the 150k pellet on iodixanol density gradient revealed that CD63$^+$ vesicles floated at a low buoyant density between 1.11 and 1.13 (Fig. 1D). Altogether, these data indicated that EPC produce EVs with exosomal characteristics, as proposed by the International Society for Extracellular Vesicles [24].

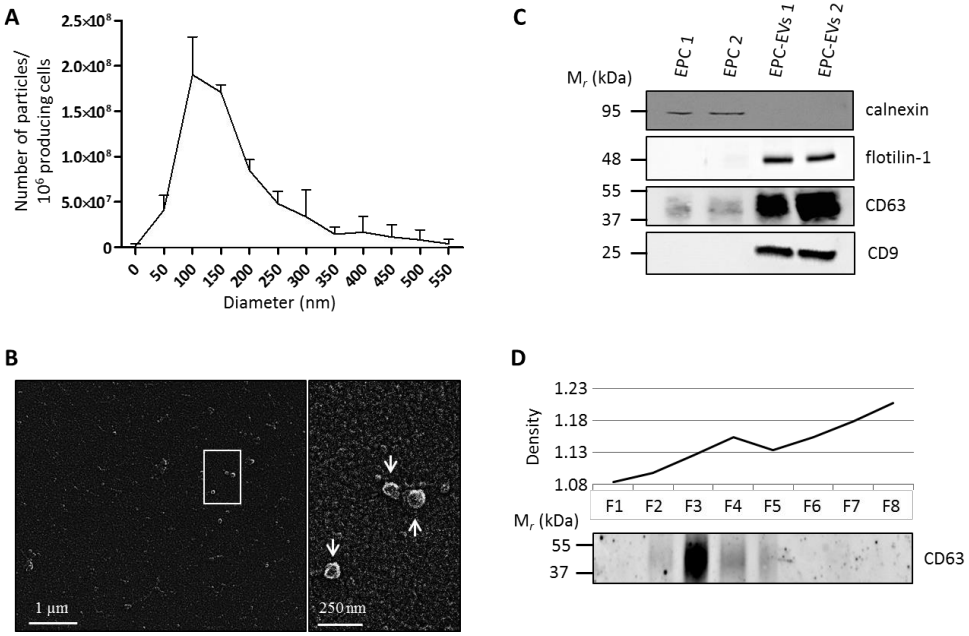

Figure 1: EVs isolated from EPC-CM display exosomal properties. **A** Quantification and size distribution of EVs obtained by Nanoparticle Tracking analysis using a Zetaview (Particle Metrix). Results are presented as the number of particles per 10^6 producing cells. **B** Representative scanning electron microscopy image of the 150k pellet obtained from EPC-CM. Enlarged view of the boxed area is shown at the right panel. EVs are indicated by arrows. **C** Western blot analysis of calnexin (ER marker) and flotilin-1, CD63 and CD9 (EVs markers) in two EPCs and two EPC-EVs lysates. **D** Western blot analysis of CD63 on 8 fractions (F1 – F8) resolved by floatation in iodixanol density gradient. Density of the 8 fractions is shown in the upper graph.

Embryonic thyroid epithelial cells incorporate EPC-EVs

We next examined whether these EVs could be incorporated by thyrocyte progenitors. To this aim, EPC-EVs were labelled with PKH67, a fluorescent lipid dye allowing imaging of EVs, then incubated with microdissected E14.5 thyroid lobes cultured on filters [16]. Despite numerous attempts (varying concentration and incubation time), we were unable to visualize fluorescent EVs in this 3D culture system of thyroid lobes due to tissue autofluorescence (see discussion). We thus simplified the culture system, by working in 2D on adherent thyroid cells. E14.5 thyroid lobes were dissociated and the cell suspension was cultured on Ibidi® µ-slides coated with type IV collagen, to improve adhesion of thyrocyte progenitors. After overnight culture, most cultured cells showed weak, but non-questionable immunoreactivity for the thyroid specific marker Nkx2.1 and for epithelial cadherin (E-cadherin; data not shown), demonstrating their thyrocyte origin but suggesting dedifferentiation [25]. All cells showed punctiform labelling for CD63, most probably corresponding to endosomes or multivesicular bodies (Fig. 2A left panel). Upon addition of EPC-EVs stained with PKH67 to the culture, exclusive colocalization of PHK67 signal with some CD63 dots indicated that PKH67-labeled vesicles were taken up into multivesicular bodies of embryonic thyroid cells (Fig. 2A right panel), confirming biochemical characterization of 150k pellet (Fig. 1C). Of note, these structures displayed a similar subcellular localization and size as endogenous $CD63^{+}/PKH67^{-}$ structures (Fig. 2A). We concluded that E14.5 thyrocyte progenitors could incorporate EVs produced by EPCs.

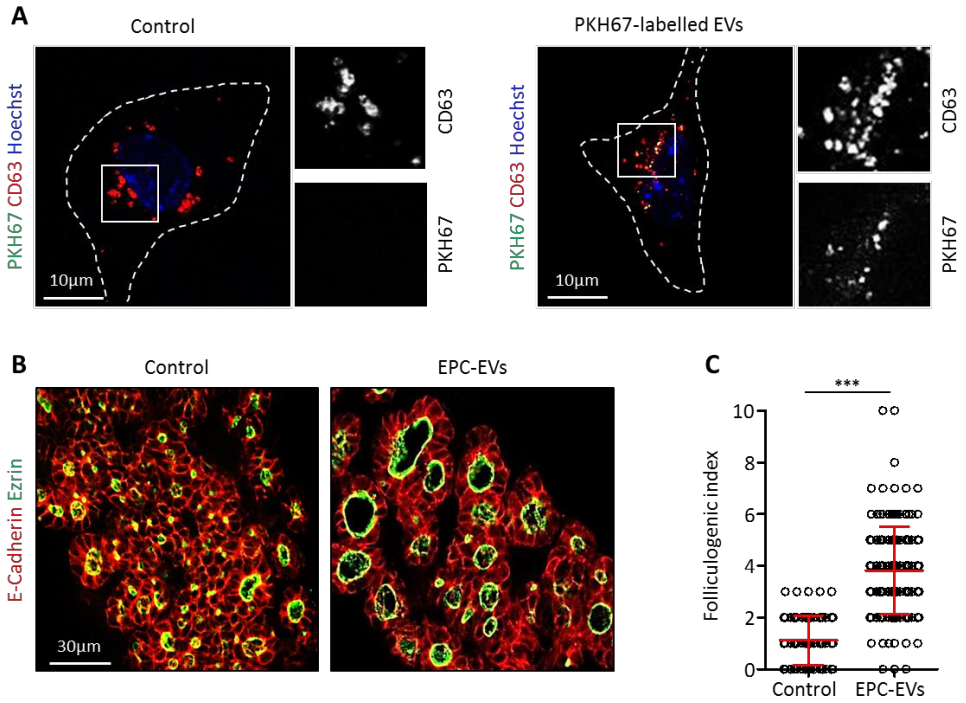

Figure 2: EPC-EVs are taken up by embryonic thyroid progenitors and stimulate folliculogenesis. **A** Immunofluorescence for CD63 (red) of cultured embryonic thyroid progenitors without (left panel) or after incubation with PKH67-labeled EVs (green; right panel). Cell contours are delineated by dotted lines. Notice clustering around cell. High magnifications of the boxed areas at left are shown at right in single channels for CD63 and PKH signals. **B** Immunofluorescence on sections of thyroid explants cultured without (control) or with EPC-EVs for E-cadherin (red) to define epithelial cells and ezrin (green) to identify their apical pole, thus lumen contour. **C** Folliculogenic index in control- and EPC-EVs-treated explants determined by quantification of ezrin+ open follicles (***, $p < 0.001$; n=5).

EPC-EVs stimulate folliculogenesis

To then test whether EPC-EVs were biologically active and able to stimulate folliculogenesis, we returned to microdissected E14.5 thyroid lobes. Such explants were cultured on semi-permeable filters at the air:liquid interface [16] with or without EPC-EVs. As consistent increase in follicular lumen opening, i.e. folliculogenic activity, was previously revealed with 10X concentrated EPC-CM [4,5], preliminary experiments were conducted with 10X concentrated EPC-EVs. At this concentration, only a weak folliculogenic effect was detected after 3 days, consistent with loss of EVs during the purification procedure. However, using an additional 2-fold concentration (i.e. 20X EPC-EVs), folliculogenesis was reproducibly induced (Fig. 2B). We therefore performed all subsequent analyses with this 20X EPC-EVs concentration. Quantification revealed that EPC-EVs were able to stimulate folliculogenesis by 3 to 4-fold (Fig. 2C).

To confirm that EVs were the bioactive factor in EPC-CM, we performed the reverse experiment and depleted EVs from the EPC-CM by ultracentrifugation of the EPC-CM (90 min, 150,000*g*). Although ultracentrifugation did not change protein abundance in the supernatant as compared to total EPC-CM (Fig. 3A, silver staining), this lead to partial depletion of EVs, as visualized by decreased CD63 intensity (Fig. 3A, western blot). Ultracentrifuged medium was thus called EV-low EPC-CM. Conversely, despite the absence of stained proteins (silver staining), abundant CD63 signal was found in the pellet (EPC-EVs). Furthermore, particle analysis revealed that ultracentrifuged EPC-CM contained only 20% of the particles present in the starting EPC-CM, while the EPC-EVs contained at least 40% (Fig. 3B). Finally, we tested the biological activity of the EV-low EPC-CM, at the same concentration (10X) as total EPC-CM. In line with our hypothesis, this EV-low EPC-CM had no folliculogenic activity (Fig. 3C and D). We concluded that EVs produced by EPCs are able to promote robust expansion of the follicular lumen.

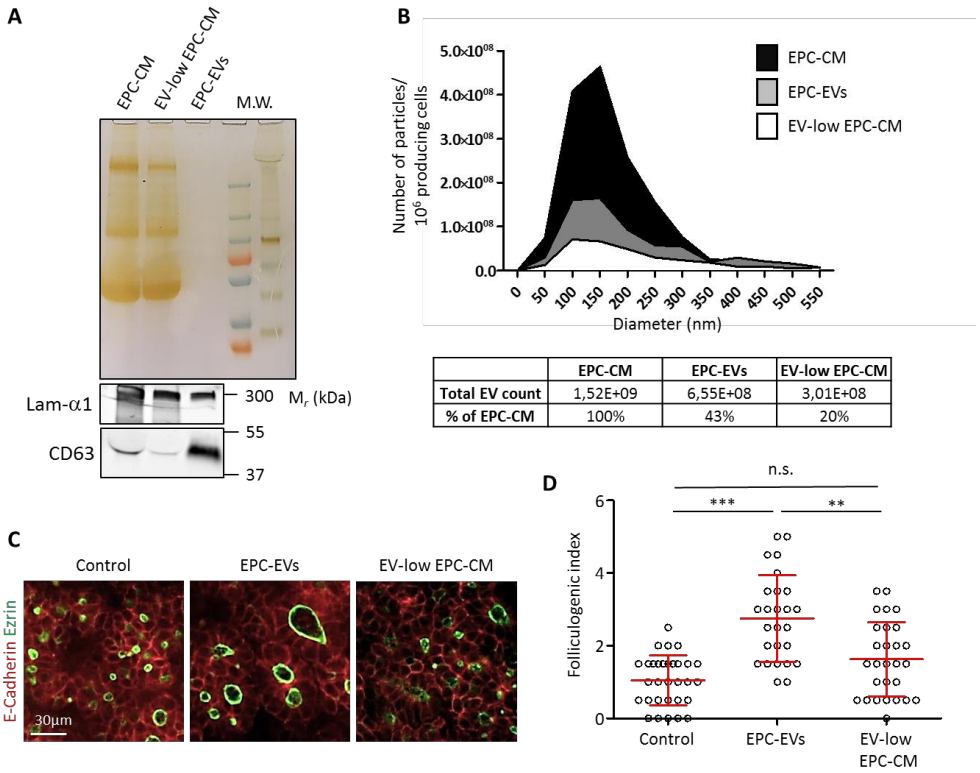

	EPC-CM	EPC-EVs	EV-low EPC-CM
Total EV count	1,52E+09	6,55E+08	3,01E+08
% of EPC-CM	100%	43%	20%

Figure 3: Depletion of EVs in the EPC-CM abrogates folliculogenic activity. **A** Silver staining and western blot analysis using CD63 and laminin-α1 antibodies on equal volume of 10X EPC-CM, 10X EV-low EPC-CM and 20X EPC-EVs. **B** Quantification and size distribution of particles in EPC-CM, supernatant (EV-low EPC-CM) and 150k pellet from ultracentrifuged EPC-CM (EPC-EVs), obtained by Nanoparticle Tracking analysis using a Zetaview (Particle Metrix). **C** Immunofluorescence of whole thyroid explant cultured without (Control) or with EPC-EVs (20X concentration) or EV-low EPC-CM (10X concentration). Epithelial cells (E-cadherin) are visualized in red and their apical pole (ezrin) is labelled in green. **D** Quantification of the folliculogenic effect of EPC-EVs and EV-depleted EPC-CM (***, $p < 0.001$; **, $p < 0.01$; 6 explants per condition were analysed in two independent experiments).

Accession	Description	Score	Coverage	# Peptides	MW [kDa]
P19137	Laminin subunit alpha-1 [LAMA1_MOUSE]	1033,99	33,72	79	338
O88322	Nidogen-2 [NID2_MOUSE]	105,16	24,52	21	153,8
P21956-2	Isoform 2 of Lactadherin [MFGM_MOUSE]	57,58	33,33	10	47,1
P80314	T-complex protein 1 subunit beta [TCPB_MOUSE]	33,07	25,61	8	57,4
Q60675	Laminin subunit alpha-2 [LAMA2_MOUSE]	32,21	0,8	2	342,5
H7BX99	Prothrombin [H7BX99_MOUSE]	29,76	6,65	5	70,2
P58022-2	Isoform 2 of Lysyl oxidase homolog 2 [LOXL2_MOUSE]	29,51	12,65	6	81,1
Q9Z1R9	MCG124046 [Q9Z1R9_MOUSE]	27,29	8,13	1	26,1
L7N202	Uncharacterized protein [L7N202_MOUSE]	24,3	32,33	8	29,9
P68033	Actin, alpha cardiac muscle 1 [ACTC_MOUSE]	23,43	16,45	5	42
P68368	Tubulin alpha-4A chain [TBA4A_MOUSE]	23,18	29,24	8	49,9
E9Q5F6	Polyubiquitin-C (Fragment) [E9Q5F6_MOUSE]	22,98	32,84	2	22,6
F6YTZ4	Uncharacterized protein [F6YTZ4_MOUSE]	20,18	24,09	5	30,1
P10852	4F2 cell-surface antigen heavy chain [4F2_MOUSE]	19,56	16,54	6	58,3
G3XA35	MCG116562, isoform CRA_a [G3XA35_MOUSE]	15,76	2,13	3	262,6
P63038	60 kDa heat shock protein, mitochondrial [CH60_MOUSE]	15,46	8,55	3	60,9
Q99JI6	Ras-related protein Rap-1b [RAP1B_MOUSE]	14,57	20,65	3	20,8
Q8VDN2	Sodium/potassium-transporting ATPase subunit alpha-1	12,41	4,3	3	112,9
F6YVP7	Uncharacterized protein [F6YVP7_MOUSE]	12,03	25,66	5	17,7
Q99PV0	Pre-mRNA-processing-splicing factor 8 [PRP8_MOUSE]	11,8	2,06	2	273,4
A2AKJ9	Syntenin-1 [A2AKJ9_MOUSE]	11,53	21,11	2	21,5
P40240	CD9 antigen [CD9_MOUSE]	5,68	11,06	1	25,2
P35762	CD81 antigen [CD81_MOUSE]	5,2	8,47	1	25,8
P41731	CD63 antigen [CD63_MOUSE]	2,67	4,62	1	25,7

Table 1: Comparative mass spectrometry analysis of the 150k pellet isolated from EPC-CM and HUVEC-CM reveal abundant laminin-α1 peptides. Upper 20 lanes (red and white) correspond to proteins identified in the EPC 150k pellet with the highest score in the mass spectrometry analysis, and for which no orthologous protein was identified in the HUVEC 150k pellet. Lower lanes (green) correspond to 4 known EV markers identified in the EPC 150k pellet. Syntenin-1 and CD9 were also identified in the HUVEC 150k pellet.

EPC-EVs preparations contain laminins and known exosomal markers

To screen for molecules responsible for the folliculogenic activity, we next aimed to define the protein composition of EPC-EVs preparations. As a further guide in the search for a putative folliculogenic factor, we compared the 150k pellets from EPC-CM and from Human Umbilical-Vein Endothelial Cells (HUVEC)-CM, as the latter does not stimulate folliculogenesis in our thyroid lobe culture system (data not shown). EPC-EVs and HUVEC-EVs preparations were thus processed in parallel, enzymatically digested and resulting peptides identified by mass spectrometry. This analysis revealed the presence of several proteins well known to be enriched in EVs

such as CD9 and syntenin-1, as well as other proteins commonly found in mass spectrometry analysis of EVs (Exocarta & Vesiclepedia). In addition, and quite interestingly, MS analysis also identified as major hit numerous peptides derived from laminin-α1 (Table 1) in EPC-EVs but not in HUVEC-EVs. Western blot indeed confirmed the presence of laminin-α1 in EPC-CM [5], and EPC-EVs (Fig. 3A). Those data suggested co-sedimentation of laminin with EVs. This extracellular matrix component has already been found to be associated with EVs (Exocarta), and to be involved in thyroid folliculogenesis [5]. As we now demonstrated that EPC-CM also contained EVs, the folliculogenic effect could be mediated by laminins, by EVs, or by their combination. To distinguish between these possibilities, we used two different approaches.

Knockdown of laminin-α1 in EPC abrogates folliculogenic activity of the 150k pellet

We first decided to reduce laminin production in EPCs using a knockdown strategy with shRNA directed against laminin-α1 [5]. EVs were isolated from the conditioned medium of silenced cells and the extent of the knockdown was evaluated in the cell lysate and the 150k pellet. Western blot analysis revealed a 75% decrease of laminin-α1 in shRNA-infected EPC (EPC-shα1), as compared to cells infected with a control shRNA (EPC-GipZ; Fig. 4A & B) and a similar decrease was observed in the EV preparation isolated therefrom (shα1-EVs; Fig. 4A). However, biochemical characterization of EVs isolated from laminin-α1 shRNA-infected EPCs also revealed a weaker signal for CD63 and flotilin-1, suggesting decreased production of total, or of a specific subpopulation of, EVs. We nevertheless tested the biological activity of shα1-EVs on thyroid lobe cultures. When shα1-EV preparation was added to E14.5 thyroid lobes, induction of folliculogenesis was abrogated (Fig. 4C and 4D). The loss of folliculogenic activity was not due to the transfection process as EVs produced by control shRNA-infected EPC (GipZ-EVs) stimulated folliculogenesis as efficiently as control EPC-EVs (Fig. 4D). These results indicated that laminin α1, present in the 150k pellet, is essential to promote expansion of follicles. However, since we observed a concomitant decrease in the abundance of two EVs markers in shα1-EVs (Fig. 4A), the lack of folliculogenic activity could be attributed to the loss of a particular EV population, enriched in CD63 and flotilin-1.

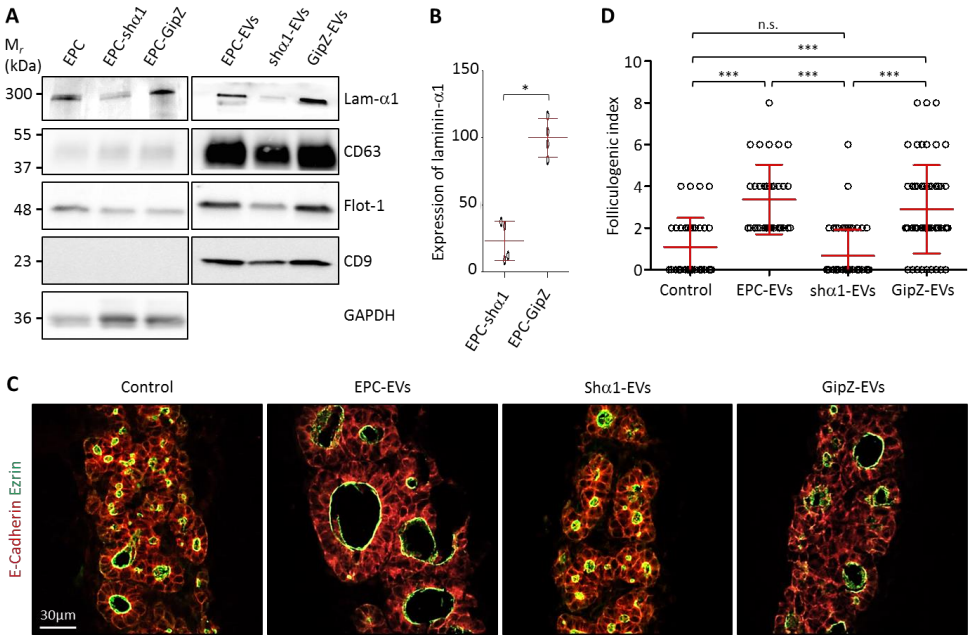

Figure 4: Knockdown of laminin-α1 in EPC abrogates folliculogenic activity of the 150k pellet. **A** Western blot analysis of laminin-α1, CD63, flotilin-1 and CD9 on EPC-EVs, shα1-EVs and GipZ-EVs lysates, as compared to parental cell line lysates. **B** Quantification of laminin-α1 knockdown in infected cell lysates using GAPDH as a control (*, $p < 0.05$; n=4). **C** Immunofluorescence of thyroid explant sections after culture without (control) or with EPC-EVs, shα1-EVS or GipZ-EVs as indicated. Epithelial cells (E-cadherin) are labelled in red and their apical pole (ezrin), in green. **D** Quantification of the folliculogenic effect of EPC-EVs, shα1-EVs and GipZ-EVs (***, $p < 0.001$; n=5).

Both EPC-EVs and laminins stimulate folliculogenesis independently

In a second approach, and in order to avoid any changes in the gene expression program, be it in the biology of the EPC or in EV production, we decided to physically separate EVs from laminins by density gradient centrifugation. After floatation of the 150k pellet isolated from EPC using an iodixanol density gradient, we were indeed able to achieve separation of EVs (predominantly floating in gradient fractions 2-3, as expected for vesicles) from the bulk of laminins, found predominantly in fractions 6-7 (dense, as expected for proteins), (Fig. 5A). We pooled separately fractions 1-4 and fractions 5-8 to generate EV-rich and laminin-rich preparations, respectively. Particle analysis indeed revealed that ~60% of the initial particles were found in F1-4 *vs* ~20% in F5-8 (data not shown). We then tested the capacity of the EV-rich fractions (F1-4) and laminin-rich fractions (F5-8) to stimulate folliculogenesis in E14.5 thyroid lobes culture. To verify that biological activity was not affected by the density gradient, we also prepared a fully reconstituted 150k pellet by mixing all fractions (F1-8). Both EV-rich (F1-4) and laminin-rich (F5-8) fractions, as well as the fully reconstituted 150k pellet (F1-8) were able to induce a robust folliculogenic response (Fig. 5B). Furthermore, we observed a slightly stronger folliculogenic activity for the laminin-depleted EVs-rich fractions as compared to EV-depleted laminin-rich fractions (Fig. 5C). Combination of all 8 fractions was not additive, indicating a saturable process (Fig. 5C).

Altogether, these results (i) confirm that laminins can stimulate folliculogenesis on their own, (ii) indicate for the first time that laminin-depleted EPC-EVs exhibit pro-folliculogenic potential and (iii) suggest that laminin impacts on the production of EVs by endothelial cells and/or their effect in thyrocytes.

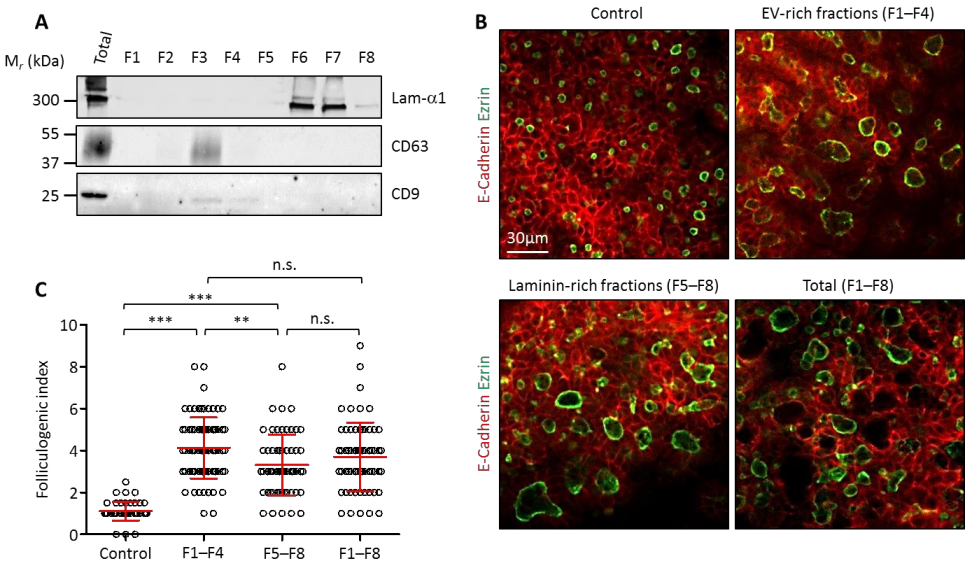

Figure 5: Independent effect of EPC-EVs and EPC-laminins on thyroid folliculogenesis. **A** Western blot analysis of laminin-α1, CD63 and CD9 after separation of EPC-EVs by floatation on iodixanol gradient. **B** Immunofluorescence of whole thyroid explant cultured without (control) or with pooled fractions 1 to 4 (F1-F4), 5 to 8 (F5-F8) and 1 to 8 (F1-F8). Epithelial cells (E-cadherin) are labelled in red and their apical pole (ezrin) in green. A single section is shown for each condition. **C** Quantification of the folliculogenic effect of F1-F4, F5-F8 and F1-F8 (***, $p < 0.001$; **, $p < 0.01$; n=3).

Discussion

In the present study, we report that embryonic endothelial progenitor cells (EPCs) produce EVs that can be internalized by thyroid progenitor cells, and are able to stimulate the expansion of follicular lumen, i.e. folliculogenesis, in thyroid lobes cultured *ex vivo*.

Characterization of the 150k pellet, obtained from the culture medium conditioned by EPCs, revealed the presence of round vesicles with a mean size between 100 and 150nm, equilibrating in iodixanol gradients at a density around 1.12 and enriched in *bona fide* EV markers such as CD63, CD9 and flotilin-1, without detectable ER marker, calnexin. These three characteristics support the claim that the 150k pellet contains EVs [11,24]. It is widely accepted that the differential ultracentrifugation protocol, used in our study and by most EVs research groups [26 – 28], does not allow optimal separation of exosomes and microvesicles (MVs). Indeed, small-sized MVs are likely present in the 150k pellet [29,30]. We nevertheless claim that the folliculogenic effect reported in this study is mediated by exosomes rather than by MVs. Indeed, we found that the 20k pellet, reported to be enriched in MVs, had no detectable effect on folliculogenesis (data not shown). Considering the heterogeneity of vesicles and the absence of definitive specific markers for the different EV subpopulations [19,31], we did not further investigate this aspect and used the term EVs to refer to the vesicles produced by EPCs and present in the 150k pellet.

We were unable to convincingly visualize incorporation of EPC-EVs in whole 3D thyroid lobes, probably due to the thickness of the samples associated with high auto-fluorescence of the 3D tissue pieces. However, we demonstrated that PKH-labelled-EVs were readily incorporated within isolated embryonic thyroid cells in culture. Although most cells had only a weak staining for E-cadherin and the thyroid transcription factor (Nkx2.1), we observed that fluorescent EVs were captured by thyroid progenitors. The loss of E-cadherin and Nkx2.1 is likely due to dedifferentiation initiated upon tissue dissociation and culture [25]. Another study reported that primary cultures of adult thyroid cells require a complex supplementation of culture medium with growth hormones to maintain the differentiated state [32]. Based on the internalization of EVs in dissociated thyroid progenitor cells, we postulate that stimulation of folliculogenesis in 3D thyroid

explants could be due to the entry of EVs, and delivery of their cargo, into the thyroid cells. However, we cannot exclude the possibility that vesicles act on thyroid cells by binding to cell surface receptors and triggering cellular changes, without entering into the target cell.

We observed that addition of the 150k pellet on embryonic thyroid lobes in culture induces a robust folliculogenic response. Mass spectrometry analysis of the 150k pellet further revealed, besides canonical EV protein markers, the presence of abundant laminin peptides. We do not think that laminins are carried within EVs. Indeed, laminins being secreted proteins could not be incorporated within EVs during microvesicle budding or intraluminal vesicle formation in multivesicular endosomes. Laminins must either co-sediment with EVs or interact biochemically with EVs. Indeed, when EPC-EVs were treated with trypsin, we observed a loss of the laminin $\alpha 1$ signal but not of CD63 (data not shown). Interestingly, we previously reported that follicular lumen expansion is promoted by the presence of trimeric laminin-$\alpha 1$, $\beta 1$, $\gamma 1$ (also known as laminin-111) in the CM produced by EPC, and that CM can rescue folliculogenesis in two different knockout models causing defective follicle formation [4,5]. Demonstration in the present report that CM contains EVs now revealed that folliculogenic effects of conditioned media could be attributed to EVs. To better define the respective role of trimeric laminins and EVs, two types of experiments were performed: (i) knockdown of laminin-$\alpha 1$; and (ii) physical separation of EVs from laminins on a density gradient. In the first approach, EVs isolated from medium produced by EPC knocked down for laminin-$\alpha 1$ failed to induce folliculogenesis, suggesting the possibility that trimeric laminin ($\alpha 1$ $\beta 1$ $\gamma 1$) could be the folliculogenic factor, or that laminin was essential for the folliculogenic response. Surprisingly, biochemical characterization of EVs produced by EPC knocked down for laminin-$\alpha 1$ revealed a concomitant decrease in EV markers as compared to control EPC, suggesting impairment of the total production of EVs, and/or orientation into a distinct EV subtype upon laminin-$\alpha 1$ silencing. In this view, suppression of the folliculogenic effect after laminin-$\alpha 1$ knockdown would be related to altered production of bioactive EVs. A role of laminin-111 on EVs biogenesis or release has not yet been shown. However, it has been demonstrated that other extracellular matrix component, i.e. heparan sulphate proteoglycans, influences EVs production by triggering intracellular signalling [33]. In the second approach, we attempted to physically separate EVs from laminins by iodixanol

gradient. Surprisingly, both laminin-rich fractions (F5-8), and EV-rich fractions (F1-4) were able to stimulate the expansion of thyroid follicles in *ex vivo* culture of embryonic thyroid lobes. However, these data do not rule out the possibilities that laminin by itself promoted the folliculogenic activity of endogenous EV, produced by cultured lobes, and that residual content of the sticky protein, laminin, in EV-rich fractions (F1-4) contributed to their effective targeting for signalling into thyrocytes. Hence, our previously reported rescues of defective folliculogenesis in *Vegfa* KO [4] and *Smad1/Smad5* double KO [5] using medium conditioned by EPC is probably due to the concerted action of EVs and of laminins released into the conditioned medium. To further test this hypothesis *in vivo* and to identify the key folliculogenic factor transported via EVs from endothelial cells to thyrocyte progenitors are therefore important future challenges. Mass spectrometry analysis of EV-rich fractions (F1-4) might also reveal if laminins are completely depleted, and whether other candidate proteins might be responsible for the folliculogenic activity. To extend our observations to a physiological situation and demonstrate a role for EVs *in vivo* during thyroid development, we initiated experiments to isolate and characterize EVs from dissociated embryonic thyroid lobes. However, despite the presence of $CD63^+$ vesicles in the 150k pellet, the number of animals required to isolate sufficient amount of EVs for biochemical analysis and functional experiment was prohibitory. Nevertheless, we hope that improvement in EV isolation and analysis methods, including omics, will help to address these questions.

In conclusion, we here demonstrated that embryonic endothelial progenitor cells produce EVs with exosomal characteristics, able to stimulate embryonic thyroid folliculogenesis in an *ex vivo* culture system of thyroid lobes. Our data also suggest that the production of folliculogenic EVs by EPCs depends on laminin-$\alpha 1$ expression and raise the possibility that laminin can promote the effect of endogenous EVs.

Disclosure statement

No potential conflict of interest was reported by the authors.

Acknowledgments

We thank T. Sasaki for laminin antibodies. This work was supported in part by grants from the Fonds pour la Recherche Scientifique (F.R.S-FNRS, Belgium), Université catholique de Louvain (Actions de Recherche concertées), The King Baudouin Foundation. The core facility for Imaging Cells and Tissues was also financed by National Lottery, Région bruxelloise, Région wallonne, Université catholique de Louvain and de Duve Institute. JD and MH held a fellowship from the Fonds pour la formation à la Recherche dans l'Industrie et l'Agriculture (FRIA, Belgium); DV, DT and CEP are Research Associate at F.R.S-FNRS.

References

[1] Fagman H, Andersson L, Nilsson M. The developing mouse thyroid: embryonic vessel contacts and parenchymal growth pattern during specification, budding, migration, and lobulation. Dev Dyn. 2006 Feb;235(2):444-55.

[2] Colin IM, Denef JF, Lengelé B, et al. Recent insights into the cell biology of thyroid angiofollicular units. Endocr Rev. 2013 Apr;34(2):209-38.

[3] Nilsson M, Fagman H. Development of the thyroid gland. Development. 2017 Jun 15;144(12):2123-2140.

[4] Hick AC, Delmarcelle AS, Bouquet M, et al. Reciprocal epithelial:endothelial paracrine interactions during thyroid development govern follicular organization and C-cells differentiation. Dev Biol. 2013 Sep 1;381(1):227-40.

[5] Villacorte M, Delmarcelle AS, Lernoux M, et al. Thyroid follicle development requires Smad1/5- and endothelial cell-dependent basement membrane assembly. Development. 2016 Jun 1;143(11):1958-70.

[6] Raposo G, Stoorvogel W. Extracellular vesicles: exosomes, microvesicles, and friends. J Cell Biol. 2013 Feb 18;200(4):373-83.

[7] Pan BT, Johnstone RM. Fate of the transferrin receptor during maturation of sheep reticulocytes in vitro: selective externalization of the receptor. Cell. 1983 Jul;33(3):967-78.

[8] Harding C, Heuser J, Stahl P. Receptor-mediated endocytosis of transferrin and recycling of the transferrin receptor in rat reticulocytes. J Cell Biol. 1983 Aug;97(2):329-39.

[9] Raposo G, Nijman HW, Stoorvogel W, et al. B lymphocytes secrete antigen-presenting vesicles. J Exp Med. 1996 Mar 1;183(3):1161-72.

[10] Valadi H, Ekström K, Bossios A, et al. Exosome-mediated transfer of mRNAs and microRNAs is a novel mechanism of genetic exchange between cells. Nat Cell Biol. 2007 Jun;9(6):654-9.

[11] Yáñez-Mó M, Siljander PR, Andreu Z, et al. Biological properties of extracellular vesicles and their physiological functions. J Extracell Vesicles. 2015 May 14;4:27066.

[12] Meehan B, Rak J, Di Vizio D. Oncosomes - large and small: what are they, where they came from? J Extracell Vesicles. 2016 Sep 27;5:33109.

[13] Tkach M, Théry C. Communication by Extracellular Vesicles: Where We Are and Where We Need to Go. Cell. 2016 Mar 10;164(6):1226-1232.

[14] Hayashi T, Lombaert IM, Hauser BR, et al. Exosomal MicroRNA Transport from Salivary Mesenchyme Regulates Epithelial Progenitor Expansion during Organogenesis. Dev Cell. 2017 Jan 9;40(1):95-103.

[15] EV-TRACK Consortium, Van Deun J, Mestdagh P, Agostinis P, et al. EV-TRACK: transparent reporting and centralizing knowledge in extracellular vesicle research. Nat Methods. 2017 Feb 28;14(3):228-232.

[16] Delmarcelle AS, Villacorte M, Hick AC, et al. An ex vivo culture system to study thyroid development. J Vis Exp. 2014 Jun 6;(88).

[17] Pierreux CE, Poll AV, Kemp CR, et al. The transcription factor hepatocyte nuclear factor-6 controls the development of pancreatic ducts in the mouse. Gastroenterology. 2006 Feb;130(2):532-41.

[18] Hatzopoulos AK, Folkman J, Vasile E, et al. Isolation and characterization of endothelial progenitor cells from mouse embryos. Development. 1998 Apr;125(8):1457-68.

[19] Kowal J, Arras G, Colombo M, et al. Proteomic comparison defines novel markers to characterize heterogeneous populations of extracellular vesicle subtypes. Proc Natl Acad Sci USA. 2016 Feb 23;113(8):E968-77.

[20] Cominelli A, Gaide Chevronnay HP, Lemoine P, et al. Matrix metalloproteinase-27 is expressed in CD163+/CD206+ M2 macrophages in the cycling human endometrium and in superficial endometriotic lesions. Mol Hum Reprod. 2014 Aug;20(8):767-75.

[21] Tyteca D, D'Auria L, Van Der Smissen P, et al. Three unrelated sphingomyelin analogs spontaneously cluster into plasma membrane micrometric domains. Biochim Biophys Acta. 2010 May;1798(5):909-27.

[22] Théry C, Amigorena S, Raposo G, et al. Isolation and characterization of exosomes from cell culture supernatants and biological fluids. Curr Protoc Cell Biol. 2006 Apr;Chapter 3:Unit 3.22.

[23] Witwer KW, Buzás EI, Bemis LT, et al. Standardization of sample collection, isolation and analysis methods in extracellular vesicle research. J Extracell Vesicles. 2013 May 27;2.

[24] Lötvall J, Hill AF, Hochberg F, et al. Minimal experimental requirements for definition of extracellular vesicles and their functions: a position statement from the International Society for Extracellular Vesicles. J Extracell Vesicles. 2014 Dec 22;3:26913.

[25] Suzuki K, Mitsutake N, Saenko V, et al. Dedifferentiation of human primary thyrocytes into multilineage progenitor cells without gene introduction. PLoS One. 2011 Apr 27;6(4):e19354.

[26] Lässer C, Eldh M, Lötvall J. Isolation and characterization of RNA-containing exosomes. J Vis Exp. 2012 Jan 9;(59):e3037.

[27] Lobb RJ, Becker M, Wen SW, et al. Optimized exosome isolation protocol for cell culture supernatant and human plasma. J Extracell Vesicles. 2015 Jul 17;4:27031.

[28] Gardiner C, Di Vizio D, Sahoo S, et al. Techniques used for the isolation and characterization of extracellular vesicles: results of a worldwide survey. J Extracell Vesicles. 2016 Oct 31;5:32945.

[29] Bobrie A, Krumeich S, Reyal F, et al. Rab27a supports exosome-dependent and -independent mechanisms that modify the tumor microenvironment and can promote tumor progression. Cancer Res. 2012 Oct 1;72(19):4920-30.

[30] Zabeo D, Cvjetkovic A, Lässer C, et al. Exosomes purified from a single cell type have diverse morphology. J Extracell Vesicles. 2017 Jun 20;6(1):1329476.

[31] Willms E, Johansson HJ, Mäger I, et al. Cells release subpopulations of exosomes with distinct molecular and biological properties. Sci Rep. 2016 Mar 2;6:22519.

[32] Barington M, Brorson MM, Hofman-Bang J, et al. Ghrelin-mediated inhibition of the TSH-stimulated function of differentiated human thyrocytes ex vivo. PLoS One. 2017 Sep 20;12(9):e0184992.

[33] Roucourt B, Meeussen S, Bao J, et al. Heparanase activates the syndecan-syntenin-ALIX exosome pathway. Cell Res. 2015 Apr;25(4):412-28.

7.2 Characterization of extracellular vesicles from mouse papillary thyroid carcinoma

Ophélie Delcorte, Jonathan Degosserie, Christophe E. Pierreux

In the second part of my project, I focused on extracellular vesicles in thyroid cancer, using the protocols and skills developed during the first years of my thesis. To study thyroid cancer, our laboratory gained access to a genetically engineered mouse model (GEMM) of papillary thyroid cancer (PTC). To initiate this work, we recruited an undergraduate student in Biomedical Sciences and I was in charge of her practical and scientific training.

Here, I will present the preliminary work that we performed together and that she performed under my close supervision during her experimental training.

This work is still in progress and opens the door for a new PhD.

7.2.1 Introduction

Thyroid cancers are the most common endocrine cancers and can be divided in medullar and follicular carcinomas according to the cancer cell of origin. Amongst follicular carcinomas, papillary thyroid carcinomas (PTC) are the most diagnosed cancers (Fagin and Wells, 2016). They are usually benign and have a good prognosis. However, some mutations have been associated with a more aggressive type of PTC with increased invasiveness and poorer prognosis. The T1799A substitution in the gene coding the B-type Raf kinase (BRAF) leads to the conversion of the valine in position 600 into glutamate, and to the constitutive activation of the kinase activity (Kimura *et al.*, 2003). By inducing activation of the Mitogen-associated protein kinase (MAPK) pathway, $BRAF^{V600E}$ causes increased proliferation. This mutation has been associated with more aggressive PTC (Fagin and Wells, 2016).

It is now widely accepted that establishment and progression of cancer, and of PTC, require continuous and reciprocal interactions with the tumor microenvironment, most importantly fibroblasts and endothelial cells. Interactions are mediated by soluble growth factors and cytokines, but since a decade, extracellular vesicles (EVs) were demonstrated to play a major role in cell:cell communication by carrying and delivering proteins and miRNA from one cell to another (Yanez-Mo *et al.*, 2015). Two main types of extracellular vesicles can be distinguished based on their biogenesis. Microvesicles are formed by budding from the plasma membrane, while exosomes are produced by intraluminal budding in specialized endosomes called multivesicular bodies (MVE), and fusion of the MVE with the plasma membrane. EVs are produced by almost every cell type and have been found in biological fluids such as blood, urine and breast milk (van Niel *et al.*, 2018). In tumors, EVs mediate local tumor:microenvironment communication by promoting cell motility and invasiveness but also distant communication with healthy tissue by preparing pre-metastatic niches (Tkach and Thery, 2016). The role of EVs in PTC establishment and progression has been poorly studied and only few miRNAs transported by PTC-EVs have been identified.

Here, we used an inducible PTC mouse model, to isolate and characterize EVs and to identify transported miRNAs. The long-term goals of this study are (i) to

determine the role of *in vivo*-produced EVs during PTC establishment, and (ii) to identify potential biomarkers of PTC progression by analyzing the miRNA profile of circulating PTC-EVs.

7.2.2 Methods

Animals and dissection

FVB mice were raised and treated according to the principles of laboratory animal care of the University Animal Welfare Committee. Mice were fed with control food (4RF21, Mucedola) or doxycyclin-containing food (4RF21 2500mg/kg doxycyclin, Mucedola) to induce $BRAF^{V600E}$ proto-oncogene expression. Mice were sacrificed by cervical dislocation at the appropriate time point and tissue pieces corresponding to the upper region of the trachea and the attached thyroid tissue were harvested for histological analysis. For RNA extraction and tissue dissociation, thyroid lobe were microdissected.

Hematoxylin Eosin staining

Dissected tissues were fixed in 4% formaldehyde for 1 to 3h and embedded in paraffin (Tissue Tek VIP, Sakura). 7µm slices were obtained from paraffin blocks and laid on glass slides. Paraffin was removed from the tissue by immersion in xylene solution and rehydration was performed by successive immersion of the tissue in ethanol solutions with decreasing concentration, and a final immersion in water. Rehydrated tissue slides were first immersed in hematoxylin solution, followed by water wash, and then immersed in eosin solution and a final wash in water. Stained tissues were observed with a panoramic slide scanner (Pannoramic P250, 3DHistech).

Immunostaining

Dissected tissues were deparaffinized as for HE staining, and then permeabilized by immersion in PBS 0.3% triton X-100. Tissues were incubated in blocking solution (PBS 0.3% triton x-100, 10% BSA, 3% milk) for 1h followed by overnight incubation with primary antibodies ; anti-E-cadherin (1:1000, BD Bioscience), anti-ezrin (1:200, Thermo Fisher Scientific) and anti-vimentin (1:100,

Cell Signaling). Tissues were washed and incubated with secondary antibodies coupled to Alexa fluorochromes (1:1000, Thermofischer Scientific) for 1h. Fluorescent signals were observed with a panoramic slide scanner (Pannoramic P250, 3DHistech).

RNA extraction

One microdissected thyroid lobe, from control or Dox-treated mice, was mechanically homogenized and lysed in TRIzol solution (Invitrogen). RNA was separated from DNA and protein using chloroform phase separation. The upper aqueous phase containing the RNA was harvested and mixed with isopropanol for RNA precipitation. RNA was washed with ethanol and resuspended in RNAse-free water. RNA levels in the samples were measured with Nanodrop ND 1000 (Thermofischer Scientific).

Reverse transcription

500ng of RNA per sample were reverse-transcribed in cDNA using M-MLV reverse transcriptase (Invitrogen) according to the manufacturers' protocol in a final volume of 20µL. At the end of the reaction, cDNA volume was raised to 50µL.

Quantitative PCR

1µl of cDNA per sample was used for qPCR reaction. qPCR were performed using SYBRgreen KAPPA Master Mix (Sopachem) and specific primers for targeted genes (*Gapdh*, *Rpl27*, *Tg*, *Nis*, *Tshr*, *Tpo*, *Nkx2-1* and *Pax8*) in a final volume of 10µL. Primer efficiency was measured for each couple of primers and was comprised between 95% and 105%. qPCR reaction were performed using the CFX96 thermocycler (Biorad). Gene expression was reported to housekeeping genes (*Gapdh* and *Rpl27*) and calculated using the $\Delta\Delta$Ct method.

Tissue dissociation

Several protocols were tested for tissue dissociation (see table at point 7.2.3). The selected protocol used in this work is presented. Four microdissected thyoid lobes from control or Dox treated mice were pooled and incubated overnight at 4°C with Trypsin-EDTA 0.5%. Mechanical dissociation, by up and down pipetting, was performed the next morning and undissociated tissue pieces were allowed to sediment. The supernatant was harvested, trypsin activity was blocked

using BSA (5% w/v) and the sample was stored at 4°C. The undissociated sedimented tissue were further incubated for 3h at 4°C with type-II collagenase solution. Every hour, a mechanical dissociation (up and down) was performed. After 3h, the dissociated tissue suspension was mixed with BSA (5% w/v) and added to the overnight supernatant. The resulting cell suspension was centrifuged at 1,000*g* for 10 min (GR 4.11, Jouan) to separate dissociated cells from the tissue dissociation supernatant.

Extracellular vesicle isolation

Supernatant from dissociated tissue was submitted to differential ultracentrifugation: a first spin at 20,000*g* for 15 min in a Ti50 rotor (Beckman) generated a 20k pellet and a supernatant, which was further spun at 150,000*g* for 90 min in a Ti80 rotor (Beckman) to generate a 150k pellet. This first 150k pellet was washed by resuspension in PBS and submitted to a second ultracentrifugation at 150,000*g* for 90 min. This washed pellet is hereafter referred to as "150k pellet" and was finally collected in PBS or in appropriate solution, depending on downstream application.

Density gradient

Floatation in iodixanol gradient was used to further purify the 20k and 150k pellets. Briefly, 1.3 mL of resuspended pellet was mixed with 1.3 mL of 60% iodixanol stock solution (Axis-Shield) to obtain a 30% iodixanol layer, placed at the bottom of a centrifuge tube. Then, 1.2 mL of 20% and 1.2 ml of 10% iodixanol, diluted from the stock solution, were sequentially added on the top of the 30% layer to obtain 3 layers in the gradient with a final volume of 5 mL. Gradients were centrifuged at 100,000*g* for 16 hours in a swinging bucket rotor (SW55 rotor, Beckman), and 8 fractions (denoted F1 to F8 from top to bottom) of 625 µL were collected by aspiration from top. Each fraction was diluted in PBS, again pelleted at 150,000*g* for 90 min in a Ti80 rotor as above, and pellets were finally resuspended in the appropriate solution.

Western blotting

For western blotting, pellets were lysed in RIPA buffer (150 mM NaCl; 1% Triton X-100; 0.5% sodium deoxycholate; 0.1% SDS; 50 mM Tris pH 8.0; 1X protease inhibitor cocktail (Roche)), and protein concentration was measured using

bicinchoninic acid. Four μg of proteins were resolved on 10% homemade polyacrylamide gels, then transferred onto PVDF membrane and incubated for 2h in blocking solution (TBS 0.05% Tween 20, 5% milk). The following primary antibodies were used overnight: anti-calnexin (1:5.000, ADI-SPA-860D Enzo Life Science), anti-CD63 (1:500, 143902 Biolegend; in non-reducing environment), anti-flotilin-1 (1:500, 610821 BD Transduction) and anti-TSG101 (1:500, sc-7964 Santa Cruz). After several washes, membrane was incubated with secondary antibodies coupled to HRP. Immuno-reactive bands were detected using chemiluminescence (Super Signal Chemiluminescent Substrate; Thermo Scientific) and images were acquired using Fusion Solo S (Vilber Lourmat).

Dynamic light scattering

Samples were analyzed by dynamic light scattering using Nanosizer device (Malver Instruments). Samples were diluted in PBS and disposed in Macro cuvettes (Greiner Bio-one) with a final volume of 1mL. PBS dispersion index was selected for measurement and 3 repeated measures were performed for each sample.

Electron microscopy

For scanning electron microscopy, 20k and 150k pellets were allowed to adhere onto poly-L-lysine-coated coverslips then fixed in 1% glutaraldehyde, washed and post-fixed with 1% OsO_4. Samples were dehydrated in ethanol, critical point-dried and coated with a 10-nm gold film.

For transmission electron microscopy, 20k and 150k pellets were negatively stained with 2% sodium silico-tungstate solution and allowed to adhere on formvar-coated grids. Samples were dried in Silicagel-containing box overnight.

Specimens were observed with CM12 electron microscope (Philips, Netherlands) at 80 kV with the use of a secondary electron detector.

7.2.3 Results

7.2.3.1 Characterization of the human PTC mouse model

A genetically engineered mouse model of papillary thyroid carcinoma

The development of genetically engineered mouse models (GEMM) by the scientific community was triggered by the increased knowledge of the genetic alterations triggering human cancer combined with the technical impossibility to study early stages of cancer development. Most of the GEMMs allow a spatial and temporal control on the expression of the oncogene. Furthermore, as compared to *in vitro* models, these *in vivo* models have an improved physiological relevance due to the cellular heterogeneity, the presence of a tumor micro-environment, and the pre-established systemic communication (Welman *et al.*, 2007).

As mentioned in the introduction, PTC is the most common thyroid cancer with an incidence of 80% amongst all diagnosed case of thyroid cancers. We thus obtained a human papillary thyroid carcinoma mouse model, which had been designed and developed by the group of Professor Jim Fagin from the Memorial Sloan-Kettering Cancer Center in New York (Chakravarty *et al.*, 2011). In this model, the sequence coding for BRAF tyrosine kinase is modified so that it bears the most frequent mutation, T1799A, observed in PTC (see Figure 9 in part 4.1.3).

The sequence coding for the $BRAF^{V600E}$ oncogene is found in a first transgene under the control of a *tetO* operator (**Fig. 1**). A second transgene contains the sequence coding for the trans-activator rtTA2S-M2, inserted downstream of the thyroglobulin promotor (**Fig. 1**). Consequently, only thyrocytes express the trans-activator rtTA2S-M2, thereby providing a spatial control. However, the trans-activator is unable to bind, by itself, to the tetO operator and $BRAF^{V600E}$ is not expressed (**Fig. 1**, left). Binding of the trans-activator, and thus expression of the $BRAF^{V600E}$ oncogene, will only be possible in the presence of doxycycline, thereby providing a temporal control of the oncogene (**Fig. 1**, right). Expression of $BRAF^{V600E}$ will trigger a sustained activation of the MAPK pathway, leading to autonomous thyrocyte proliferation, decreased thyroid-specific gene expression and finally loss of thyroid gland anatomy and function.

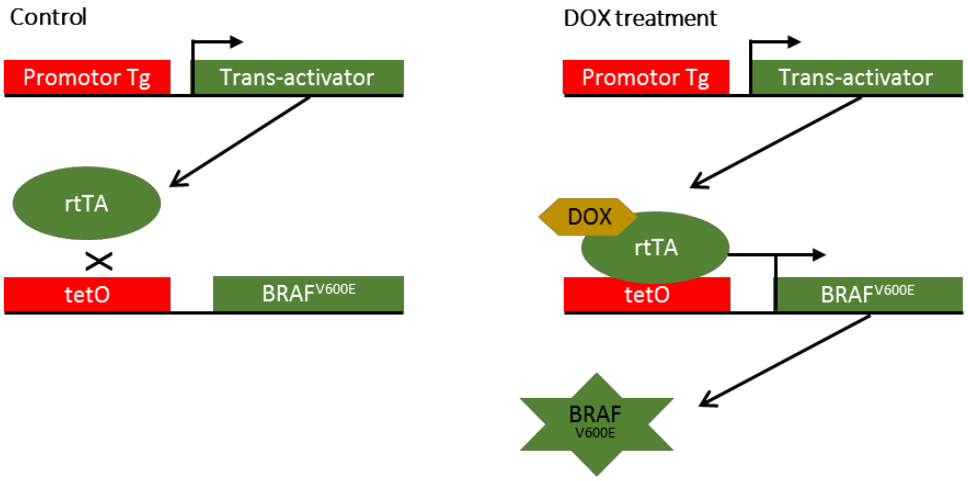

Figure 1: Spatiotemporal control of BRAFV600E oncogene in human PTC mouse model. See text for explanations.

Histological and molecular consequences of oncogenic BRAF^{V600E} expression

To induce BRAF^{V600E} expression, mice were fed with a doxycycline-containing diet for six days. At the end of the treatment, mice were sacrificed and the upper part of the trachea surrounded by the thyroid lobes was dissected. One lobe was precisely microdissected and used for RNA extraction and gene expression analysis and the remaining piece of tissue (trachea + one lobe) was fixed in 4% formaldehyde and embedded for histological analysis.

Sections of control and DOX-treated tissues were first stained with hematoxylin and eosin (**Fig. 2**). We observed that, after only six days of DOX treatment, the follicular architecture of the thyroid tissue is completely lost (**Fig. 2A**). At higher magnification, thyrocytes from DOX-treated mice did not display a flat shape, as in control mice, but are rather cuboidal (**Fig. 2B**). Moreover, thyrocytes also present irregular cell border and cytoplasmic inclusions (data not shown). Finally, we also observed a huge cellular component in DOX-treated mice (**Fig. 2B**, right). These characteristics are compatible with human PTC.

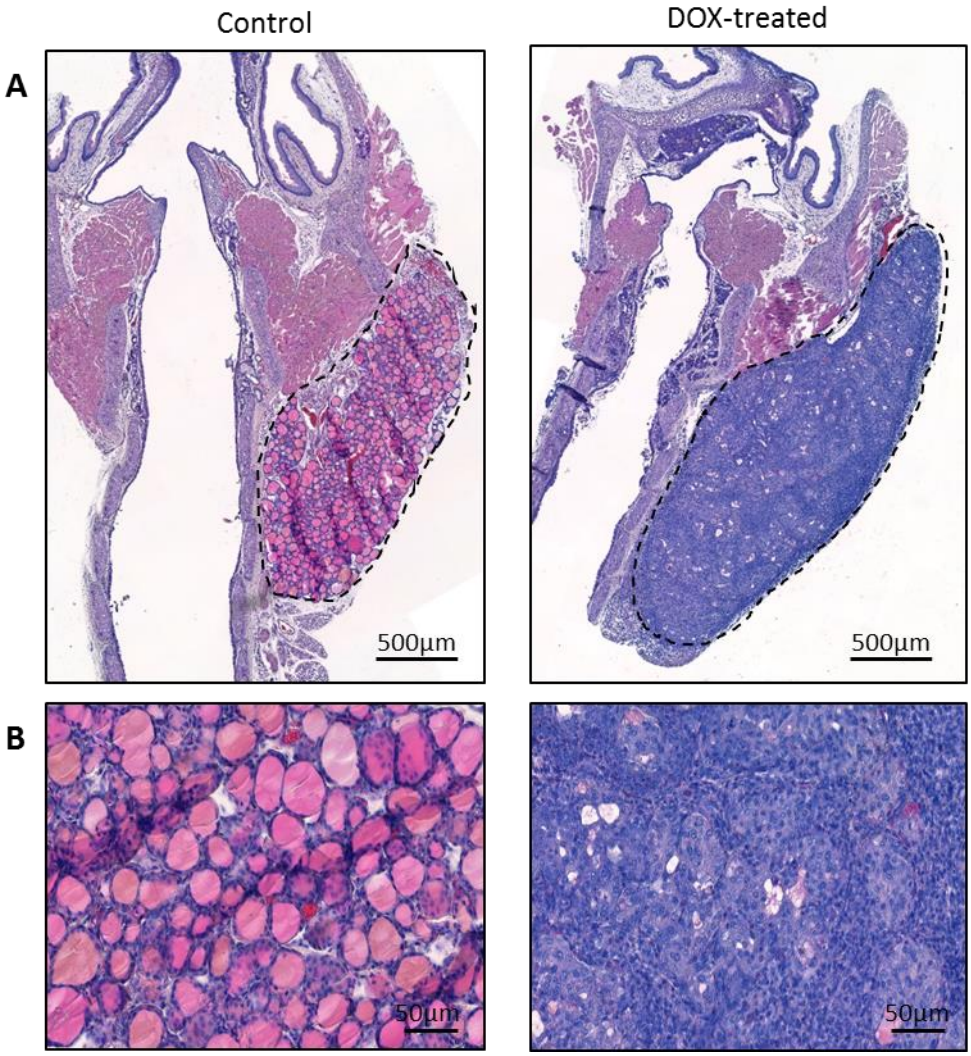

Figure 2: Hematoxylin eosin staining of control (left) and DOX-treated thyroid (right), at low (A) and high (B) magnification. In Dox-treated mice, note global gland enlargement and total loss of pink colloid, causing only blue stain. Thyroid contours are delimited by a broken line; Tr is trachea.

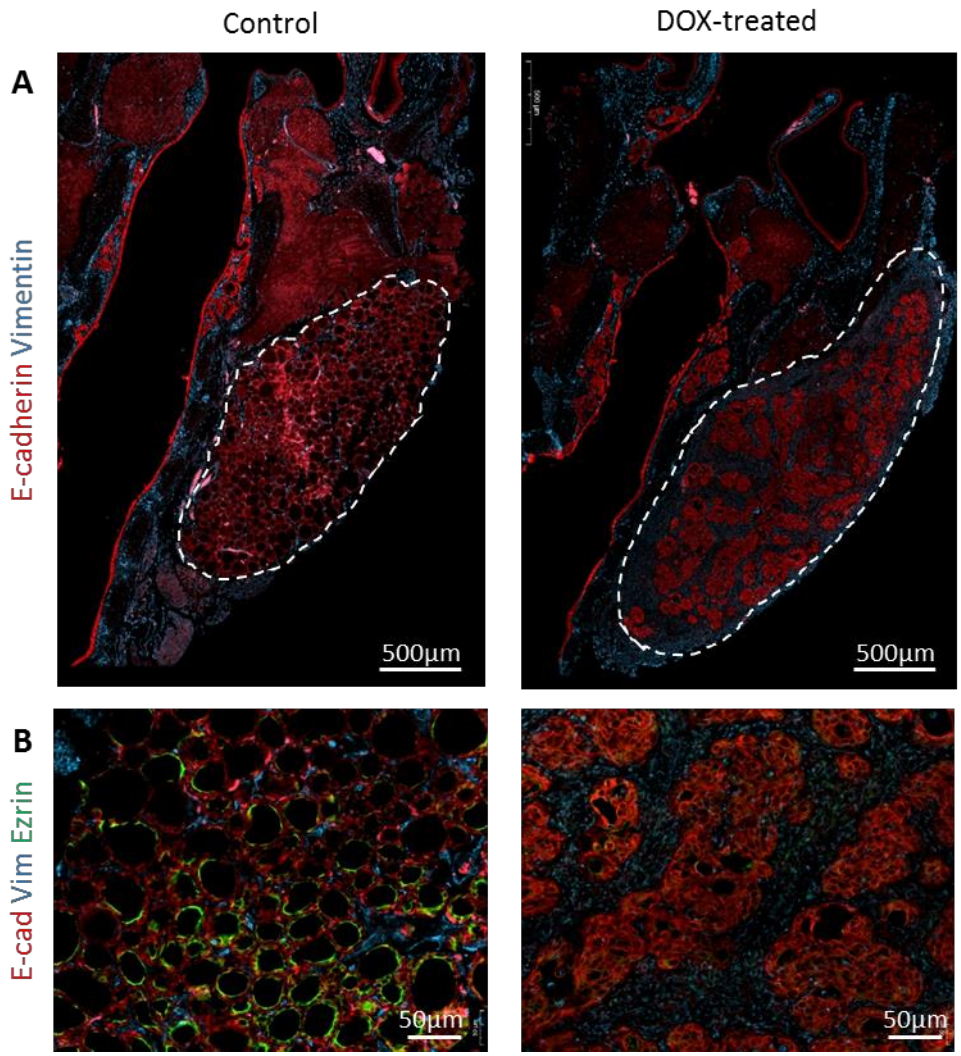

Figure 3: Immunofluorescent labeling of control (left) and DOX-treated (right) thyroid lobe sections at low (A) and high (B) magnification. Sections were labeled with antibodies against E-cadherin, to detect epithelial cells (E-cad, red), vimentin to detect fibroblasts (Vim, blue), and ezrin, to detect the apical pole of polarized cells (green). In Dox-treated mice, note loss of epithelial cell polarity and huge inter-epithelial compartment immunoreactive to vimentin. Thyroid contours are delimited by a broken line. Tr is trachea.

To further explore the modifications triggered by PTC development, adjacent sections we used for immunolocalization. We identified epithelial cells with an antibody against epithelial cadherin (E-Cad), mesenchymal cells with an antibody against vimentin and apical pole with an antibody against ezrin. The control tissue revealed polarized epithelial cells organized in follicles and surrounded by diffuse mesenchyme (**Fig. 3A&B**, left). By comparison, in DOX-treated thyroid tissue, large clusters of non-polarized epithelial cells surrounded by a dense mesenchymal compartment were detected (**Fig. 3A&B**, right). These data, supporting the classical H&E histological staining, confirm the loss of follicular architecture and epithelial polarity, and the important stromal reaction.

Microdissected thyroid lobes were used to measure thyroid-specific gene expression, and to indirectly evaluate the function of the gland. RNA, from control and DOX-treated lobes, was extracted and reverse-transcribed into cDNA. Expression of several genes involved in thyroid function was then measured by qPCR. The expression level of each gene was compared to the expression of *Rpl27*, which was stable in both conditions and was thus considered as a good housekeeping gene. The expression of another housekeeping gene (*Gapdh*) was also measured and also showed stable expression. The quantification revealed a dramatic decrease, in DOX-treated thyroid lobes, of *Pax8* and *Nkx2-1*, two thyroid transcription factors involved in thyroid homeostasis but also of *Nis*, *Tg*, *Tpo* and *Tshr,* genes coding for proteins involved in hormone synthesis or regulation (**Fig. 4**). This analysis revealed a complete dedifferentiation of the tissue after 6 days of DOX-induced $BRAF^{V600E}$ expression.

Altogether, these data indicate that DOX treatment of $BRAF^{V600E}$ GEMM induces a rapid, homogeneous and complete transformation of the thyroid tissue resulting in the loss of follicular architecture and complete thyroid dedifferentiation, associated with a strong stromal reaction.

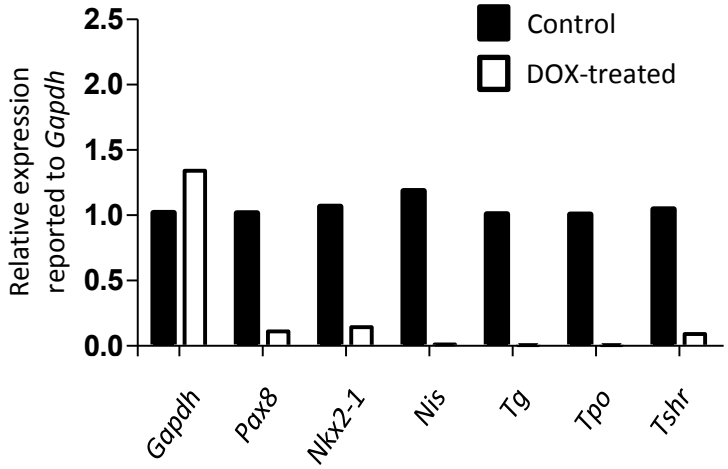

Figure 4: Gene expression analysis in control and DOX-treated thyroid. The expression of 2 thyroid transcription factors (*Pax8* and *Nkx2-1*) and of 4 genes involved in thyroid hormone synthesis or regulation (*Nis, Tg, Tpo* and *Tshr*) is decreased upon DOX treatment.

7.2.3.2 Isolation of extracellular vesicles from thyroid tissue

Since $BRAF^{V600E}$ expression in the thyroid transforms the thyroid tissue and causes dedifferentiation, we next set up a tissue dissociation protocol to collect EVs released by the cancerous tissue in the extracellular spaces. The challenge here was to dissociate the tissue to release the EVs, without affecting cellular integrity. Indeed, dying cells would produce unwanted vesicles that would contaminate EV preparations.

Classical dissociation protocols to obtain a cellular suspension from a tissue piece combine enzymatic digestion with mechanical separation. Enzymatic digestion is usually performed with a solution containing collagenase, for gentle digestion of the extracellular matrix; trypsin, to digest junctional proteins; and EDTA to further destabilize cell-cell junctions. We tested several enzymes or combinations of enzymes, varying incubation times and temperature. For mechanical dissociation, we tested the MacsMix dissociator (Milteniy Biotec) but mainly used up and down pipetting with a Gilson pipette (Up-Down). Cell mortality was assessed at the end of the dissociation using trypan-blue (see table below).

Protocol	Enzymatic dissociation	Temperature (°C)	Time	Mechanical dissociation	Cell mortality
1	Accutase®	37	3*10’	MacsMix Dissociator	/
2	Collagenase (type II)	37	30’	Up-Down	40%
3	Collagenase (type II)	37	3*10’	Up-Down	28%
4	Collagenase (type II)	4	16h+3h	Up-Down	27%
5	Trypsine-EDTA 0.5% + Collagenase (type II)	4	16h+3h	Up-Down	11%
6	Trypsine-EDTA 0.25% + Collagenase (type II)	4	16h+3h	Up-Down	14%

We selected protocol 5 (highlighted in green). This protocol consists of overnight tissue dissociation in trypsin-EDTA 0.5% at 4°C followed by a 3 hours dissociation with type II collagenase, also at 4°C. This protocol gave the lowest mortality rate, confirmed in further experiments. After pelleting the dissociated cells from the suspension, we started EVs isolation using differential ultra-centrifugation. In a first experiment, we collected a medium-speed pellet (called the 20k pellet), and then a high-speed pellet (called the 150k pellet) after each dissociation step (16h and 16h+3h). We then evaluated the presence of EVs in the 20k and 150k pellets by western blotting using a CD63 antibody (**Fig. 5**). This revealed that the first dissociation step (Trypsin-EDTA for 16h) already releases some $CD63^+$ material in the 20k and 150k pellet. Strikingly, the second step of dissociation (type-II collagenase for 3 hours after the first dissociation) released much more $CD63^+$ material in both 20k and 150k pellet (**Fig. 5**). We concluded that

the two-step dissociation protocol at 4°C, using first Trypsin-EDTA 0.5% for 16 hours, followed by another 3 hours of incubation with type-II collagenase, allowed the isolation of $CD63^+$ material in the medium- and high-speed pellets, while triggering the lowest mortality. In addition, this experiment revealed a stronger CD63 signal in DOX-treated thyroid than in control thyroid (**Fig. 5**), suggesting either increased production of CD63 material or increased recovery from a more disorganized tissue.

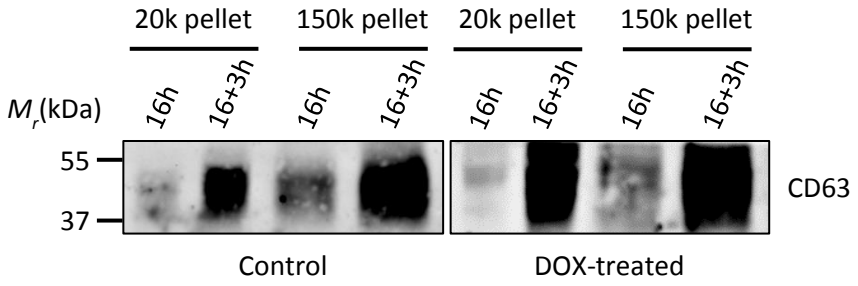

Figure 5: Biochemical analysis of sedimentable material isolated from dissociated control and DOX-treated thyroid tissue. CD63 signal is more important after the two dissociation steps, in the 150k pellet and in DOX-treated thyroid tissue.

7.2.3.3 Characterization of PTC EVs

To better characterize the $CD63^+$ material isolated from dissociated PTC tissue, and to verify that the 20k and 150k pellets do contain EVs, we analyzed the size and the shape of the particles present in the pellet and further characterized the pellet biochemically.

First, we resorted to transmission electron microscopy (TEM) and scanning electron microscopy (SEM) to visualize the content of the pelleted material. Both techniques revealed the presence of round-shaped structures compatible with small vesicles (**Fig. 6**). In the 20k pellet, the objects had a size between 400nm and 1µm (data not shown), while in the 150k pellet, the size of the vesicles was smaller than 100nm. Although very informative, EM only allows the analysis of a tiny part of a biological sample and therefore may not be representative of the whole sample. To circumvent this problem, the EM analysis was complemented with

dynamic light scattering analysis. Using light scattering properties of vesicles in a solution, the device (Nanosizer) determines the average size of the particles present in a sample. In the 20k pellet, the Nanosizer evaluated the size of the particles between 300 and 800nm, which is similar to what we found by EM (data not shown). In the high-speed 150k pellet, we observed a more heterogeneous profile with the Nanosizer (**Fig. 7**). A main peak was found around 200nm, and a smaller one peaked at 60 nm. The large (200 nm) peak could be due to aggregation of small particles, a phenomenon frequently reported upon ultra-centrifugation. Aggregates were also observed by EM.

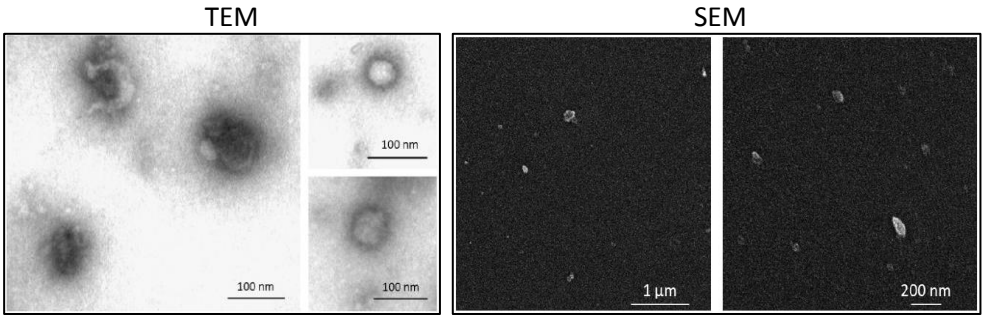

Figure 6: Electron microscopy analysis of the 150k pellet isolated from DOX-treated thyroid. Transmission electron microscopy (TEM) images of 150k pellet show mostly spherical structures (left panel). We could also observe some elongated and twisted structures. Scanning electron microscopy (SEM) images of 150k pellet show spherical-ovoid structures with an average size of 100nm (right panel).

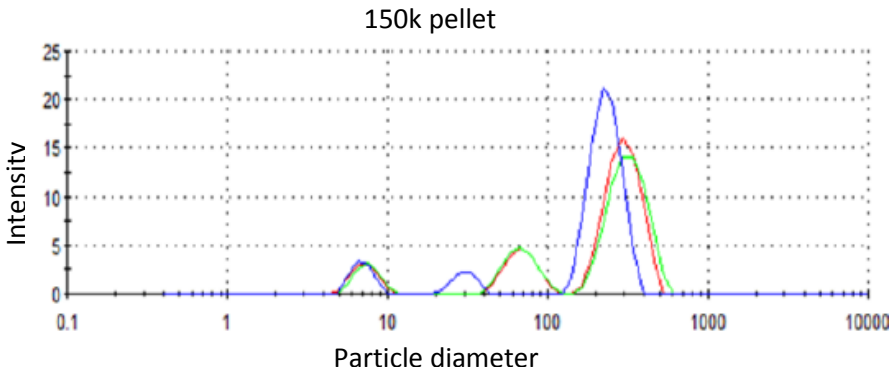

Figure 7: Dynamic light scattering analysis of the 150k pellet isolated from DOX-treated thyroid. Superposition of three repeated measurements (blue, green and red line) of a representative 150k pellet.

We finally analyzed the enrichment of EV markers by western blot analysis in the 20k and 150k pellets, as compared to cell lysates from the dissociated thyroid tissue (**Fig. 8**). Equal amounts of proteins were loaded in each condition and the membranes were blotted with anti-CD63, flotilin-1 and TSG101 antibodies, three known EV markers. We observed a strong enrichment of all markers in both 20k and 150k pellets, as compared to the cell lysate of DOX-treated thyroid (**Fig. 8**). Furthermore, lack of detectable calnexin in the 20k and 150k pellets as opposed to cell lysate indicates negligible contaminant by intracellular organelles (**Fig. 8**).

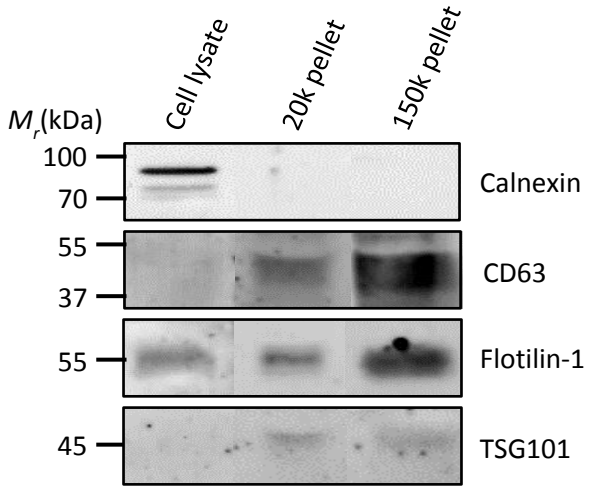

Figure8: Biochemical analysis of 20k and 150k pellet isolated from DOX-treated thyroid. CD63 is strongly enriched in the 20k and 150k pellets while the enrichment of flotilin-1 and TSG101 is mostly detected in the 150k pellet as compared to the original cell lysate. The endoplasmic reticulum protein, calnexin, is readily detected in the cell lysate but not in the high-speed pellets.

Finally, we wished to determine the equilibrium density of the vesicles present in the 20k and 150k pellets. After differential ultra-centrifugation, the medium-speed (20k) and the high-speed (150k) pellets were suspended in a buffer and mixed with 60% iodixanol, to obtain a first layer of 30% iodixanol laid at the bottom of two centrifuge tubes. We then added sequentially a layer of 20% and 10% of iodixanol on top of the suspended pellets. After overnight centrifugation and gradient equilibration, eight fractions were harvested in each tube, from top

(low density) to bottom (high density), and washed in PBS before ultra-centrifugation to concentrate the diluted fractions of each gradient. The fractions (F1 to F8) from 20k pellets and 150k pellets were then analyzed by western blotting using CD63 and flotilin-1 (not shown) antibodies (**Fig. 9**). Surprisingly, signals for both EVs markers were detected in the same low density fraction (**Fig. 9**, F3 and F4) for the two pellets, indicating that (i) markers are associated with floating vesicles rather than high-density protein aggregates, as expected; and (II) vesicles present in both pellets have a similar density, again suggesting that vesicles form aggregates during the harvesting process.

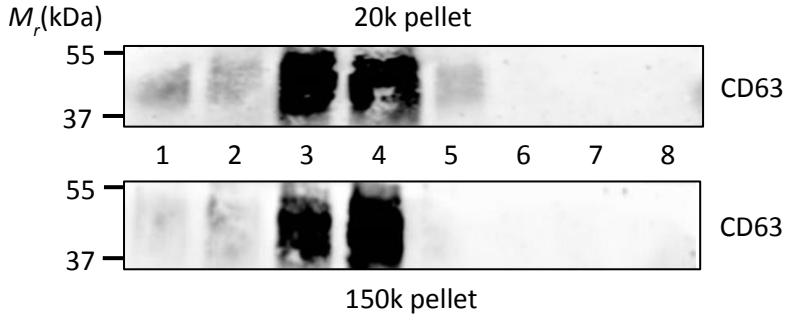

Figure 9: Biophysical analysis of 20k and 150k pellet produced by DOX-treated thyroid. $CD63^+$ vesicles are detected in the same fractions (mainly #3 and #4) for both 20k and 150k pellet. Density increases from fraction #1 to #8. Density of fraction #1 was around 1.05, of #3 and #4 was around 1.09, and of fraction #8 was 1.23.

Altogether, these data indicate that, after six days of $BRAF^{V600E}$ expression with doxycycline, thyroid cancer cells produce vesicles that are released in the extracellular space and have a size, a density and biochemical characteristics compatible with microvesicles (20k pellet) and exosomes (150k pellet); even if we could not differentiate these two populations by their density or markers.

7.2.4 Conclusions and perspectives

In the course of this preliminary work on thyroid cancer, we validated the doxycycline-induced formation of PTC in the $BRAF^{V600E}$ mouse model and demonstrated that the expression of mutated $BRAF^{V600E}$ protein in thyrocytes results in the appearance of a cancerous lesion bearing PTC characteristics with loss of follicular structure, cell dedifferentiation and stromal expansion. We set up a gentle tissue dissociation protocol that allows isolation of EVs, with a low cellular mortality rate. Finally, we demonstrated that, after six days of treatment with doxycycline, transformed thyrocytes produce both microvesicle-like and exosome-like vesicles in their environment.

Based on these experiments, the undergraduate student continued to work on this project without my direct supervision. First, she detailed the time-course production of EVs with PTC development. Indeed, after 6 days of DOX treatment, the tissue was dramatically altered and expression of thyroid-specific genes was lost (**Fig. 2, 3** and **4**). She thus analyzed EVs production and histology along PTC development using thyroid tissue from mice treated for 2, 4 and 6 days with doxycycline. After two days of treatment, the well-known histological signs of PTC (i.e. numerous papillae in follicles) were visible and decreased expression of some thyroid-specific genes was measured. However, after 2 days of treatment, EV production was still very low. The best compromise was 4 days of $BRAF^{V600E}$ induction. Some follicles with papillae were still visible and EV production was higher than at 2 days. She also decided to focus on the 150k pellets. The second major step was the establishment of the RNA extraction protocol from this ultra-centrifuged material to elucidate the catalogue of microRNAs contained in PTC-derived exosomes. 150k pellets were first treated with RNAses to remove RNA potentially bound on the surface of EVs. Then, RNA was extracted from the EVs and Exiqon/QIAGEN performed next generation sequencing on 3 independent 150k pellets isolated from thyroid treated with DOX for 4 days. In parallel, she also performed the miRNAs sequencing on the dissociated tissues from control and DOX-treated mice at 4 days. Out of the ~60 microRNAs identified with high confidence in the EVs from the 150k pellets, 2/3 were differentially expressed in PTC as compared to the control thyroid tissue. Some of the miRNAs identified in

EVs have already been identified in human PTC samples or in other cancers, and some have never been demonstrated to be involved in cancer.

The next obvious steps of this work are first to analyze in detail the RNA sequencing results and to cross the results with the literature and cancer databases to identify microRNA candidates that could be involved in PTC development and/or be used as PTC biomarkers. The best candidates should then be further studied in a detailed time-course following $BRAF^{V600E}$ expression. The relevance of "functional" microRNA candidates could be tested *in vitro* in classical transfection experiments with miR-mimic and antagomiR, or by deleting miRNA candidate(s) by Crispr/Cas9 *in vivo* in the $BRAF^{V600E}$/rtTA colony. If biomarker microRNA candidates emerge, we will first confirm their presence in EVs harvested from the blood of DOX-treated mice after 2, 4 or 6 days. In collaboration with the St Luc Hospital, we will also analyze the presence of these candidate microRNA in the blood of patients diagnosed with PTC before surgery, and after surgery.

8 Discussion, conclusions and perspectives

The aim of my thesis was to determine if extracellular vesicles could mediate intercellular communications during thyroid gland ontogenesis and oncogenesis. I mainly focused on thyroid folliculogenesis and demonstrated that extracellular vesicles produced by endothelial progenitor cells stimulate follicle formation. In the last year, I initiated the second part of my project on the role of extracellular vesicle in papillary thyroid cancer. This project yielded very promising results that constitute a very good basis for a new PhD thesis.

In this section, I will discuss the techniques that I implemented in the lab to be able to work with extracellular vesicles and the general need for improvement and standardization of those techniques. I will then discuss extracellular vesicles, their physiological relevance and their potential for medicine. Finally, I will integrate the results of my work in the state-of-the-art on thyroid development.

8.1 Experimental procedures: how to work with EVs?

Harvesting methods

During my thesis, I had the opportunity to work in the exciting field of extracellular vesicles. However, every great opportunity has its dark side. As a relatively new field of research, the EV field was lacking guidelines and precise report of experimental procedures, resulting in a huge diversity of protocols, most of the time not very well detailed. The international society for extracellular vesicles (ISEV) recognized and started to tackle this problem in 2013 (Witwer *et al.*, 2013). Luckily, I performed my thesis in a research institute with experience in differential-ultracentrifugation (d-UC), epitomized by the discovery of lysosome by Professor Christian de Duve in 1955. Furthermore, ultracentrifugation followed by iodixanol density gradient was used in the lab to isolate microvesicles (Thoene *et al.*, 2013) and to prepare conditioned medium (Hick *et al.*, 2013). Consequently, I resorted to d-UC to harvest extracellular vesicles from EPC-conditioned medium and improved our protocol by complementing it with expert protocols found in the literature (Lasser *et al.*, 2012; Raposo *et al.*, 1996; Thery *et al.*, 2006). The crucial need for more detailed protocols in EV research was further highlighted by Cvjetkovic and

collaborators upon demonstration that the rotor type and the centrifugation speed impact on the purity and yield of extracellular vesicles (**Fig. 18**) (Cvjetkovic *et al.*, 2014). In addition, recent data obtained in the lab suggest that at each 150,000*g* spin in the TI 80 rotor, 20-30% of the vesicular material is lost. Finally, although it was observed that d-UC promotes aggregation of vesicles, it was still the most widely used primary method to harvest extracellular vesicles according to a report in 2016 (Gardiner *et al.*, 2016).

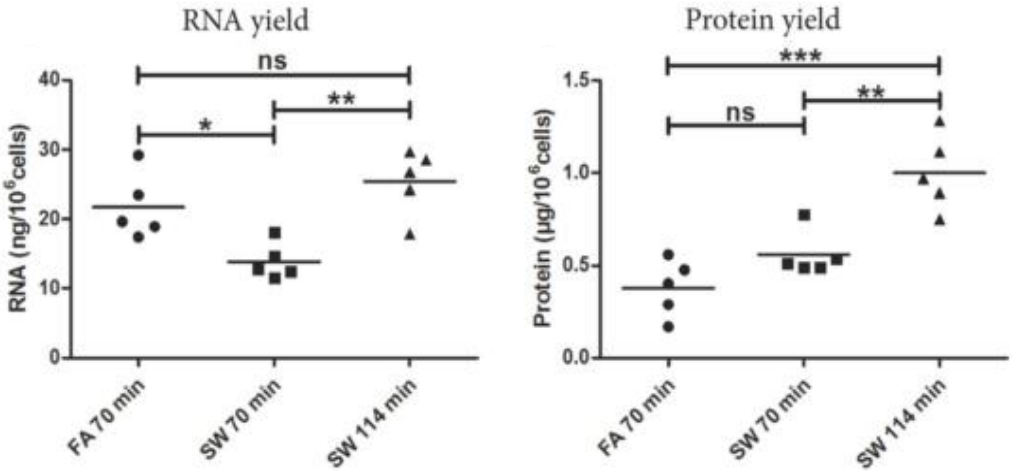

Figure 18: Influence of the rotor type and centrifugation time on the RNA and protein yield. Left graph: The RNA yield is greater with fixed angle (FA) rotor as compared to the swinging buckets rotor (SW) after 70min of centrifugation. Increased centrifugation time (114min) with the SW rotor results in a similar RNA yield to the FA rotor after 70min of centrifugation. Right graph: At equivalent centrifugation time (70min), there is no significant difference in the protein yield with the FA and SW rotor. Increased centrifugation time (114min) results in an increased protein yield with the SW rotor as compared with 70min of centrifugation. (Cvjetkovic *et al.*, 2014)

However, several other methods such as size exclusion chromatography and filtration on 0.22µm filters (i.e. based on the size as is d-UC), density gradient (i.e. based on the size and the density) and affinity purification on magnetic beads (i.e. based on the affinity for EV markers) are also used to harvest extracellular vesicles. When choosing an isolation technique, it is important to think about the downstream experiment. Each technique has its pros and cons but they all struggle

to deal with the heterogeneity of extracellular vesicles, which is emphasized in more and more studies. For example, the group of Thery isolated EVs from medium conditioned by dendritic cell using d-UC and was able to identify by proteomic analysis five groups of proteins expressed preferentially in certain type of EVs (Kowal *et al.*, 2016). Moreover, using d-UC followed by density gradient, Willms demonstrated that melanoma cells release "low-density" and "high-density" exosomes that bears different biological functions (Willms *et al.*, 2016). More recently, Zabeo *et al.* observed by transmission electron microscopy and cryo-electron microscopy that exosomes from human mast cells present different morphological characteristics (Zabeo *et al.*, 2017). I believe that tackling the problem of EVs' heterogeneity is one of the biggest challenge for the EV community and that the development of methods and tools allowing proteomic and transcriptomic analysis on single particle is thus critically needed.

Characterization of extracellular vesicles

A well accepted nomenclature for EVs, even though evolving due to the aforementioned heterogeneity, distinguishes two types of EVs produced by healthy cell: microvesicles and exosomes. These two types of vesicles mainly differ by their mode of production. Nevertheless, other characteristics such as protein enrichment, density and size are used in the literature to distinguish microvesicles from exosomes. Before starting functional experiments with extracellular vesicles it was thus imperative to characterize the vesicular populations present in the biological material of interest. Although this statement seems rather trivial, it is discouraging to see how many (recent) published studies are still lacking EV characterization, and thus attributing any kind of function to so-called EVs. To avoid this problem, the ISEV published a "minimal experimental requirements to study extracellular vesicles" in 2014 (Lotvall *et al.*, 2014). Since the publication of these recommendations, the quality of EV characterization is improving, as these guidelines are broadly accepted. However, more than 25% of ISEV members recognized that they did not follow the minimal requirements in their last publication, leaving room for more improvement (Witwer *et al.*, 2017).

During the first years of my thesis, I thus struggled to find detailed information, technical or descriptive, to perform a complete characterization of EPC-EVs. The first challenge was to find suitable antibodies and their working conditions for biochemical characterization of EVs by western blotting. Although

publications mentioned the antibody name, details about the manufacturer, dilution and blotting conditions were often simply lacking. This resulted in a waste of time and money for new groups in the EV field, like ours, and more importantly in non-reproducible experiments. At the end of the journey, and thanks to advices from the lab of P. Zimmermann, I have been able to perform an adequate biochemical characterization of EPC-EVs, and highlighted the enrichment of CD63, Flotilin-1 and CD9 (three EV markers) while excluding the presence of calnexin (an endoplasmic reticulum protein), therefore fulfilling the previously mentioned minimal requirements for a biochemical characterization.

For biophysical (i.e. density) characterization of EPC-EVs, I performed iodixanol density gradients, from which I learned the basics thanks to the great expertise of Francisca N'Kuli, a former technician in the lab, which had been extensively trained by Prof. Pierre Courtoy. Gradient, either continuous or discontinuous, and particulate (PercoIL) or soluble (hypertonic sucrose or isotonic iodixanol), equilibration is achieved after layering a sample at the bottom (bottom-top migration; i.e. floatation; most appropriate to buoyant particles) or at the top (top-bottom migration; i.e. equilibration by sedimentation; most appropriate to dense particles) of the gradient. Here, using a discontinuous iodixanol bottom-top floatation, I reported that EPC-EVs float at a density around 1.12g/mL, a density compatible with exosomes. However, using the same protocol in the PTC project, $CD63^+$ vesicles floated at a density of 1.09g/mL and we were not able to distinguish microvesicles (20k pellet) from exosomes (150k pellet) based on their density, suggesting possible aggregation of exosomes during differential ultracentrifugation and highlighting again the difficulty to differentiate the types of extracellular vesicles. It would be very interesting to test top-bottom equilibration or to increase the number of layers in the gradient to improve its resolution.

To determine the size of EPC-EVs, I resorted to electron microscopy and dynamic light scattering. Dr. Patrick Van Der Smissen, who is in charge of the platform for imaging cell and tissue (PICT) of the Institute, performed sample preparation and image acquisition for electron microscopy. Although electron microscopy is the only technique allowing visualization of EVs, the images obtained only represent a tiny part of the sample. Therefore, electron microscopy must be complemented with a technique that will analyze the broad vesicular population of the sample. Here, I used dynamic light scattering analysis, which was performed

with a Nanosizer (i.e. a device used in the pharmacology department to determine the size of molecules). Dynamic light scattering analysis uses a laser beam and Brownian motion of particles, which defines the random motion of small particles in fluids (the smaller the particle, the faster the motion), which can be a measure of variations of scattered light intensity in time (**Fig. 19**). These variations are transformed, using complex mathematical formulas, to obtain a size distribution of the particles present in the sample. Using these techniques, I could visualize that EPC-EVs display a mean size of 100nm by electron microscopy, while Nanosizer analysis of EPC-EVs showed a mean particle diameter of 140nm of the same sample in the hydrated state. Another method using dynamic light scattering is nanoparticle-tracking analysis. The advantage of this method is that it allows quantification of the number of particles in the sample. I could get access to a nanoparticle-tracking device (Zetaview from Particle Metrix), which was available on our campus for a demo, during the reviewing of my paper (presented in 6.1). The acquisition of such device (planned for this year) will improve the characterization of EV samples and provide important quantification information that we are currently lacking in the PTC project but that I could provide in the revised version of our manuscript submitted to the Journal of Extracellular Vesicles.

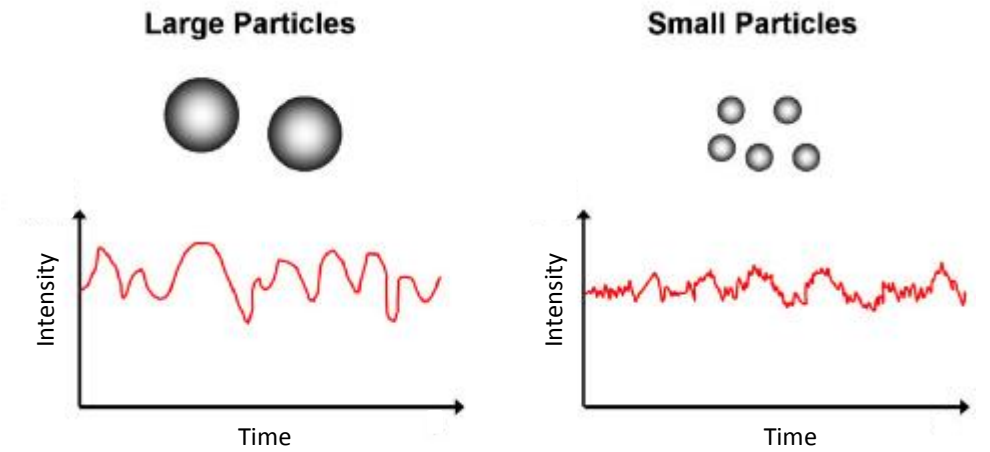

Figure 19: Representation of raw data in dynamic light scattering analysis. Variation of the intensity of scattered light in time. The slower motion of large particles will result in slower variation of scattered light intensity (left graph). The faster motion of small particles will result in faster variation of scattered light intensity (right graph. (Lim *et al.*, 2013)

Incorporation by target cells and functional experiments

As previously stated, visualization of exosomes is best achieved by resorting to electron microscopy. Nevertheless, it is possible to visualize exosomes with classical optical microscope by using lipophilic fluorochromes. However, it remains difficult to claim that only one exosome, and not a cluster of exosomes, is visualized. Amongst the commonly used fluorochromes (PKH, CellMask, DiI, DiD…), I used PKH67. PKH67 is a fluorescent molecule that is stably incorporated into lipid regions of the cell/vesicle membrane thanks to long aliphatic tails. After incorporation into the vesicles, it is mandatory to eliminate unbound fluorochrome. Failure to do so may lead to cell labeling by free contaminating PKH67. To avoid this, PKH-labeled EVs were submitted to a density gradient that allows separation of the labeled vesicles from the free fluorochrome. After incubation of dissociated thyrocyte progenitors with labeled EPC-EVs, I was able to demonstrate EPC-EVs incorporation. However, it was recently reported that other contaminants associated with EVs such as lipoproteins could be confounding factors for incorporation studies (Takov *et al.*, 2017). This recent report highlights once again the importance of choosing the appropriate EV isolation method.

A strong evidence for a biological property of extracellular vesicles is a dose-dependent response (Lotvall *et al.*, 2014). Most publications rely on gene expression assay performed on *in vitro* cell culture to demonstrate biological properties. In our project, I used an *ex vivo* culture system of embryonic thyroid explants. This system allows thyrocyte progenitors to develop and differentiate in their 3D environment while in contact with neighboring cell populations present in the organ *in vivo*. I was able to demonstrate the EPC-EVs *stimulate* ongoing follicle expansion in this system. An extended dose-dependent analysis was not performed, to limit animal usage. However, I observed that EPC-EVs used at the same concentration as the EPC-CM, i.e. 10X-concentrated (Hick et al. 2013), failed to promote follicle expansion in a convincing and reproducible manner. On the contrary, a 2-fold increase in the concentration of EPC-EVs reproducibly stimulated follicle expansion. However, failure to evidence a dose-response effect could be explain by: (i) variations in the reproducibility of biological EV preparation (that could impact bio-activity); (ii) the accessibility of EVs to complex tissues that may vary dramatically; (iii) the fact that the biological effect that we observed with exogenous factor is probably already stimulated by endogenous factors; and (iv)

the dynamic range between constitutive and enhanced response, which varies around three-fold. These considerations could also explain why no additivity of stimulation by laminin and purified EVs could be observed. Finally, this system is not perfect and could be improved. One key component, present *in vivo* but absent in the *ex vivo* system, is the blood flow. Implementing a microfluidic-like system to the *ex vivo* culture system, using the already established vasculature of the explant, would improve the physiological relevance of our system.

To conclude, I would like to remind the difficulty, for newcomers in the EV field, to find suitable protocols to characterize properly their EVs. The publication of the minimal requirements was a good start towards the right track (Lotvall *et al.*, 2014). However, many research groups, including those affiliated to ISEV and aware of those guidelines, do not refer to them (Witwer *et al.*, 2017) and more importantly do not provide sufficient details to allow replication of their experiments. With the steady increase in the number of EV-related publications, it is more and more difficult to find reliable information on the way to perform experiments. Recently, a group of ISEV members created EV-TRACK, a database to centralize knowledge in the EV field (Van Deun *et al.*, 2017). This platform has two main interests: (i) it helps the authors to evaluate compliance of their work with the ISEV guidelines and to estimate the reproducibility of their experiments by giving a score, an information to be included in their manuscript (we obtained 100%); and (ii) it allows other investigators to find detailed information to perform comparable experiments with extracellular vesicles. Adequate usage of this platform by journal editors worldwide should standardize and optimize the quality of published EV investigations.

8.2 Physiological relevance of extracellular vesicles

In 2016, 83% of published EV research used as starting source EVs isolated from medium conditioned by cultured cells. Moreover, 72% of the studies performed *in vitro* biological readouts, and only 29% used *in vivo* functional assays (**Fig. 20**) (Gardiner *et al.*, 2016). In addition, it should be mentioned that most *in vivo* functional analyses were performed with *in vitro* produced EVs injected at very high doses in mice, resulting in preferential biodistribution to the liver, regardless of the producing cell type (Smyth *et al.*, 2015; Takahashi *et al.*, 2013). These

observations suggest that most of the effects attributed to EVs have questionable physiological relevance. There are several solutions for this problem.

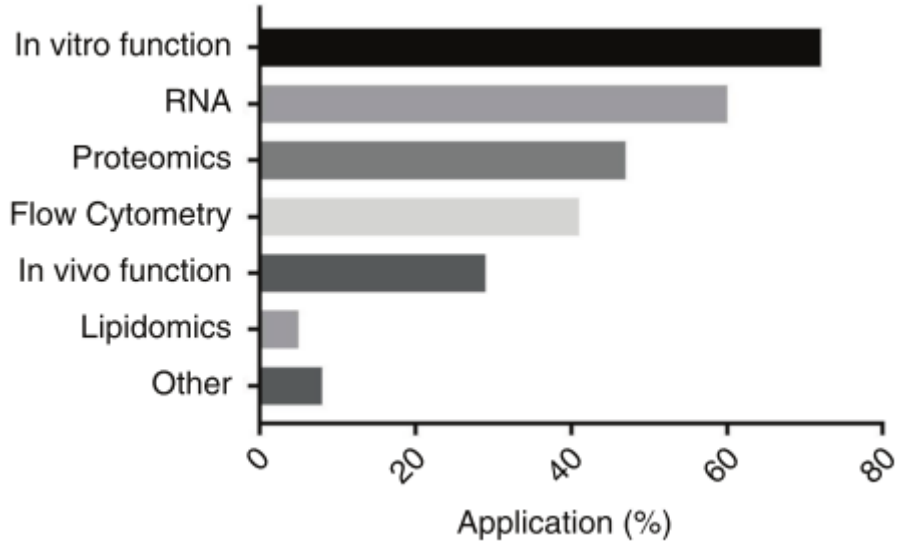

Figure 20: Survey of literature: percentage of EV-based publications. Most research groups focus on *in vitro* functional analysis as compared to *in vivo* functional analysis. (Gardiner *et al.*, 2016)

First, I think that *in vitro* experiments should be designed to be transposable to *in vivo* models. An outstanding example is the study demonstrating the effect of $BRAF^{V600E}$ inhibition on the cargo of vesicles produced by malignant melanoma cells. First, Lunavat *et al.* established the proof-of-concept *in vitro* by demonstrating that $BRAF^{V600E}$ inhibition by Vemurafenib in the malignant melanoma cell line MML-1 affected miRNA loading in the extracellular vesicles. The authors further identified miR-211-5p to be the only up-regulated miRNA in treated cells and in released vesicles, as compared with untreated cells and vesicles derived therefrom. To confirm the *in vivo* relevance of their observations, the authors then transplanted MML-1 cells into mice and treated the mice with Vemurafenib or a vehicle. As compared to the continuous growth of the MML-1-derived tumor in untreated mice, they observed a reduced growth in the Vemurafenib-treated group. After few days, tumors from treated and untreated mice were resected and EVs were isolated from the dissociated tumor tissues. Analysis of the EV cargo in both condition confirmed the up-regulation of miR-211-5p *in vivo* after $BRAF^{V600E}$

inhibition. Further *in vitro* experiments suggest that miR-211-5p could play a role in the resistance to Vemurafenib treatment (Lunavat *et al.*, 2017).

Second, I think that scientists in the EV field should put more energy on the role and cargo of *in vivo*-produced EVs, even if the function is studied *in vitro*. It is of course more laborious than using *in vitro*-produced EVs but it is feasible, as we demonstrated by harvesting EVs from dissociated PTC dissected from mice. The group of Lötvall also used *in vivo*-produced EVs in a study published in 2016. In this publication, the authors harvested EVs from nasal lavage fluid collected from healthy and asthmatic patients. They demonstrated that nasal exosomes were able to stimulate immune cells migration *in vitro* and that their protein cargo was modified by the health status of the patient (Lasser *et al.*, 2016).

Finally, the ideal study would be achieved by using *in vivo*-produced EVs and by also testing their biological properties *in vivo*. It is surely the most difficult option but also the most relevant approach to address the role of EVs. To date, I could not find any publication combining these features. However, the study of Anoek Zomer published in Cell in 2015 is, to me, the closest to the previously mentioned settings (Zomer *et al.*, 2015). In their study, the authors demonstrated that malignant CRE recombinase-expressing tumor cells are able to transfer their malignant phenotype to benign RFP/STOP/GFP-expressing cells *in vivo* via extracellular vesicles. First, the authors observed such transfer *in vitro* by visualizing the light emission switch of benign tumor cells (from red to green) after incubation with EVs produced by malignant tumor cells and by measuring the migration capacities of those cells. Then, *in vivo*, using a double xenograft mouse model of benign and malignant tumor cells, they visualized the light emission switch of benign tumor cells, which must be due to EV-mediated transfer of the CRE from the malignant cells (Zomer *et al.*, 2015). One key criterion to design relevant experiments with EVs is the evaluation of the physiological EV-load of an organism. This information would not only help to understand if, and how, cells of a tissue use EVs to communicate at long distances but also give clues to appreciate the targeting capacities of EVs. Of note, we here evaluated stimulation of thyroid folliculogenesis by exogenous EVs, in an environment producing unknown amount of endogenous EVs, and possibly of different composition and specific effects.

The accuracy of EVs to target specific recipient cell is still a matter of debate amongst the scientific community. In a recent review, Van Niel and Raposo state that " probably, the most frequent fate of extracellular vesicles is their targeting to lysosomes" where they would be degraded (van Niel *et al.*, 2018). Even though this degradation would provide some metabolite source for the recipient cells (Zhao *et al.*, 2016), this pathway would strongly argue against target specificity of EVs. On the other hand, Hoshino *et al.* demonstrated that tumor exosomes, via their integrins, were able to target specific organs and prepare metastatic niches (more details on this study are given at point 5.3.4 pg. 51) (Hoshino *et al.*, 2015). I think that one answer to the question of specificity *vs* unspecificity of EVs is that we are lacking precision in the vocabulary that is broadly used (target/targeting) in the literature to describe two completely different phenomena: one unspecific, the incorporation of EVs within cells; and one very specific, the transmission of a message by EVs to cells. Both processes are non-mutually exclusive even if they may still occur independently of each other. My point of view is that, in order to communicate at long distances, cells (in a healthy organ or in a tumor) produce large amount of extracellular vesicles that can spread into the whole body through the blood flow. EVs will be incorporated and degraded by most cells, while only transmitting a message to cells that are equipped to decode its signal (i.e. specific receptor, integrin ligands…).

8.3 Extracellular vesicles: therapeutic tools of the future

In parallel to the study of the natural role and mode of action of extracellular vesicles, another important area of research in the field is their use as therapeutic tools. Despite the lack of solid knowledge in basic field of EV research, a lot of effort is already put on the use of EVs as therapeutic tools. Indeed, as soon as the communication potential of exosomes was demonstrated (Raposo *et al.*, 1996), therapy assays using exosomes were performed already. In 1998, Zitvogel et al. reported eradication of murine tumors using dendritic cells exosomes (Zitvogel *et al.*, 1998). This work led to a first clinical trial using EVs to vaccinate patient against malignant melanoma (Escudier *et al.*, 2005). While this trial was not conclusive, the authors demonstrated the feasibility of large-scale exosome production and the safety of exosome administration to patients.

Those viewing EVs as therapeutic tools follow two main trends: either to harness the intrinsic biological properties of EVs, or to use EVs as drug delivery vehicle. The first option will probably be limited to EVs produced by cells from the immune system (as illustrated in the previous paragraph) or by stem cells. Mesenchymal stem cells have been broadly studied for their regenerative and immunosuppressive effects. Those effects were first attributed to the migration and attachment of MSCs to an injured tissue. However, it is increasingly clear that the effects of MSCs can be attribute to their secretome, including EVs (Zhang *et al.*, 2016a). The molecular mechanisms behind the therapeutic effects of MSC-EVs are still obscure but it has been postulated that those effects could be due to the enrichment of signaling protein (e.g. chemokines, cytokines, interleukins and growth factors) in MSC-EVs (Ferguson and Nguyen, 2016).

To use EVs as drug delivery vehicles, several processes need to be better understood. Regardless of the *in vivo* physiology of EVs and the specificity of interaction with targeted cells that were discussed previously, using EVs as drug delivery vehicle require to find ways to produce or synthetize EVs, and to load them with a specific cargo. In 2013 the group of Yong Song Gho was the first to achieve exosome-mimetic nanovesicle (NV) production by submitting monocytes to serial extrusion through filters with decreasing pore size. The authors were able to load NV with doxorubicin and induce endothelial cell death both *in vitro* and *in vivo*. Interestingly, the author noticed that they were able to obtain 100-fold higher yield of vesicles using serial extrusion as compared with classical EV production in cell culture. Furthermore, they demonstrated that doxorubicin-loaded NV had fewer side effects and were more effective than the classical doxorubicin treatment (Jang *et al.*, 2013). More recently, using the same protocol for NV production, Lunavat et al. were able to load miRNA in NV by direct NV electroporation. Furthermore, the authors demonstrated that the NV-loaded miRNA were active *in vitro* in target cells (Lunavat *et al.*, 2016). Lots of effort are being done on modification of exosomes at the cellular level (i.e. before their release), and on post-isolation modification of *in vitro* produced exosomes. Recently, Yin *et al.* proposed a very elegant light-dependent double fusion protein tool to load preferential molecules into HEK293T exosomes (Yim *et al.*, 2016). This tool is described as “engineered exosomes for protein loading via optically reversible protein–protein interactions” and relies on two-fusion protein, transiently expressed in cells. One fusion protein is composed of a photoreceptor (CRY2) linked with the cargo of interest. The second fusion

protein is composed of a truncated CRY-receptor (CIBN) linked to an exosome-associated tetraspanin (e.g. CD9). Light stimulation of the cytoplasm induces a transient docking of CRY2-cargo to CIBN-CD9 and the cargo is introduced into the intraluminal vesicles (ILVs) during the biogenesis process. Once introduced into the ILVs, the cargo is detached from CIBN-CD9 by switching off the light source. This tool provides an excellent solution for an efficient intracellular delivery of soluble proteins into exosomes (Yim *et al.*, 2016). As stated, it is also possible to modify exosomes after isolation. Modification of the surface of exosomes by adding a fluorescent molecule to pre-engineered exosomes could be a powerful tool to track them and determine their fate *in vivo* (**Fig. 21A**). Modification of exosome surface molecules as well as loading hydrophobic and hydrophilic molecules into exosomes could have a therapeutic impact (**Fig. 21**) (Hood, 2016).

Unfortunately, those promising breakthrough will only be useful once we better understand the fate of EVs *in vivo* and when it will be proven that therapeutics through EVs have limited off-target effects.

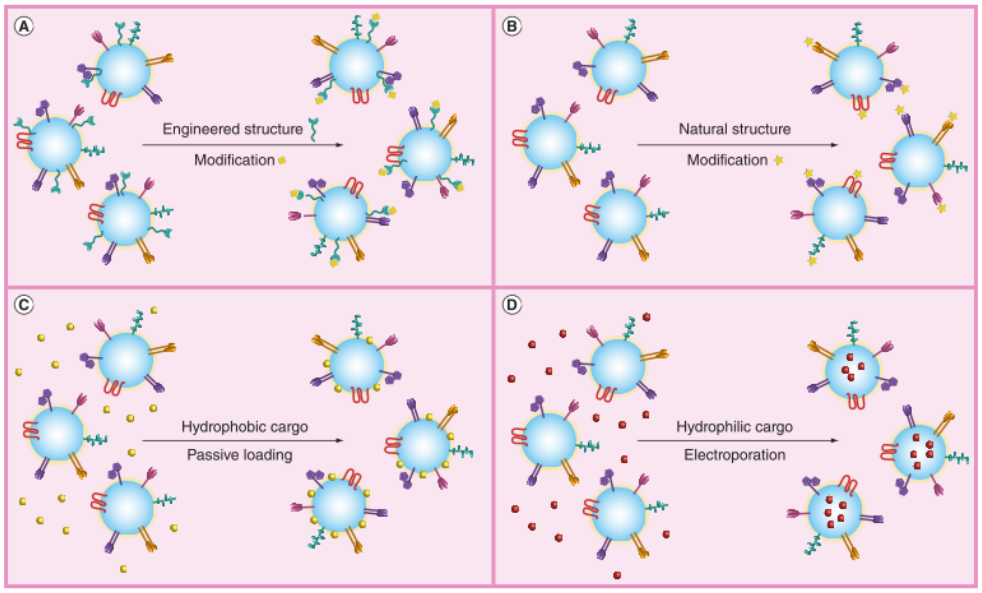

Figure 21: Post-isolation modification of exosomes produced *in vitro*. A, Modification of a pre-engineered structure could allow *in vivo* tracking of exosomes. B, modification of a protein at the surface of exosomes could shift the effect on the target cell. C and D, hydrophobic and hydrophilic cargo loading to use exosomes as therapeutic nanocarriers. (Hood, 2016)

8.4 Introducing extracellular vesicles into thyroid ontogenesis

As mentioned in the introduction, the developing thyroid gland migrates into different environment, suggesting that EV from different cell types (i.e. epithelial, mesenchymal or endothelial) could impact thyroid development at several key steps of the process (e.g. specification, budding, migration, bilobation or folliculogenesis). Here, I focused on endothelial-produced EVs during follicle formation and expansion.

What did we learn from the *Vegfa* KO study? (Hick *et al.*, 2013)

At early stage of thyroid development, thyrocyte progenitors produce large amount of the angiocrine factor, VEGFa, resulting in efficient recruitment of endothelial cells into the mass of thyrocyte progenitors and ultimately leading to formation of the thyroid angiofollicular units. By knocking-out *Vegfa* in thyrocyte progenitors, my host laboratory was able to prevent endothelial cells recruitment. More interestingly, it was observed that, in absence of endothelial cells, thyroid follicles formation was impaired, suggesting that endothelial cells play an important role in thyroid follicle formation.

Using a VEGFR2 inhibitor in an *ex vivo* system of thyroid explant cultures, the phenotype observed *in vivo* by depletion of endothelial cells was fully reproduced. Furthermore, this phenotype could be rescued by adding embryonic endothelial progenitor cells (EPCs) to endothelium-depleted explants. To test a contact-independent role of endothelial cells in the folliculogenic process, endothelium-depleted explants were incubated with medium conditioned by EPCs (EPC-CM). Strikingly, EPC-CM was able to rescue thyroid follicle formation, indicating that endothelial cells secrete one or several factor(s) that promote(s) thyroid folliculogenesis.

What did we learn from the *Smad1/5* double KO study? (Villacorte *et al.*, 2016)

Our lab further showed that inactivation of *Smad1* and *Smad5* in thyroid progenitors causes a defective follicle phenotype, similar to the *Vegfa* KO. However, in the *Smad1/5* dKO, endothelial cell recruitment and density was similar to wild type thyroid. This suggests that the BMP intracellular signaling mediated by

Smad1/5 in thyrocyte progenitors is downstream of the endothelial cell signal or parallel. Surprisingly, incubation of *Smad1/5* dKO thyroid explants with EPC-CM also rescued follicle formation.

Deeper *in vivo* analysis of *Vegfa* KO and *Smad1/5* dKO revealed basement membrane defects, suggesting a concerted action of endothelial cell signaling and thyrocytes Smad1/5 intracellular signaling on the deposition or assembly of the basement membrane. Using mass spectrometry for proteomic analysis, laminin-α1, -β1 and -γ1 were identified as top hits. To test the hypothesis that laminin111 could mediate the folliculogenic effect of EPC-CM, the authors knocked-down laminin-α1 in EPCs and tested the CM produced by KD-EPCs on thyroid explants. Conditioned medium from EPC cells depleted of laminin-α1 did not promote folliculogenesis, indicating that EPCs promote thyroid follicle formation through deposition of laminin111.

This led to the proposal that, *in vivo*, endothelial cell recruitment and invasion in the thyroid mass, together with thyrocyte Smad1/5 signaling, act to promote basement membrane formation. Basement membrane deposition would then orient thyrocyte progenitor and promotes follicle formation.

What is the role of extracellular vesicles in thyroid development?

During my thesis, I demonstrated that EPCs also produce extracellular vesicles (EVs) in the conditioned medium, and that EPC-EVs are able to stimulate thyroid follicle formation in *ex vivo* culture of thyroid explants. However, proteomic analysis on EPC-EVs revealed that laminin111 was co-isolated with EPC-EVs during the isolation procedure, raising the possibility that the folliculogenic effect attributed to the high-speed pellet could be due to laminin111 (as suggested by Villacorte *et al*. 2016) and not to EVs.

To distinguish between these two possibilities, I first resorted to laminin-α1 KD-EPC and tested the effect of EVs harvested therefrom on thyroid explants. Such KD-EPC-EVs did not promote thyroid folliculogenesis, arguing against a role of EPC-EVs in thyroid follicle formation. However, biochemical characterization of EVs from KD-EPCs displayed differences (i.e. decreased signal) in EV markers as compared with wild-type EPC-EVs, suggesting that KD-EPC might produce either less EVs or a different set of EVs as compared to wild-type EPCs.

I then used another strategy to separate EVs from laminins. I floated EPC-EVs in an iodixanol gradient to separate the low-density EVs-rich from the high-density protein complexes (i.e. laminin111). Then, the folliculogenic activity of the EV-rich fractions and proteins/laminin111-rich fractions were tested on thyroid explants. As expected, EV-depleted laminin111-rich fractions stimulated thyroid follicle formation. However, laminin111-depleted EPC-EVs were also able to stimulate thyroid follicle formation.

Altogether, my results suggest that (i) EPCs produce EVs, (ii) EVs production depends partially on laminin production, and (iii) both laminin-depleted EV-rich and EV-depleted laminin-rich fractions are able to stimulate thyroid folliculogenesis *ex vivo*. It now remains to examine, *in vivo*, whether endothelial cell recruitment is associated with increased EV production around the thyroid.

Reviewing the timeline of thyroid follicles formation

Combining the results obtained by our laboratory, I would like to propose an updated model for follicle formation during thyroid embryogenesis. This model should stimulate and define further experimental challenges.

In this model based on intimate connections between thyrocyte progenitors and endothelial cells, I propose that, as demonstrated by Hick et al., a first message is sent by thyrocyte progenitors to endothelial cells through production of the angiocrine messenger VEGFa (**Fig. 22A**). This results in the recruitment of endothelial cells. Conversely, endothelial cells, while invading the mass of thyrocyte progenitors, produce extracellular vesicles that trigger or facilitate intracellular Smad1/5 signaling in thyrocyte progenitors (**Fig. 22B**). In turn, Smad1/5 signaling in thyrocyte progenitors promotes the production and assembly of basal lamina components that sustains the polarization of thyrocyte progenitors and their organization into follicular structures (**Fig. 22B**), ultimately forming the angiofollicular units in association with the surrounding endothelial cells. Of note, difficulties, presented in the introduction, for EVs to access the tissue would not be problem in the present model if, indeed, endothelial-produced EVs trigger basement membrane production and promote lumen expansion of developing angio-follicular units.

This cascade of events is supported by the following experimental observations: (i) endothelial cells are required for follicle expansion, (ii) EPC-EVs promote thyroid follicles formation independently of laminin111, and (iii) despite the presence of endothelial cells, *Smad1/5* dKO do not assemble a basal lamina and do not form follicle *in vivo*. In this cascade, the mode of action of endothelial cell-released EVs on the Smad1/5 signaling pathway needs to be demonstrated. However, before digging into the molecular mechanism, a critical rescue experiment should be performed: to test the folliculogenic activity of the EV-rich and laminin-rich fractions, combined and separated, on *Vegfa* KO and *Smad1/5* dKO thyroid. If the model is correct, both fractions should rescue the *Vegfa* KO phenotype, while the *Smad1/5* dKO phenotype should be rescued by the laminin-rich fraction but not by the EV-rich fraction.

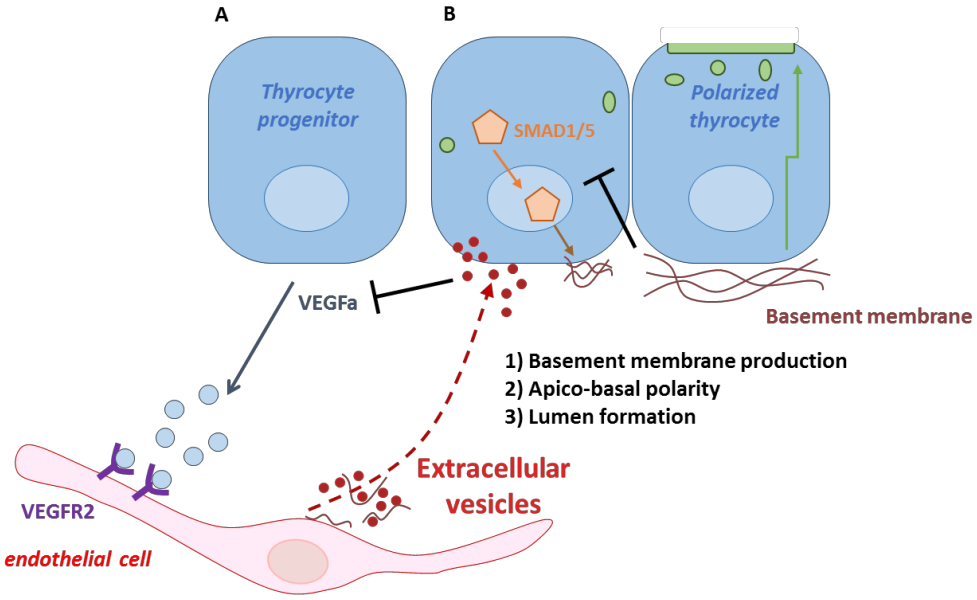

Figure 22: Extracellular vesicles-mediated instruction of thyrocyte progenitors promotes thyrocytes' polarization and organization in follicles. **A**, the mass of thyrocyte progenitors produce VEGFa to recruit endothelial cells. **B**, while invading the mass of thyrocyte progenitors, endothelial cells produce extracellular vesicles that will induce basement membrane components production (1) through SMAD1/5 signaling. In turn, basement membrane establishment will trigger polarization of thyrocytes (2) and lumen formation (3) to obtain a follicular architecture.

9 Annex

Bioprinting of functional vascularized mouse thyroid gland construct

Elena A. Bulanova*, Elizaveta V. Koudan*, Jonathan Degosserie, Charlotte Heymans, Frederico Pereira, Vladislav A. Parfenov, Yi Sun, Qi Wang, Suraya A. Akhmedova, Irina K Sviridova, Natalia S. Sergeeva, Georgy A. Frank, Yusef D. Khesuani, Christophe E. Pierreux and Vladimir A. Mironov

*Authors contributed equally to this work

This project was collaboration with the laboratory of Vladimir Mironov, from the Laboratory for Biotechnological Research '3D Bioprinting Solution', Moscow, Russia. Our lab trained the main investigators (Dr. Bulanova and Miss Koudan) to thyroid explants culture and immunostaining. We performed all confocal microscopy image acquisitions and helped with the manuscript.

Biofabrication

PAPER

Bioprinting of a functional vascularized mouse thyroid gland construct

RECEIVED
16 April 2017

REVISED
22 June 2017

ACCEPTED FOR PUBLICATION
14 July 2017

PUBLISHED
18 August 2017

Elena A Bulanova[1,6], Elizaveta V Koudan[1,6], Jonathan Degosserie[2], Charlotte Heymans[2], Frederico DAS Pereira[1], Vladislav A Parfenov[1], Yi Sun[3], Qi Wang[3], Suraya A Akhmedova[4], Irina K Sviridova[4], Natalia S Sergeeva[4], Georgy A Frank[5], Yusef D Khesuani[1], Christophe E Pierreux[2] and Vladimir A Mironov[1]

[1] Laboratory for Biotechnological Research '3D Bioprinting Solutions', Moscow 115409, Russia
[2] de Duve Institute, Université Catholique de Louvain (UCL), B-1200 Brussels, Belgium
[3] Department of Mathematics and Interdisciplinary Mathematics Institute, University of South Carolina, Columbia, SC 29208, United States of America
[4] National Medical Research Radiological Centre of the Ministry of Health of the Russian Federation, Moscow 125284, Russia
[5] Russian Medical Academy of Postgraduate Education Studies, Moscow 125993, Russia
[6] Both authors contributed equally to this paper.

E-mail: vladimir.mironov54@gmail.com

Keywords: 3D bioprinting, mouse thyroid gland, tissue spheroids, vascularization

Supplementary material for this article is available online

Abstract

Bioprinting can be defined as additive biofabrication of three-dimensional (3D) tissues and organ constructs using tissue spheroids, capable of self-assembly, as building blocks. The thyroid gland, a relatively simple endocrine organ, is suitable for testing the proposed bioprinting technology. Here we report the bioprinting of a functional vascularized mouse thyroid gland construct from embryonic tissue spheroids as a proof of concept. Based on the self-assembly principle, we generated thyroid tissue starting from thyroid spheroids (TS) and allantoic spheroids (AS) as a source of thyrocytes and endothelial cells (EC), respectively. Inspired by mathematical modeling of spheroid fusion, we used an original 3D bioprinter to print TS in close association with AS within a collagen hydrogel. During the culture, closely placed embryonic tissue spheroids fused into a single integral construct, EC from AS invaded and vascularized TS, and epithelial cells from the TS progressively formed follicles. In this experimental setting, we observed formation of a capillary network around follicular cells, as observed during *in utero* thyroid development when thyroid epithelium controls the recruitment, invasion and expansion of EC around follicles. To prove that EC from AS are responsible for vascularization of the thyroid gland construct, we depleted endogenous EC from TS before bioprinting. EC from AS completely revascularized depleted thyroid tissue. The cultured bioprinted construct was functional as it could normalize blood thyroxine levels and body temperature after grafting under the kidney capsule of hypothyroid mice. Bioprinting of functional vascularized mouse thyroid gland construct represents a further advance in bioprinting technology, exploring the self-assembling properties of tissue spheroids.

Introduction

The thyroid gland is an endocrine organ required for the production of hormones such as thyroxine (T4) and triiodothyronine (T3). These are essential for normal growth, neurological development and homeostasis. Hypofunctionality of the thyroid gland or its complete removal due to thyroid cancer requires compensation for the lost function [1]. Hypothyroidism is usually treated with synthetic hormone replacement therapy, which is a lifelong treatment [2]. Although hormone replacement therapy does provide a certain level of thyroid hormones it almost completely excludes fine regulation of thyroid status according to current physiological conditions. The use of autologous thyrocytes and thyroid follicles derived

from induced pluripotent stem cells opens up the unique possibility of developing a new therapeutic modality to compensate for loss of thyroid function and eliminate the subsequent lifelong dependence of patients on treatment with synthetic hormones [3].

The recent advances in rapidly emerging three-dimensional (3D) bioprinting technology will eventually enable the biofabrication of functional and vascularized tissue from autologous human cells suitable for clinical transplantation [4]. The original concept of robotic layer-by-layer biofabrication of 3D human tissues and organs according to a digital model, using tissue spheroids as building blocks, was proposed more than a decade ago and has been gradually improved [5–8]. Tissue fusion is a recurrent process during embryonic development [9] and a fundamental biomimetic principle of the proposed 3D bioprinting technology. The fusion of closely placed tissue spheroids enables rapid post-printing self-assembly of the 3D tissue construct.

The anatomical and histological structure of the thyroid gland is relatively simple compared with more complex organs such as the lung, liver or kidney due to the absence of a ductal system. The thyroid gland is thus an attractive target for testing the feasibility of bioprinting technology. The structural and functional unit of the thyroid gland consists of independent thyroid follicles composed of a polarized epithelium surrounded by fenestrated blood capillaries, thereby enabling import of iodine and delivery of thyroid hormones directly into the blood circulation. Branched segments of thyroid arteries and veins are connected with microvessels of multiple angio-follicular units and form the vascularized thyroid gland [10]. Moreover, it has been demonstrated recently that thyroid folliculogenesis is closely associated with and guided by angiogenesis [11], thus indicating that during thyroid organogenesis the level of vascularization regulates functional differentiation of thyroid follicles.

Vascularization, i.e. the development of a microvascular network, remains a big challenge and a major technological impediment in bioprinting. The microvascular network within an engineered tissue should maintain high cell viability and function, providing the requisite nutrients and oxygen. Without vasculature the size of a bioprinted construct is limited to 200 μm, the diffusion limit of oxygen [12]. Different approaches exist for engineering vascularized tissues. The classical seeding of sacrificial scaffolds with endothelial cells (EC) supported by angiogenic factors has showed promising results but is limited to construction of simple tissues only [13, 14]. Theoretical research based on mathematical modeling and computer simulation [15], along with a growing body of experimental evidence [16], strongly indicates that it is possible to bioprint 3D tissue and organ constructs with a built-in intra-organ branched vascular tree using different types of self-assembling vascular tissue spheroids as building blocks. It has been shown that: (i) solid vascular tissue spheroids could be effectively used for biofabrication of large-diameter extraorgan and intra-organ arterial and venous blood vessels [6]; (ii) lumenized vascular tissue spheroids could be used for biofabrication of arteriolar and venular vascular segments with intermediate diameter [9, 17]; and, finally, (iii) prevascularized organospecifc tissue spheroids or adjacently placed endothelial tissue spheroids could be used for bioprinting of tissue constructs with a well-developed microvascular network [18]. We propose a solid scaffold-free approach in which the 'self-assembling spheroid' strategy enables generation of a complex bioprinted tissue construct with a built-in vascular system consisting of hierarchically branched blood vessels.

In our previous paper [19] we demonstrated that tissue spheroids when closely placed in fusion-permissive collagen hydrogel can coalesce and form a toroid-like construct, exactly as predicted by mathematical modeling and computer simulation. Here we report the bioprinting of a functional and vascularized mouse thyroid gland construct using two types of tissue spheroids, thyroid spheroids (TS) and allantoic spheroids (AS), obtained from embryonic thyroid and allantoic tissues, respectively. We demonstrate that EC from AS are endowed with the capacity to completely vascularize thyroid explants, even when the endothelial pool of TS is ablated by selective inhibition of vascular endothelial growth factor receptor 2 (VEGFR2). More importantly, we confirmed the functionality of bioprinted tissue construct in radioiodine-ablated thyroid (hypothyroid mice).

Materials and methods

Reagents and materials

The following reagents and materials were used: Hank's Balanced Salt Solution (Paneco, cat. no. R020), tungsten wire (Goodfellow, cat. no. W 005160), anti-E-cadherin (BD Biosciences, cat. no. 610182, 1:1000), anti-Ezrin (Thermo Scientific, cat. no. MS-661-P1, 1:400), anti-PECAM (BD Biosciences, cat. no. 550274, 1:100), anti-caspase-3a (Cell Signaling, cat. no. 9661), anti-pHH3 (Cell Signaling, cat. no. 9701), anti-TTF1 (Dako, cat. no. M3575), Hoechst 33258 (Sigma, cat. no. B2883), Alexa Fluor 488 goat anti-mouse IgG1 (γ1) antibody (Thermo Scientific, cat. no. A-21121), Alexa Fluor 647 goat anti-mouse IgG2a (γ2a) (Thermo Scientific, cat. no. A-21241), Alexa Fluor 647 chicken anti-rat IgG (H + L) (Thermo Scientific, cat. no. A-21472), sodium hydroxide (Merck, cat. no. 106498), sodium bicarbonate (Paneco, cat. no. F022), phosphate-buffered saline (PBS; Gibco, cat. no. 18912-014), Corning Transwell®-COL collagen-coated polytetrafluoroethylene (PTFE) membrane inserts (Corning, cat. no. 3491, 0.4 μm), gelatin (Fluka, cat. no. 48723-500G-F), sucrose (Sigma, cat. no.

S0389), SU5416 (Cayman, cat. no. 13342), 100 mm plastic cell culture dish (Corning, cat. no. 430167).

Complete culture medium

The complete culture medium comprised Dulbecco's modified Eagle's medium (DMEM; Gibco, cat. no. 12491-015) containing 10% fetal bovine serum (FBS; Gibco, cat. no. 16000-044) supplemented with an antibiotic/antimycotic mix (Gibco, cat. no. 15240-062) and 1 mM L-glutamine (Paneco, cat. no. F032).

Collagen isolation from rat tails and collagen gel preparation

Rat tail type I collagen was prepared according to the method described by Rajan *et al* [20]. The established concentration of collagen in solution was 3.12 mg ml^{-1}. For preparation of collagen gel 890 μl of collagen solution was mixed with 60 μl of 1 M sodium hydroxide, 250 μl of 7.5% sodium bicarbonate and 300 μl of PBS.

Generation of spheroids

Thyroid explants were microdissected from e14.5 mouse embryos as described by Delmarcelle *et al* [21]. Allantoic tissue was microdissected from e8.5 mouse embryos as described by Drake and Fleming [22]. Dissection was not performed under a sterile atmosphere, so explants and allantoides were washed several times in sterile culture medium. Individual thyroid explants and allantoides were then suspended in 20 μl of complete culture medium and spotted onto the underside of a lid of a 100 mm plastic cell Petri dish. The lids were then inverted and placed onto culture dishes to create hanging drops. SU5416 (VEGFR2 kinase inhibitor) was dissolved in dimethyl sulfoxide (DMSO; 20 mM stock solution) and added at 5 μM to the culture medium for thyroid explants. Control thyroid explants were exposed to the same concentration of vehicle as the test samples. The hanging drop cultures were placed in a humidified atmosphere and cultured at 37 °C, 5% CO_2 for 18–24 h. After 18–24 h of culture, the resulting spheroidal thyroid explants and allantoides were used for bioprinting of mouse thyroid gland constructs.

Kinetics of spheroid fusion

Fusion angles between adjacent spheroids were measured as described by Susienka *et al* [23]. Briefly, fusion angles were measured manually and plotted as a function of time using GraphPad Prism software (GraphPad Software, Inc., La Jolla, CA, USA).

Bioprinting process

To print the thyroid mouse gland construct within the collagen hydrogel spread on a transparent PTFE membrane we used a multifunctional Fabion 3D bioprinter with the turnstile system (see figures 3(A)–(C)). This device consists of the following functional systems: syringe pump; fluidic chip; loading piston (d); trapping piston (e); depositing piston (f) with groove for liquid removal (g) (figure 3(B)). The syringe loaded with spheroid suspension was installed into the syringe pump and thus connected to printing head. As soon as the spheroid suspension entered the printing head, the automation system switched the syringe pump on and then switched it off at the moment when spheroids came into contact with trapping piston. The depositing piston (f) moved upward, closing the liquid removal outlet (g) and freeing the channel for spheroid passage; the trapping piston (e) slides downward, opening the passage for spheroids. Then loading piston (d) immediately moved the spheroids rightward and under the depositing piston (f). The depositing piston transported spheroids downward until contact with the printing surface and then returned to its initial position, thus completing one bioprinting cycle. The depositing piston features a groove slightly above the base (g) providing a channel for the draining of liquid. This resource is applied to minimize the amount of liquid being deposited with the tissue spheroids. This section with reduced diameter is positioned between the outlet and the horizontal channel. A vacuum pump removes the liquid, while the tissue spheroids are held in place by the piston itself.

The bioprinter has three air-free syringe dispensers, with one of them able to keep the temperature down to 4 °C, one spray nozzle and one pneumatic syringe dispenser. The *XY* table moves with the resolution of 5 μm and has a heating base with a maximum temperature of 100 °C. An experimental single spheroid printer head was developed in house and took the place of one syringe for this experiment. The configuration was designed for convenient incorporation into a bioprinter and subsequent maintenance. The printing head module can be sterilized with either UV irradiation or ethyl alcohol aqueous solution.

To enable collagen hydrogel printing, a special cooling/heating system was developed in house. The system consists of a controllable heating aluminum base (with temperature is ranging from room temperature up to 200 °C in steps of 0.1 °C) and a cooling system (with temperature ranging from room temperature down to −4 °C in steps of 0.1 °C) to cool down the syringe contents. Supplementary figure 2(A), available online at stacks.iop.org/BF/9/034105/mmedia, shows the elements and their connections. The temperature of the syringe was controlled by a cooling system based on a Peltier module. This module allowed cooling by a recirculating liquid that transfers the heat via a coiled bronze tube around the syringe. The cooled syringe kept the collagen mix liquid at 4 °C. The base plate uses a cartridge heater to change its temperature up to 100 °C. Upon deposition on the heated plate (28 °C), the collagen mix polymerizes, allowing a controlled 3D print shape (supplementary figures 2(B), (C)).

Culture of printed thyroid constructs

After the printing, thyroid gland constructs were further cultured within collagen hydrogel spread on the surface of a transparent PTFE membrane for 4 days. The culture medium did not cover the printed constructs but reached the level of the PTFE membrane to allow better oxygenation of the tissue. After 4 days in culture the printed samples were subjected to immunolabeling or grafting. Bright-field imaging was performed on a Nikon Eclipse Ti-E inverted microscope with a Nikon DS-Qi2 camera. Images were processed with NIS-Elements D Research software version 4.0. Photoshop CS5 (Adobe) was used to adjust brightness, contrast and picture size.

Immunolabeling

After the culture, printed constructs were fixed at 4 °C in 4% paraformaldehyde in PBS for 2 h, transferred in sucrose 20%/PBS and then embedded in 15% sucrose/7.5% gelatin/PBS. Immunofluorescence on thin tissue sections was performed as described [24]. Primary antibodies and dilutions were as follows: monoclonal mouse anti-E-cadherin at 1:250, rat anti-PECAM at 1:100, monoclonal mouse ant-Ezrin at 1:300, rabbit anti-caspase-3a at 1:200, rabbit anti-pHH3 at 1:100, monoclonal mouse anti-TTF1 at 1:200. Nuclei were counterstained with Hoechst in PBS during incubation with secondary antibodies. Fluorescence on sections was observed with a Zeiss Cell Axiovert 200 inverted fluorescence microscope or with a Zeiss Cell Observer Spinning Disk (COSD) microscope.

Generation of ^{131}I-induced hypothyroidism mouse model and transplantation of bioprinted mouse thyroid gland constructs

A hypothyroidism mouse model was generated as described previously [25, 26]. Briefly, experimental hypothyroidism was induced by administering 150 μCi of [^{131}I] by intraperitoneal injection to mice. Eight weeks after the administration of [^{131}I], plasma levels of T4 were analyzed to confirm the hypothyroid status. For transplantation of bioprinted mouse thyroid gland constructs the hypothyroid mice were anesthetized with 5 ml kg^{-1} of an anesthetic solution composed of a 5% solution of ketamine (Moscow Endocrine Plant, Russia) and 2.5 mg ml^{-1} droperidol (Moscow Endocrine Plant), then constructs were placed under the renal capsule using a blunt-pointed needle. After surgery, the skin wound was treated with gluten BF-6 (Vertex, Russia). Three and 5 weeks later, the grafted mice were subjected to body temperature measurement, blood sampling for plasma T4 measurements and 5 weeks after transplantation sacrifice for histological examination of the kidneys.

All mice were of the CD1 strain. Mice were raised and treated according to the principles of laboratory animal care of the institute's animal ethical committee. All animal experiments and care were in compliance with institutional guidelines and local ethical committees. Animals were maintained on a 12 h light/12 h dark schedule (light on at 6 am) and fed with laboratory chow and water *ad libitum*.

Body temperature measurement

Body temperature was measured in conscious mice using a 'Precision' 841 thermometer (RST, cat. no. RST07841). Animals were restrained and kept motionless to obtain a stable body temperature.

Plasma T4 level measurements

The total T4 level was assayed using a T4 mouse/rat enzyme-linked immunosorbent assay (ELISA) kit (BioVision, cat. no. K7421-100), according to the manufacturer's instructions.

Results

Mathematical modeling and computer simulation of bioprinted thyroid gland

In order to demonstrate the feasibility of using tissue spheroids as building blocks in 3D bioprinting we first started with mathematical modeling and computer simulation (figure 1). We capitalized on previously published data and experimental results, which reported 3D bioprinting of sequential segments of a branched vascular tree. Here, for the first time, we report mathematical modeling and computer simulation for biofabrication of a complete intra-organ branched vascular tree including proximal and distal vascular segments. The fusion of spheroids composed of tightly packed epithelial cells or EC was theoretically modeled and simulated. To investigate the fusion process, a multicellular lattice-based model, which describes the interactions between cells based on the differential adhesion hypothesis (DAH), was used [27]. This hypothesis states that: (i) cell adhesion in multicellular systems depends on energy differences between different cell types and (ii) cells in aggregates are motile enough to reach the configuration which minimizes the interfacial energy of the system. In the model, each site of a 3D cubic lattice is occupied either by a cell or a similar-sized volume unit of hydrogel medium. For simulation of the evolution of a multicellular system, the kinetic Monte Carlo (KMC) method was applied [28]. In the KMC method, self-assembly of cells in the cellular aggregate system is described in terms of the transition rates corresponding to possible conformational changes of the system, and then the corresponding time evolution of the system is expressed in terms of these rates. The dynamics of the cells depend on the transition rates of cell swapping with adjacent cells of different type and/or with hydrogel particles [29, 30], which are given by

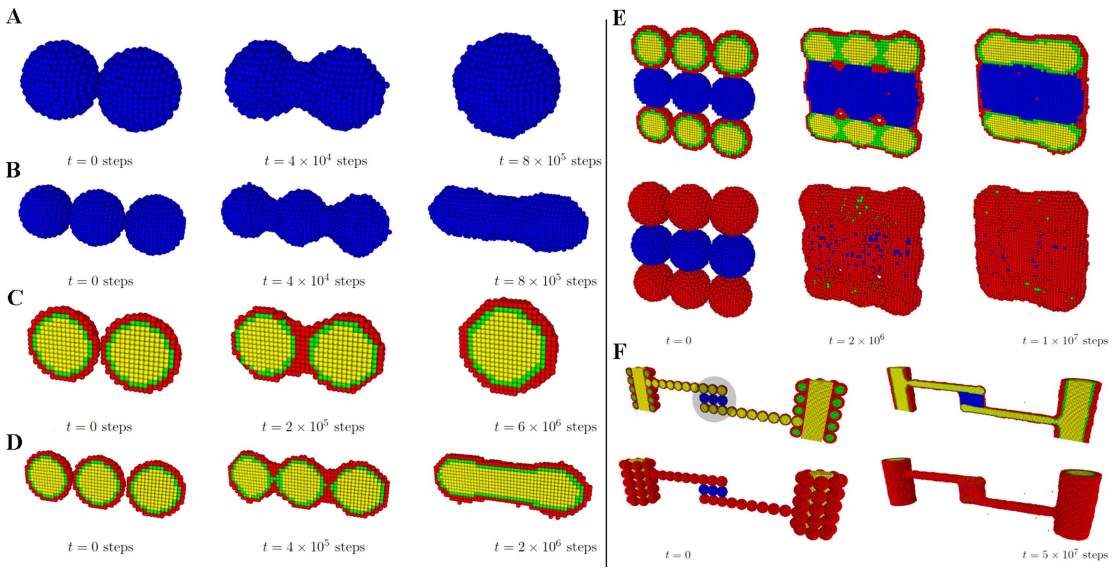

Figure 1. Mathematical modeling and computer stimulation of fusion processes starting from different initial settings for bioprinting of mouse thyroid gland construct. (A) Time evolution of the fusion between two thyroid spheroids (TS) in KMC simulations. Initially, each spheroid contains 2176 cells. The three snapshots are taken at $t = 0, 4 \times 10^4$ and 2×10^6 steps, respectively. (B) Time evolution of three fusing TS. The three snapshots are taken at $t = 0, 4 \times 10^4$ and 8×10^5 steps, respectively. (C) Time evolution of two fusing vascular spheroids. Initially, each spheroid contains 1336 cells, which include 848 smooth muscle cells (SMCs in red) in the outer layer and 488 endothelial cells (ECs in green) in the inner layer that engulfs 840 internal hydrogel medium particles (in yellow). The three snapshots of cross-sectional views are taken at $t = 0, 2 \times 10^5$ and 6×10^6 steps, respectively. (D) Time evolution of three fusing vascular spheroids. The three snapshots of cross-sectional views are taken at $t = 0, 4 \times 10^5$, and 2×10^6 steps, respectively. (E) Time evolution of a system of six vascular spheroids with three TS in the middle, which form the central part of the bioprinted thyroid gland. The three snapshots of cross-sectional views (top) and external views (bottom) are taken at $t = 0, 2 \times 10^6$ and 1×10^7 steps, respectively. (F) Time evolution of a system of vascularized thyroid gland construct with two large-diameter vessels fabricated from vascular tissue spheroids. The two snapshots of cross-sectional views (top) and external views (bottom) are taken at $t = 0$ and 5×10^7 steps, respectively.

the Arrhenius relation. In each step, the transition rates for all possible changes from the current configuration are calculated and then a new configuration is chosen with a probability proportional to the rate of the corresponding transition. Figures 1(A)–(D) depict the computer simulations of the fusion processes between two or three tissue spheroids from different initial settings for bioprinting of the thyroid gland construct. Next, in order to examine the bioprinting settings we modeled the fusion of three TS surrounded by six vascular spheroids which form the core structure of the engineered thyroid construct (figure 1(E)). This particular setting was then tested experimentally (see below). The model of thyroid gland construct (see inside the circle) is placed in the context of branched vascular tree bioprinting using self-assembly of vascular tissue spheroids (figure 1(F)). Such an approach is necessary in the case of orthotopic implantation using surgical vascular anastomoses. In the case of heterotopic implantation under a highly vascularized kidney capsule, which has been implemented in our study, the proposed bioprinting of a complete branched vascular tree is not required to achieve a desirable level of vascularization in the implanted thyroid gland construct.

A detailed description of the mathematical model and computer simulation is given as supplementary information (SI).

Generation of tissue spheroids from mouse thyroid and allantoides

Based on the self-assembly principle, we aimed to print mouse thyroid gland constructs using rounded mouse embryonic thyroid explants for the follicular compartment and rounded mouse allantois explants as a vascular, i.e. EC, source. Thyroid explants were microdissected from e14.5 mouse embryos as described in [21] and cultured overnight in a hanging drop to obtain rounded pieces of tissue suitable for bioprinting (figure 2(A)). It has been demonstrated previously that mouse embryonic thyroid folliculogenesis starts at e14.5 and is concomitant with vascularization of embryonic thyroid tissue [11, 21].

Allantoides were microdissected from e8.5 mouse embryos as described in [22] and cultured overnight in a hanging drop to obtain rounding of the tissue pieces (figure 2(B)). Dissected e8.5 mouse allantoides have an elongated rod-like shape and consist of cells with angioblastic phenotype. It has been previously reported that isolation of allantoides at this stage with sequential incubation in hanging drop in the presence of VEGF induces endothelial differentiation and formation of a cluster of EC, with subsequent generation of blood microvessels [22]. Allantoides were thus used as a source of EC; thyroid explants as a source of follicular cells and of VEGF [21].

When thyroid explants and allantoides were cultured in hanging drops, they took on a spherical shape overnight

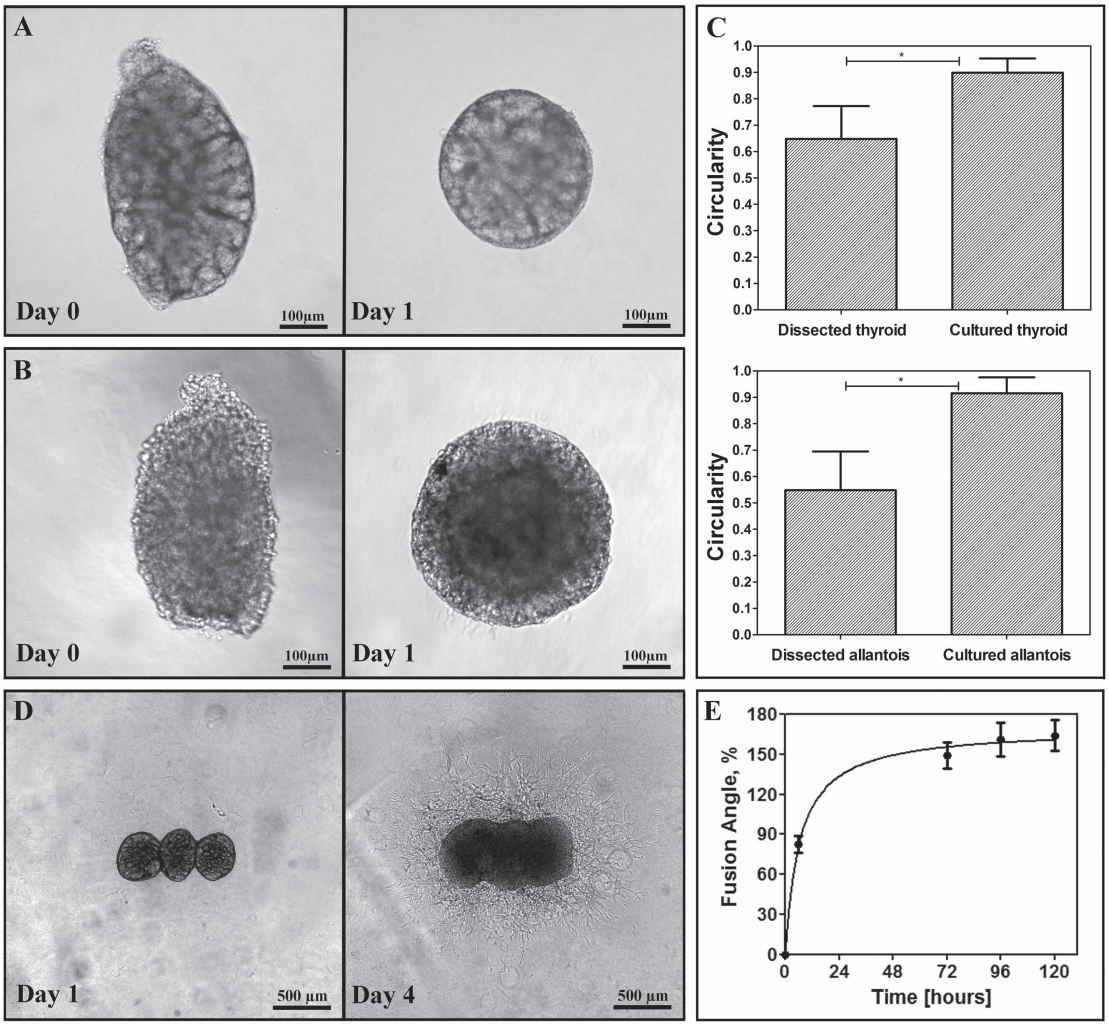

Figure 2. Generation of rounded building blocks for mouse thyroid gland construct printing. Representative images of dissected tissue and spheroids of thyroid lobes (A) and allantoides (B) after hanging drop culture. The circularity before and after hanging drop culture was calculated (C). The circularity of thyroid lobes and allantoides increased after hanging drop culture. An unpaired *t*-test was used for statistical analysis ($^*P < 0.001$). (D) Fusion of three thyroid spheroids (TS) within collagen gel after 4 days. TS fused completely and formed a solid flattened construct with thin sprouts. The fusion angle between individual spheroids increased up to 162 °C showing complete spheroid fusion (E).

with mean outer diameters of 388.2 μm $\pm$ 45.3 ($n = 168$) and 493.6 μm $\pm$ 114.3 ($n = 28$), respectively. On assessing the circularities of AS and TS, they were estimated close to a value of 1.0, 0.92 $\pm$ 0.06 ($n = 28$) and 0.90 $\pm$ 0.05 ($n = 168$), respectively, indicating an almost perfect circle (figure 2(C)). This study was performed using Image J software (NIH, Bethesda, MD, USA).

Fusion of thyroid explants and allantoides in a hanging drop and within collagen hydrogel

In order to investigate the capacity of TS to fuse, a pair of them of equal size were first placed in contact with each other in a hanging drop and incubated overnight (supplementary figure 1(A)). Eighteen hours later they were found to merge together as a single spheroid (supplementary figure 1(B)). This fusion was observed in the case of a pair of allantoides as well, incubated under similar conditions. Fusion is an inherent property of tissue spheroids, and hence this acts as a proof of principle that spheroids can be used as building blocks in our bioprinting technology.

We then evaluated the consequence of fusion of embryonic TS under conditions in which the spheroids are capable of engaging in adhesive interactions with their culture environment. For that matter, three spheroids were placed within collagen hydrogel (figure 2(D)). In contrast to the spherical structure generated earlier, an oviform, elongated structure was formed within the collagen. A few cells, endowed with migratory properties, left the elongated structure and invaded the 3D collagen hydrogel. The cohesiveness of the TS was measured using the fusion angle, which increased to 162 °C during culture within the collagen gel indicating complete spheroid fusion (figure 2(E)).

We concluded that TS and AS are endowed with the property of endogenous fusion, thereby validating their use as building blocks for organ bioprinting technology.

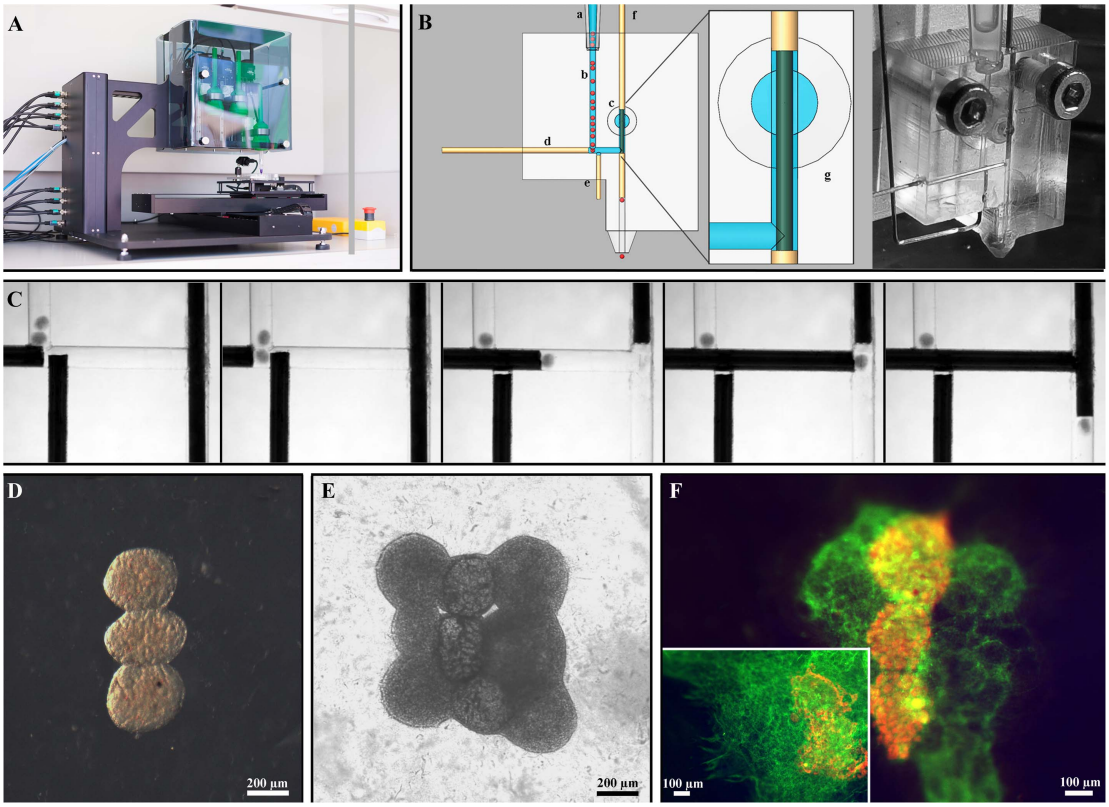

Figure 3. Bioprinting of mouse thyroid gland construct using the turnstile device. (A) The Fabion 3D bioprinter developed by 3D Bioprinting Solutions and used for thyroid gland construct printing with single tissue spheroids. (B) Turnstile device for bioprinting of single spheroids: spheroids loading point (a), channel with spheroids inline (b); output for media culture (c); loading piston (d); trapping piston (e); deposition piston (f); recess in the piston for media extraction (g). (C) Step-by-step progression of a single tissue spheroid using the turnstile device for bioprinting. (D) Bioprinted mouse thyroid gland construct composed of three spheroids from embryonic thyroid explants (3TS) or (E) composed of three spheroids from embryonic thyroid explants in between six allantoides spheroids (3TS + 6AS) after 1 day in culture. (F) Bioprinted mouse thyroid gland construct labeled, after 1 day in culture, with antibodies against platelet and endothelial cell adhesion molecule (PECAM; green) and E-cadherin (red) to visualize endothelial and epithelial cells, respectively. The insert in F shows the widespread localization of PECAM-positive cells in bioprinted mouse thyroid construct (TS + AS) after 4 days in culture.

Bioprinting using mouse thyroid and allantoic spheroids

For this study we developed a novel original multi-functional 3D bioprinter, Fabion (figure 3(A)), with two unique functional characteristics: first, it is equipped with a technology, based on the turnstile principle [31, 32] that facilitates dispensing of a single tissue spheroid at a time (figures 3(B), (C)); second, it includes a cooling/heating system for better control over the polymerization of the collagen hydrogel (supplementary figure 2). Our system allows the use of a collagen mix with a physiological pH and prevents its premature gelation while being stored at 4 °C in an extrusion needle and during the printing. The polymerization starts as soon as the hydrogel is deposited on the hot base plate, resulting in a collagen gel with a stable and predictable structure. The first step was to print a 2 mm × 2 mm collagen bed on cell strainers in the Petri dish to serve as a base. After polymerization, three e14.5 TS were loaded into the print head and placed in a line and adjacent to each other on top of the collagen bed according to the mathematical model (figure 3(D)). We also developed a more advanced version of the bioprinted construct (TS + AS). Six e8.5 mouse AS were loaded into the printing head and printed adjacent to and on both sides of the three TS, again to mimic the mathematical model (figures 3(C), (F); compare with figure 1(E)). To complete the printing process, a thin layer of collagen hydrogel was deposited on top of three TS, or three TS with six AS, depending on the construct version.

Endothelial cells from allantoic spheroids are responsible for the vascularization of thyroid gland construct

The vascularization of bioprinted thyroid gland construct is the most important and critical issue since it is required for a surrogate endocrine organ to be functional and both capture iodine and deliver hormones into the blood flow. We first analyzed the printed thyroid constructs containing TS only. After 4 days in culture, constructs were fixed and immunolabeled with antibodies against TTF1, E-cadherin and ezrin to visualize thyrocyte nuclei, basolateral and apical domains, respectively. $TTF1^{+}$ nuclei displayed a monolayered and organized circular pattern.

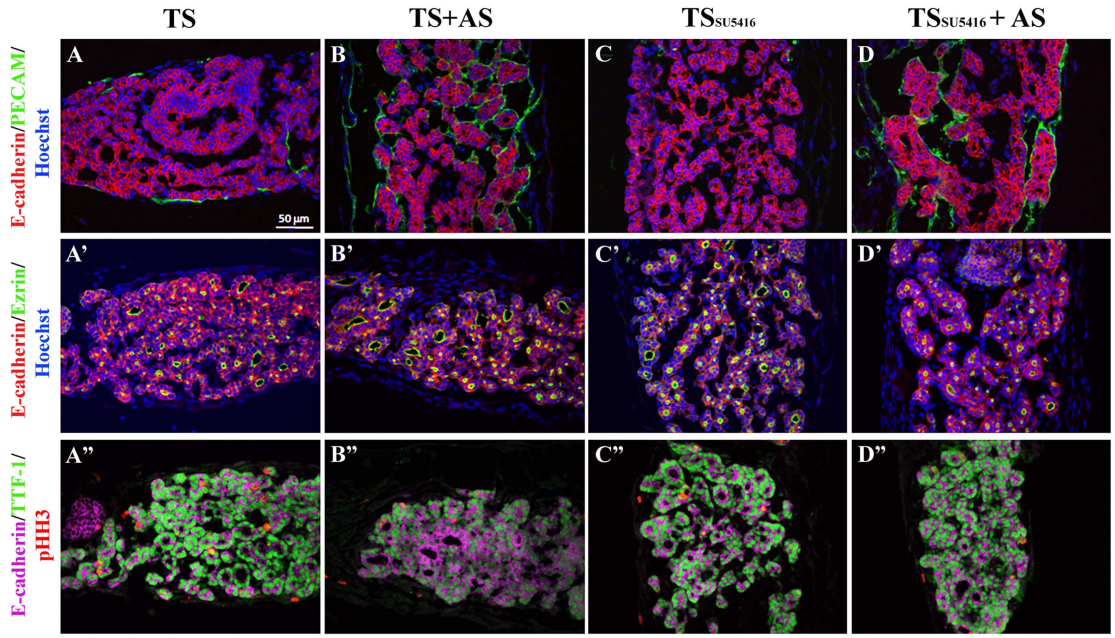

Figure 4. Vascularization of bioprinted mouse thyroid constructs. Immunolabeling of thin sections of bioprinted constructs after 4 days of culture with antibodies as indicated. (A) Bioprinted thyroid spheroids (TS) display endothelial cells (EC) only at the periphery of the tissue. (B) TS bioprinted together with allantoic spheroids (AS) reveal intense PECAM labeling around and inside the TS. (C) TS pretreated with SU5416 (TS_{SU5416}) during hanging drop culture do not show endothelial labeling. (D) In the presence of AS, TS depleted of EC (TS_{SU5416}) are invaded by EC from AS. Thyroid follicle formation (A′)–(D′) as well as cell proliferation (A″)–(D″) was comparable in all the cultured bioprinted constructs.

E-cadherin confirmed the formation of epithelial monolayers, each delineating a central space. $Ezrin^+$ epithelial cells demonstrated apical polarization of cells facing a lumen (figures 4(A), (A′), (A″)). Printed spheroid tissue was alive and growing as cells positive for the proliferation marker pHH3 were found in the construct (figure 4(A″)). However, compared with the widespread localization of EC in the TS at the end of the hanging drop culture (supplementary figure 3.), EC were only found at the periphery of thyroid tissue after 4 days in collagen (figure 4(A)). This suggests that thyroid EC localized deep inside the tissue construct do not support long-term culture in collagen, probably due to low pO_2. Interestingly, the constructs printed from TS and AS (3TS + 6AS) displayed abundant and widespread localization of EC around epithelial cells of the thyroid tissue after 4 days in collagen. Ezrin and TTF1 visualization revealed developing follicular structure in thyroid tissue (figures 4(B′), (B″)). These observations suggest that endothelial progenitors present in AS responded and were attracted by the angiogenic factor, VEGF-A, highly secreted by thyrocyte progenitors of the TS [11]. However, one cannot exclude that thyroid EC responded to survival and proliferating signals secreted by the allantoides. To distinguish between these two possibilities, we cultured e14.5 thyroid explants in hanging drops in the presence of the specific VEGFR2/Flk-1 kinase inhibitor SU5416 (TS_{SU5416}). As VEGFR2 signaling is essential for EC survival, inhibition of this signaling pathway leads to progressive EC death [11]. Addition of 5 μM SU5416 to the culture medium of thyroid explants for 24 h indeed removed all PECAM-positive EC from TS (figure 4(C)), indicating that SU5416 treatment was effective. We then bioprinted three SU5416-treated TS (TS_{SU5416}) with six AS, as above, and cultured the construct in collagen hydrogel for 4 days. Bioprinted constructs showed invasion of EC deep into thyroid tissue (figure 4(D)), resulting in the generation of a dense capillary network surrounding epithelial cells. This indicates that EC detected around follicles on these thin sections were clearly derived from allantoides. SU5416 treatment did not affect the proliferation of thyrocytes (figures 4(C″), (D″)) or the formation of prefollicular structures (figures 4(C′), (D′), (C″), (D″)). Altogether, these experiments demonstrate that addition and fusion of allantoides to thyroid tissue within collagen hydrogels allow improved vascularization of bioprinted TS.

Bioprinted mouse thyroid gland constructs are functional *in vivo*

In order to validate the functionality of bioprinted cultured mouse thyroid constructs (3TS + 6AS), we grafted these latter under the kidney capsule of hypothyroid mice, following ^{131}I injection (figure 5(A)). Implantation of tissue pieces under the vascularized kidney capsule is a standard and well-established approach for *in vivo* testing [33–36]. Experiments on hypothyroid animals were performed 8 weeks after the administration of ^{131}I, when all mice

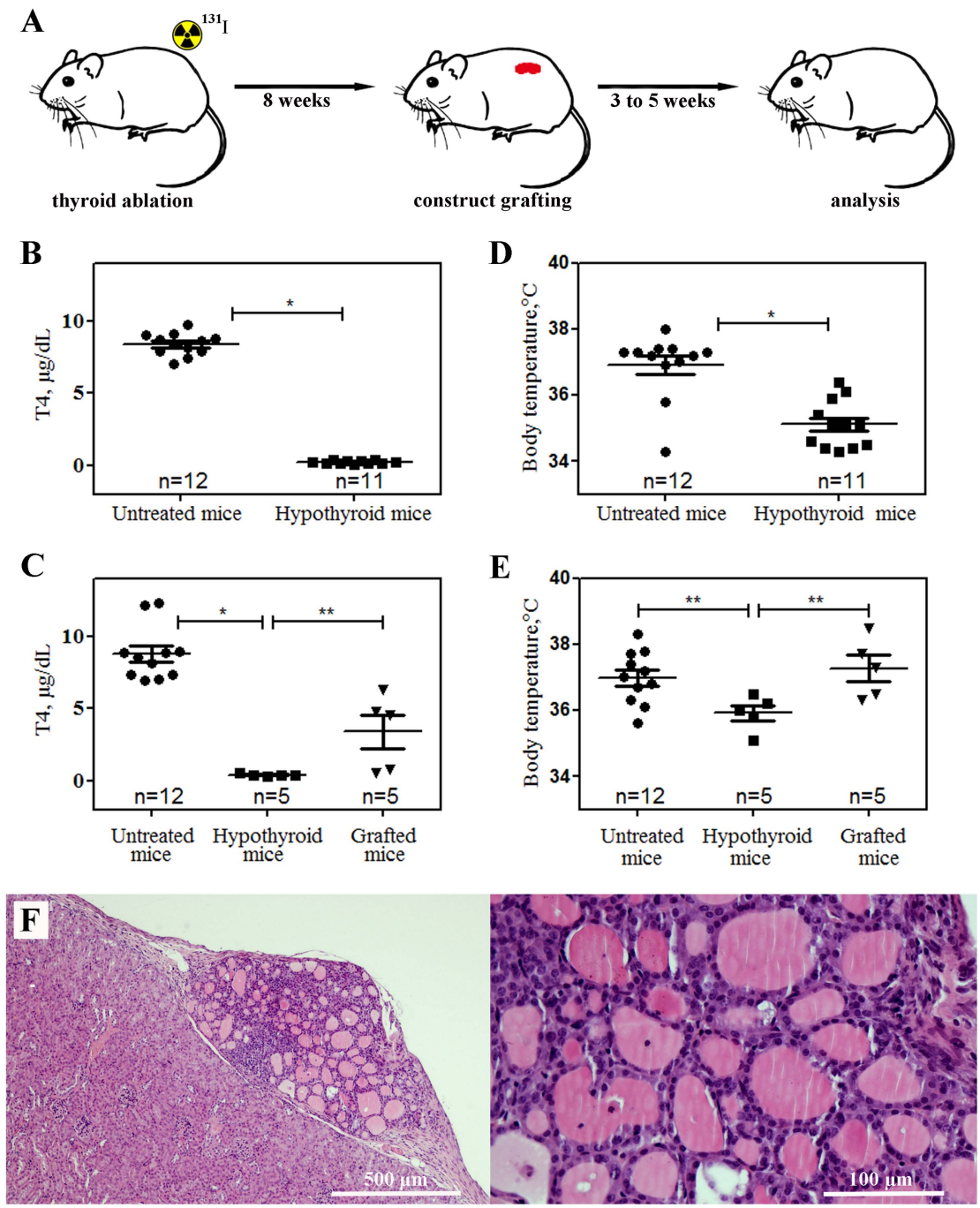

Figure 5. Functional rescue of *in vivo* thyroid function using bioprinted mouse thyroid construct. (A) Schematic representation and time line of mouse ^{131}I-induced thyroid ablation and construct grafting. (B) T4 blood level and (D) body temperature in untreated and hypothyroid mice 8 weeks after ^{131}I-induced thyroid ablation. ^{131}I-treated mice present clear hypothyroidism. An unpaired *t*-test was used for statistical analysis ($^{*}P < 0.001$). (C) T4 blood level and (E) body temperature 5 weeks after thyroid construct (TS + AS) grafting in recipient hypothyroid mice. Tukey's multiple comparison test was used for statistical analysis ($^{*}P < 0.001$, $^{**}P < 0.05$). (F) Histological analysis of kidneys section 5 weeks after grafting. Hematoxylin and eosin staining on grafted kidney showed follicular organization in grafted tissue and colloid accumulation (see supplementary figure 5 for results at 3 weeks).

had undetectable blood concentrations of T4 (figure 5(B)). Histological evaluation of the native thyroid region 8 weeks after administration of ^{131}I revealed loss of thyroid tissue (supplementary figures 4(A), (B)). The blood level of T4 was measured as a specific and most informative marker. Three and 5 weeks after grafting, recipient mice showed a substantial elevation of T4 blood levels (figure 5(C) and supplementary figure 5(A)), indicating functional rescue with the bioprinted thyroid construct (3TS + 6AS).

Additionally, we analyzed the body temperature in mice from the different groups. As expected, decreased body temperature was found in hypothyroid mice (figure 5(D)). Mice grafted with the printed and cultured thyroid gland construct showed a gradual normalization of body temperature at 3 and 5 weeks after transplantation, providing a reliable

example for symptomatic recovery (figure 5(E), supplementary figure 5(B)).

Histological evaluation of the kidney region 3 and 5 weeks after transplantation demonstrated successful integration and maturation of grafted organoids in the host niche. At the grafting site, numerous follicles containing a monolayered epithelium were present at the cortical area of the host organ (figure 5(F)). Regions of new capillary formation filled with erythrocytes were detectable (supplementary figure 5(C)).

Our *in vivo* data clearly demonstrate that printed thyroid gland constructs have potent functional capacity to compensate for the lack of native thyroid tissue allowing functional rescue of experimentally induced hypothyroidism.

Discussion

In the present study we validated the earlier proposed principle of bioprinting technology based on the use of tissue spheroids as building blocks [5, 6]. Our data on bioprinting of functional vascularized mouse thyroid gland construct from TS and AS represents further advance in the emerging solid scaffold-free approach for 3D bioprinting, exploring self-assembling properties of tissue spheroids [6, 15, 37]. Tissue spheroids capable of fusion are already used for scaffold-free biofabrication of cartilage [38], bone [39], liver [40], ovary [41] and blood vessels [9, 42]. Using tissue spheroids as opposed to single cells has substantial advantages [43, 44]. First, tissue spheroids represent densely packed spherical aggregates of living cells. Spheroids thus ensure the maximum achievable cell density during the printing, while displaying a higher resistance to shear stress, radiation and other unfavorable factors, which results in decreasing risks of karyotype alteration [45]. Secondly, precise embedding of tissue spheroids into sequentially applied layers of hydrogel ensures the desired allocation of closely placed tissue spheroids contacting each other in both horizontal and vertical directions [19]. This creates proper conditions for formation of 3D tissue constructs as a result of tissue fusion. Finally, the spherical form of tissue spheroids is ideal for their robotic dispensing through the cylindrical nozzle of 3D bioprinter.

However, tissue spheroid printing has also some drawbacks, and problems can emerge during bioprinting: (i) spontaneous fusion of spheroids resulting in the formation of clusters or aggregates seriously complicates bioprinting with individual tissue spheroids; (ii) adhesion of tissue spheroids to the walls of dispensing tubes obstructs the passage of further tissue spheroids; (iii) both the above phenomena cause undesired damage, defects, deformation and even destruction of tissue spheroids. To overcome the aforementioned problems, we created a device allowing 3D bioprinting of individual tissue spheroids, using the turnstile principle. Bioprinting achieved with our device is stable and reliable.

Collagen is a major component of the extracellular matrix, it supports cell adhesion and culture but its application in 3D bioprinting still has limitations because it is sensitive to both pH and temperature and forms a gel at physiological pH and 37 °C [46]. It is thus difficult to keep a collagen mix liquid when printing and produce a solid scaffold immediately after printing [47]. The first approach to printing with collagen was changing its pH by addition of sodium hydrogen carbonate ($NaHCO_3$) before deposition to initiate the transition of collagen solution to a gel when the temperature gradually increases during the printing. Although this system improved deposition of the hydrogel by the bioprinter, the process was time consuming, resulting in clogging inside the extrusion needle due to anticipatory polymerization caused by gradual transition to room temperature. We improved the printing of collagen hydrogel by implementing a cooling/heating system in our extrusion bioprinter, which had been previously used [48], but its biocompatibility was not evaluated.

Bioprinting of thyroid gland construct containing a dense network of EC is another important achievement of this study. 3D bioprinted tissue constructs quickly develop necrotic regions without sufficient vascularization [49]. Printing the channels from sacrificial hydrogels followed by the seeding of EC and smooth muscle cells for vessel wall formation is an approach developed recently [13, 50]. Carbohydrate glass [13] or pluronic acid F-127 [50] was used to print sacrificial tunnels within a supporting matrix and then extruded by dissolution, leaving room for EC population. This approach is highly effective and reproducible for simple homogeneous constructs. However, natural tissues and organs are effectively perfused by a hierarchically branched complex intra-organ vascular tree. These will be difficult to mimic using sacrificial matrices. In this study we employed the self-assembly approach which represents an alternative to the scaffold-free technique for engineered tissue vascularization. It has been demonstrated that large-diameter blood vessels could be bioprinted from vascular tissue spheroids biofabricated from smooth muscle cells and EC [43]. The capacity of lumenized vascular AS to fuse into linear and branched intermediate-diameter vascular segments has been reported [6]. Finally, the microvascular networks can be self-assembled either from single cells placed into hydrogel by vacuole accumulation [51] or from endothelial tissue spheroids [52]. Thus, all three main parts of the intra-organ branched vascular tree—large-diameter vessel segments, intermediate-diameter vascular segments and microvascular segments—could be bioprinted using vascular tissue spheroids as building blocks.

In the present study we showed that sufficient development of a microvascular network could be

achieved in the engineered tissue construct by placing AS adjacent to TS, known to produce high levels of VEGF-A [11]. Indeed, we found that the endothelial density was more prominent in AS + TS than in TS alone. More importantly, TS depleted of EC were effectively invaded by EC when AS were added in the engineered construct. The presence of a dense microvascular network is not only significant for survival of the cells upon *in vivo* grafting. In the developing thyroid, EC invasion, from e12.5 onwards also positively controls the induction of thyroid folliculogenesis by promoting basal lamina deposition [11, 24]. Thus, allantoides-derived 'vasculature' could contribute to advancing thyroid folliculogenesis and sequential differentiation and maturation of follicles in the thyroid gland construct. Most importantly, better survival and expansion of EC from AS could allow formation of large, intermediate and microvessels in the construct, thereby allowing functional connection with the vascularization from the host mice. Taken together these results strongly support the practical feasibility of developing vascularized-competent tissue using bioprinting of vascular tissue spheroids. It should not escape to our attention that the advance in bioprinting of functional tissue depends on our understanding of the principles of cellular self-assembly and the ability to take advantage of this knowledge.

The thyroid gland construct must include the artery and the vein to establish anastomosis with the vascular system of the receiving organism. This is important for orthotopic implantation, when the printed construct is to be transplanted to the usual thyroid gland site. However, this is not critical if the implantation is heterotopic. It is well known that thyroid gland transplants can survive under the skin, in muscles or under the kidney capsule and still produce hormones [53, 54]. In case of heterotopic implantation under highly vascularized kidney capsula there is no need for large-diameter blood vessels connected to the bioprinted thyroid gland construct. Our results suggest that the connection of the microvascular network from the bioprinted construct, with that of the kidney capsula allows vascularization of the thyroid follicles.

Validation of the functionality of bioprinted mouse thyroid gland construct is another significant result of our study. Grafting of the bioprinted mouse thyroid construct under the kidney capsula of hypothyroid mice restored blood T4 level and body temperature, demonstrating functionality of bioprinted mouse thyroid construct. The amplification of TS, improvement of thyroid follicle vascularization and the level of their histological differentiation and maturation should eventually achieve 100% rescue of lost function in athyroid mice.

A consistent question arises concerning the possible clinical translation of our proposed variant of bioprinting technology. In order to bioprint human thyroid tissue in the future it is necessary to have clinically relevant source of therapeutic-grade thyroid epithelial cells. However, the effective propagation and scalable generation of large number of autologous differentiated human thyroid epithelial cells from biopsy is still a challenge. As of today, our efforts to isolate and propagate human thyroid epithelium or even viable thyroid follicles directly from human thyroid gland have not been successful (data not shown). So this direct approach is looking increasingly elusive and practically unfeasible. In this context, scalable generation of functional thyroid epithelium from human stem cells looks much more promising. The reported generation of thyroid follicles at first from mouse embryonic stem cells [25], then from human embryonic stem cells [55], and most recently, from human induced pluripotent stem cells [56] opens an opportunity for bioprinting of human thyroid gland. Tissue spheroids biofabricated from human smooth muscle and EC could be successfully generated from human fat tissue stem cells [57] or from human induced pluripotent stem cells using directed tissue differentiation [58, 59]. Alternatively, it would be possible to employ human endothelial tissue spheroids, which are capable of forming a vascular network *in vitro* and *in vivo* [52, 60]. Autologous EC could be isolated in sufficient number from human fat tissues [61]. Thus, 3D bioprinting of thyroid human tissue from organo-specific tissue spheroids and vascular tissue spheroids capable of post-printing tissue fusion is technologically feasible.

Conclusion

A thyroid gland construct has been bioprinted using two types of rounded embryonic tissue spheroids: thyroid spheroids were printed in close association with allantoic spheroids within collagen hydrogel using a novel bioprinter capable of precise placing of one spheroid at a time. Within 4 days, tissue spheroids fused into a single and integral thyroid gland construct, in which endothelial cells from allantoic spheroids invaded and vascularized thyroid spheroids, generating a dense capillary network around developing follicles. The bioprinted construct is functional as it could restore thyroid homeostasis after grafting under the kidney capsule of hypothyroid mice. Thus, our data demonstrated that bioprinting of tissue spheroids (i) derived from dissected embryonic mouse tissues, (ii) used as building blocks and (iii) capable of fusion can develop in vascularized-competent thyroid gland construct, functional *in vivo*. Our data represent a significant advance in the development of organ printing technology and important step toward eventual bioprinting of vascularized functional human tissue.

Acknowledgments

We thank Dr Sabina Costagliola for expertise in establishing a radioiodine-ablated animal model of thyroid gland hypofunction and helpful discussions, Anne-Sophie Delmarcelle for thyroid microdissection procedure and Emy Tassenoey for immunohistological analyses of bioprinted constructs. This work was supported in part by grants from: Fonds de la Recherche Scientifique (FNRS) (FRS-FNRS; J.0126.16); Action de Recherche Concertées from UCL (ARC 15/20-065); Fondation Roi Baudouin to CEP; JD was supported by FRIA, and CEP is a Research Associate of the FRS-FNRS. Y Sun is partially supported by the NSF Grants DMS-1318866, DMS-1620212 and a SC EPSCoR GEAR Award. Qi Wang's research is partially supported by NIH and NSF through awards DMS-1200487, DMS-1517347 and R01GM078994-05A1 and a SC EPSCoR GEAR award.

Author contributions

EAB, CEP and VAM designed the research; EVK, VAP, FDP, JD, CH and SAA performed the research; YS and QW created the mathematical model and computer simulation, EVK, NSS, GAF, EAB and CEP analyzed the data; EAB, YDK, CEP and VAM wrote the paper.

ORCID iDs

Elena A Bulanova https://orcid.org/0000-0001-8460-3113

References

[1] Eligar V, Taylor P N, Okosieme O E, Leese G P and Dayan C M 2016 Thyroxine replacement: a clinical endocrinologist's viewpoint *Ann. Clin. Biochem.* **53** 421–33
[2] Biondi B and Wartofsky L 2014 Treatment with thyroid hormone *Endocr. Rev.* **35** 433–512
[3] Ma R, Morshed S A, Latif R and Davies T F 2015 Thyroid cell differentiation from murine induced pluripotent stem cells *Front Endocrinol.* **6** 56
[4] Bajaj P, Schweller R M, Khademhosseini A, West J L and Bashir R 2014 3D biofabrication strategies for tissue engineering and regenerative medicine *Annu. Rev. Biomed. Eng.* **16** 247–76
[5] Mironov V, Boland T, Trusk T, Forgacs G and Markwald R R 2003 Organ printing: computer-aided jet-based 3D tissue engineering *Trends Biotechnol.* **21** 157–61
[6] Mironov V, Visconti R P, Kasyanov V, Forgacs G, Drake C J and Markwald R R 2009 Organ printing: tissue spheroids as building blocks *Biomaterials* **30** 2164–74
[7] Morimoto Y, Hsiao A Y and Takeuchi S 2015 Point-, line-, and plane-shaped cellular constructs for 3D tissue assembly *Adv. Drug. Deliv. Rev.* **95** 29–39
[8] Schon B S, Hooper G J and Woodfield T B F 2017 Modular tissue assembly strategies for biofabrication of engineered cartilage *Ann. Biomed. Eng.* **45** 100–14
[9] Fleming P A, Argraves W S, Gentile C, Neagu A, Forgacs G and Drake C J 2010 Fusion of uniluminal vascular spheroids: a model for assembly of blood vessels *Dev. Dyn.* **239** 398–406
[10] Mohebati A and Shaha A R 2012 Anatomy of thyroid and parathyroid glands and neurovascular relations *Clin. Anat.* **25** 19–31
[11] Hick A C *et al* 2013 Reciprocal epithelial: endothelial paracrine interactions during thyroid development govern follicular organization and C-cells differentiation *Dev. Biol.* **381** 227–40
[12] Radisic M, Malda J, Epping E, Geng W, Langer R and Vunjak-Novakovic G 2006 Oxygen gradients correlate with cell density and cell viability in engineered cardiac tissue *Biotechnol. Bioeng.* **93** 332–43
[13] Miller J S *et al* 2012 Rapid casting of patterned vascular networks for perfusable engineered three-dimensional tissues *Nat. Mater.* **11** 1–7
[14] Rouwkema J, Rivron N C and van Blitterswijk C A 2008 Vascularization in tissue engineering *Trends Biotechnol.* **26** 434–41
[15] Visconti R P, Kasyanov V, Gentile C, Zhang J, Markwald R R and Mironov V 2010 Towards organ printing: engineering an intra-organ branched vascular tree *Expert Opin. Biol. Ther.* **10** 409–20
[16] Richards D, Jia J, Yost M, Markwald R and Mei Y 2017 3D Bioprinting for vascularized tissue fabrication *Ann. Biomed. Eng.* **45** 132–47
[17] Gentile C, Fleming P A, Mironov V, Argraves K M, Argraves W S and Drake C J 2008 VEGF-mediated fusion in the generation of uniluminal vascular spheroids *Dev. Dyn.* **237** 2918–25
[18] Kelm J M *et al* 2005 VEGF profiling and angiogenesis in human microtissues *J. Biotechnol.* **118** 213–29
[19] Jakab K, Neagu A, Mironov V, Markwald R R and Forgacs G 2004 Engineering biological structures of prescribed shape using self-assembling multicellular systems *Proc. Natl Acad. Sci. USA* **101** 2864–9
[20] Rajan N, Habermehl J, Coté M-F, Doillon C J and Mantovani D 2006 Preparation of ready-to-use, storable and reconstituted type I collagen from rat tail tendon for tissue engineering applications *Nat. Protoc.* **1** 2753–8
[21] Delmarcelle A-S, Villacorte M, Hick A-C and Pierreux C E 2014 An *ex vivo* culture system to study thyroid development *J. Vis. Exp.* 8–15
[22] Drake C J and Fleming P A 2000 Vasculogenesis in the day 6.5 to 9.5 mouse embryo *Blood.* **95** 1671–9
[23] Susienka M J, Wilks B T and Morgan J R 2016 Quantifying the kinetics and morphological changes of the fusion of spheroid building blocks *Biofabrication* **8** 45003
[24] Villacorte M *et al* 2016 Thyroid follicle development requires Smad1/Smad5- and endothelial-dependent basement membrane assembly *Development* **143** 1958–70
[25] Antonica F *et al* 2013 Generation of functional thyroid from embryonic stem cells *Nature* **491** 66–71
[26] Abel E D *et al* 1999 Divergent roles for thyroid hormone receptor beta isoform inthe endocrine axis and auditory system *J. Clin. Invest.* **104** 291–300
[27] Steinberg M S 1963 Reconstruction of tissues by dissociated cells *Science* **141** 401–8
[28] Bortz A, Kalos M and Lebowitz J 1975 A new algorithm for Monte Carlo simulation of Ising spin systems *J. Comput. Phys.* **17** 10–8
[29] Flenner E, Janosi L, Barz B, Neagu A, Forgacs G and Kosztin I 2012 Kinetic Monte Carlo and cellular particle dynamics simulations of multicellular systems *Phys. Rev.* E **85** 1–10
[30] Sun Y *et al* 2013 Modeling and simulations of multicellular aggregate self-assembly in biofabrication using kinetic Monte Carlo methods *Soft Matter* **9** 2172
[31] Lang M, Wang W, Chen X Q and Woodfield T 2010 Integrated system for 3D assembly of bio-scaffolds and cells *2010 IEEE Int. Conf. Autom. Sci. Eng. CASE 2010* pp 786–91
[32] Lang M, Chen X, Wang W and Woodfield T B F 2012 Injection system for cellular assembly of 3D bio-tissue engineered constructs *IEEE Int. Conf. Autom. Sci. Eng.* pp 291–6
[33] Ma S N, Yuan Y H, Guo X R and Li D S 2016 Subcapsular implantation of pancreatic islets in syngeneic, allogeneic, and xenogeneic mice *Transplant Proc.* **48** 2821–5

[34] van Gurp L *et al* 2016 Sequential intravital imaging reveals *in vivo* dynamics of pancreatic tissue transplanted under the kidney capsule in mice *Diabetologia* **59** 2387–92
[35] Raikwar S P, Kim E M, Sivitz W I, Allamargot C, Thedens D R and Zavazava N 2015 Human iPS cell-derived insulin producing cells form vascularized organoids under the kidney capsules of diabetic mice *PLoS One* **10** 1–15
[36] Xinaris C *et al* 2012 *In vivo* maturation of functional renal organoids formed from embryonic cell suspensions *J. Am. Soc. Nephrol.* **23** 1857–68
[37] Rezende R A *et al* 2013 Scalable biofabrication of tissue spheroids for organ printing *Procedia CIRP* **5** 276–81
[38] Lee J I, Sato M, Kim H W and Mochida J 2011 Transplantatation of scaffold-free spheroids composed of synovium-derived cells and chondrocytes for the treatment of cartilage defects of the knee *Eur. Cell Mater.* **22** 275–90
[39] Tang D, Tare R S, Yang L Y, Williams D F, Ou K L and Oreffo R O C 2016 Biofabrication of bone tissue: approaches, challenges and translation for bone regeneration *Biomaterials* **83** 363–82
[40] Lee J, Cuddihy M J, Cater G M and Kotov N A 2009 Engineering liver tissue spheroids with inverted colloidal crystal scaffolds *Biomaterials* **30** 4687–94
[41] Liao J *et al* 2014 Ovarian cancer spheroid cells with stem cell-like properties contribute to tumor generation, metastasis and chemotherapy resistance through hypoxia-resistant metabolism *PLoS One* **9** 1–13
[42] Inamori M, Mizumoto H and Kajiwara T 2009 An approach for formation of vascularized liver tissue by endothelial cell-covered hepatocyte spheroid integration *Tissue Eng.* A **15** 2029–37
[43] Itoh M *et al* 2015 Scaffold-free tubular tissues created by a bio-3D printer undergo remodeling and endothelialization when implanted in rat aortae *PLoS One* **10** e0136681
[44] Rago A P, Dean D M and Morgan J R 2009 Controlling cell position in complex heterotypic 3D microtissues by tissue fusion *Biotechnol. Bioeng.* **102** 1231–41
[45] Yamada K M and Cukierman E 2007 Modeling tissue morphogenesis and cancer in 3D *Cell* **130** 601–10
[46] Roth E A, Xu T, Das M, Gregory C, Hickman J J and Boland T 2004 Inkjet printing for high-throughput cell patterning *Biomaterials* **25** 3707–15
[47] Rutz A L, Hyland K E, Jakus A E, Burghardt W R and Shah R N 2015 A multimaterial bioink method for 3D printing tunable, cell-compatible hydrogels *Adv. Mater.* **27** 1607–14
[48] Nocera A D, Salvatierra N A and Cid M P 2014 Printing Collagen 3D Structures *IFMBE Proc.* **49** 136–9
[49] Griffith C K *et al* 2005 Diffusion Limits of an *in vitro* thick prevascularized tissue *Tissue Eng.* **11** 257–66
[50] Bertassoni L E *et al* 2014 Hydrogel bioprinted microchannel networks for vascularization of tissue engineering constructs *Lab Chip* **14** 2202–11
[51] Kamei M, Saunders W B, Bayless K J, Dye L, Davis G E and Weinstein B M 2006 Endothelial tubes assemble from intracellular vacuoles *in vivo Nature* **442** 453–6
[52] Alajati A *et al* 2008 Spheroid-based engineering of a human vasculature in mice *Nat. Methods* **5** 439–45
[53] Iwai H *et al* 1993 Thyroid follicle transplantation by percutaneous injection *Acta Oto-Laryngol.* **113** 135–7
[54] La Rosa F G, Smilek D, Talmage D W, Lafferty K J, Bauling P and Ammons T J 1992 Evidence that tolerance to cultured thyroid allografts is an active immunological process. Protection of third-party grafts bearing new antigens when associated with tolerogenic antigens *Transplantation* **53** 903–13
[55] Ma R, Latif R and Davies T F 2015 Human embryonic stem cells form functional thyroid follicles *Thyroid.* **25** 455–61
[56] Kurmann A A *et al* 2015 Regeneration of thyroid function by transplantation of differentiated pluripotent stem cells *Cell Stem Cell* **17** 527–42
[57] Mineda K *et al* 2015 Therapeutic potential of human adipose-derived stem/stromal cell microspheroids prepared by three-dimensional culture in non-cross-linked hyaluronic acid gel *Stem Cells Transl. Med.* **4** 1511–22
[58] Vodyanik M A *et al* 2010 A mesoderm-derived precursor for mesenchymal stem and endothelial cells *Cell Stem Cell* **7** 718–29
[59] Patsch C *et al* 2015 Generation of vascular endothelial and smooth muscle cells from human pluripotent stem cells *Nat. Cell Biol.* **17** 994–1003
[60] Pfisterer L and Korff T 2016 Spheroid-based *in vitro* angiogenesis model *Methods Mol. Biol.* **1430** 167–77
[61] Tiwari A, Salacinski H J, Hamilton G and Seifalian A M 2001 Tissue engineering of vascular bypass grafts: role of endothelial cell extraction *Eur. J. Vasc. Endovasc. Surg.* **21** 193–201
[62] Graner F and Glazier J A 1992 Simulation of biological cell sorting using a 2-dimensional extended potts-model *Phys. Rev. Lett.* **69** 2013–6
[63] Glazier J A and Graner F 1993 Simulation of the differential adhesion driven rearrangement of biological cells *Phys. Rev. Lett.* **47** 2128–54

10 References

Afelik, S., and Jensen, J. (2013). Notch signaling in the pancreas: patterning and cell fate specification. Wiley interdisciplinary reviews Developmental biology *2*, 531-544.

Alt, B., Elsalini, O.A., Schrumpf, P., Haufs, N., Lawson, N.D., Schwabe, G.C., Mundlos, S., Gruters, A., Krude, H., and Rohr, K.B. (2006). Arteries define the position of the thyroid gland during its developmental relocalisation. Development *133*, 3797-3804.

Andersson, L., Westerlund, J., Liang, S., Carlsson, T., Amendola, E., Fagman, H., and Nilsson, M. (2011). Role of EphA4 receptor signaling in thyroid development: regulation of folliculogenesis and propagation of the C-cell lineage. Endocrinology *152*, 1154-1164.

Andreu, Z., and Yanez-Mo, M. (2014). Tetraspanins in extracellular vesicle formation and function. Front Immunol *5*, 442.

Antonica, F., Kasprzyk, D.F., Opitz, R., Iacovino, M., Liao, X.H., Dumitrescu, A.M., Refetoff, S., Peremans, K., Manto, M., Kyba, M.*, et al.* (2012). Generation of functional thyroid from embryonic stem cells. Nature *491*, 66-71.

Antonyak, M.A., Li, B., Boroughs, L.K., Johnson, J.L., Druso, J.E., Bryant, K.L., Holowka, D.A., and Cerione, R.A. (2011). Cancer cell-derived microvesicles induce transformation by transferring tissue transglutaminase and fibronectin to recipient cells. Proc Natl Acad Sci U S A *108*, 4852-4857.

Baietti, M.F., Zhang, Z., Mortier, E., Melchior, A., Degeest, G., Geeraerts, A., Ivarsson, Y., Depoortere, F., Coomans, C., Vermeiren, E.*, et al.* (2012). Syndecan-syntenin-ALIX regulates the biogenesis of exosomes. Nat Cell Biol *14*, 677-685.

Boelaert, K., and Franklyn, J.A. (2005). Thyroid hormone in health and disease. The Journal of endocrinology *187*, 1-15.

Bonifacino, J.S., and Glick, B.S. (2004). The mechanisms of vesicle budding and fusion. Cell *116*, 153-166.

Bort, R., Martinez-Barbera, J.P., Beddington, R.S., and Zaret, K.S. (2004). Hex homeobox gene-dependent tissue positioning is required for organogenesis of the ventral pancreas. Development *131*, 797-806.

Bort, R., Signore, M., Tremblay, K., Martinez Barbera, J.P., and Zaret, K.S. (2006). Hex homeobox gene controls the transition of the endoderm to a pseudostratified, cell emergent epithelium for liver bud development. Developmental biology *290*, 44-56.

Bray, S.J., and Gomez-Lamarca, M. (2017). Notch after cleavage. Current opinion in cell biology *51*, 103-109.

Chakravarty, D., Santos, E., Ryder, M., Knauf, J.A., Liao, X.H., West, B.L., Bollag, G., Kolesnick, R., Thin, T.H., Rosen, N.*, et al.* (2011). Small-molecule MAPK inhibitors restore radioiodine incorporation in mouse thyroid cancers with conditional BRAF activation. J Clin Invest *121*, 4700-4711.

Charrin, S., Jouannet, S., Boucheix, C., and Rubinstein, E. (2014). Tetraspanins at a glance. Journal of cell science *127*, 3641-3648.

Chou, S.Y., Hsu, K.S., Otsu, W., Hsu, Y.C., Luo, Y.C., Yeh, C., Shehab, S.S., Chen, J., Shieh, V., He, G.A.*, et al.* (2016). CLIC4 regulates apical exocytosis and renal tube luminogenesis through retromer- and actin-mediated endocytic trafficking. Nat Commun *7*, 10412.

Colin, I.M., Denef, J.F., Lengele, B., Many, M.C., and Gerard, A.C. (2013). Recent insights into the cell biology of thyroid angiofollicular units. Endocrine reviews *34*, 209-238.

Colombo, M., Moita, C., van Niel, G., Kowal, J., Vigneron, J., Benaroch, P., Manel, N., Moita, L.F., Thery, C., and Raposo, G. (2013). Analysis of ESCRT functions in exosome biogenesis, composition and secretion highlights the heterogeneity of extracellular vesicles. Journal of cell science *126*, 5553-5565.

Colombo, M., Raposo, G., and Thery, C. (2014). Biogenesis, secretion, and intercellular interactions of exosomes and other extracellular vesicles. Annu Rev Cell Dev Biol *30*, 255-289.

Cvjetkovic, A., Lotvall, J., and Lasser, C. (2014). The influence of rotor type and centrifugation time on the yield and purity of extracellular vesicles. Journal of extracellular vesicles *3*.

de Cristofaro, T., Di Palma, T., Fichera, I., Lucci, V., Parrillo, L., De Felice, M., and Zannini, M. (2012). An essential role for Pax8 in the transcriptional regulation of cadherin-16 in thyroid cells. Molecular endocrinology (Baltimore, Md) *26*, 67-78.

De Felice, M., and Di Lauro, R. (2004). Thyroid development and its disorders: genetics and molecular mechanisms. Endocrine reviews *25*, 722-746.

De Felice, M., and Di Lauro, R. (2011). Minireview: Intrinsic and extrinsic factors in thyroid gland development: an update. Endocrinology *152*, 2948-2956.

De Felice, M., Ovitt, C., Biffali, E., Rodriguez-Mallon, A., Arra, C., Anastassiadis, K., Macchia, P.E., Mattei, M.G., Mariano, A., Scholer, H.*, et al.* (1998). A mouse model for hereditary thyroid dysgenesis and cleft palate. Nature genetics *19*, 395-398.

de Gassart, A., Geminard, C., Fevrier, B., Raposo, G., and Vidal, M. (2003). Lipid raft-associated protein sorting in exosomes. Blood *102*, 4336-4344.

de Jong, O.G., van Balkom, B.W., Gremmels, H., and Verhaar, M.C. (2016). Exosomes from hypoxic endothelial cells have increased collagen crosslinking activity through up-regulation of lysyl oxidase-like 2. Journal of cellular and molecular medicine *20*, 342-350.

Del Conde, I., Shrimpton, C.N., Thiagarajan, P., and Lopez, J.A. (2005). Tissue-factor-bearing microvesicles arise from lipid rafts and fuse with activated platelets to initiate coagulation. Blood *106*, 1604-1611.

Donahue, H.J., Qu, R.W., and Genetos, D.C. (2017). Joint diseases: from connexins to gap junctions. Nature reviews Rheumatology *14*, 42-51.

Durante, C., Montesano, T., Torlontano, M., Attard, M., Monzani, F., Tumino, S., Costante, G., Meringolo, D., Bruno, R., Trulli, F.*, et al.* (2013). Papillary thyroid cancer: time course of recurrences during postsurgery surveillance. J Clin Endocrinol Metab *98*, 636-642.

Escudier, B., Dorval, T., Chaput, N., Andre, F., Caby, M.P., Novault, S., Flament, C., Leboulaire, C., Borg, C., Amigorena, S*., et al.* (2005). Vaccination of metastatic melanoma patients with autologous dendritic cell (DC) derived-exosomes: results of thefirst phase I clinical trial. Journal of translational medicine *3*, 10.

Fagin, J.A., and Wells, S.A., Jr. (2016). Biologic and Clinical Perspectives on Thyroid Cancer. The New England journal of medicine *375*, 1054-1067.

Fagman, H., Amendola, E., Parrillo, L., Zoppoli, P., Marotta, P., Scarfo, M., De Luca, P., de Carvalho, D.P., Ceccarelli, M., De Felice, M*., et al.* (2011). Gene expression profiling at early organogenesis reveals both common and diverse mechanisms in foregut patterning. Developmental biology *359*, 163-175.

Fagman, H., Andersson, L., and Nilsson, M. (2006). The developing mouse thyroid: embryonic vessel contacts and parenchymal growth pattern during specification, budding, migration, and lobulation. Developmental dynamics : an official publication of the American Association of Anatomists *235*, 444-455.

Fagman, H., Grande, M., Edsbagge, J., Semb, H., and Nilsson, M. (2003). Expression of classical cadherins in thyroid development: maintenance of an epithelial phenotype throughout organogenesis. Endocrinology *144*, 3618-3624.

Fagman, H., Grande, M., Gritli-Linde, A., and Nilsson, M. (2004). Genetic deletion of sonic hedgehog causes hemiagenesis and ectopic development of the thyroid in mouse. The American journal of pathology *164*, 1865-1872.

Fagman, H., Liao, J., Westerlund, J., Andersson, L., Morrow, B.E., and Nilsson, M. (2007). The 22q11 deletion syndrome candidate gene Tbx1 determines thyroid size and positioning. Human molecular genetics *16*, 276-285.

Fais, S., O'Driscoll, L., Borras, F.E., Buzas, E., Camussi, G., Cappello, F., Carvalho, J., Cordeiro da Silva, A., Del Portillo, H., El Andaloussi, S*., et al.* (2016). Evidence-Based Clinical Use of Nanoscale Extracellular Vesicles in Nanomedicine. ACS nano *10*, 3886-3899.

Ferguson, S.W., and Nguyen, J. (2016). Exosomes as therapeutics: The implications of molecular composition and exosomal heterogeneity. Journal of controlled release : official journal of the Controlled Release Society *228*, 179-190.

Gardiner, C., Di Vizio, D., Sahoo, S., Thery, C., Witwer, K.W., Wauben, M., and Hill, A.F. (2016). Techniques used for the isolation and characterization of extracellular vesicles: results of a worldwide survey. Journal of extracellular vesicles *5*, 32945.

Geers, C., Colin, I.M., and Gerard, A.C. (2011). Delta-like 4/Notch pathway is differentially regulated in benign and malignant thyroid tissues. Thyroid : official journal of the American Thyroid Association *21*, 1323-1330.

Genetos, D.C., Kephart, C.J., Zhang, Y., Yellowley, C.E., and Donahue, H.J. (2007). Oscillating fluid flow activation of gap junction hemichannels induces ATP release from MLO-Y4 osteocytes. Journal of cellular physiology *212*, 207-214.

Gerard, A.C., Poncin, S., Caetano, B., Sonveaux, P., Audinot, J.N., Feron, O., Colin, I.M., and Soncin, F. (2008). Iodine deficiency induces a thyroid stimulating hormone-independent early phase of microvascular reshaping in the thyroid. The American journal of pathology *172*, 748-760.

Greco, V., Hannus, M., and Eaton, S. (2001). Argosomes: a potential vehicle for the spread of morphogens through epithelia. Cell *106*, 633-645.

Gross, J.C., Chaudhary, V., Bartscherer, K., and Boutros, M. (2012). Active Wnt proteins are secreted on exosomes. Nat Cell Biol *14*, 1036-1045.

Hanahan, D., and Weinberg, R.A. (2011). Hallmarks of cancer: the next generation. Cell *144*, 646-674.

Harding, C., Heuser, J., and Stahl, P. (1983). Receptor-mediated endocytosis of transferrin and recycling of the transferrin receptor in rat reticulocytes. J Cell Biol *97*, 329-339.

Harvey, C.B., and Williams, G.R. (2002). Mechanism of thyroid hormone action. Thyroid : official journal of the American Thyroid Association *12*, 441-446.

Hayashi, T., Lombaert, I.M., Hauser, B.R., Patel, V.N., and Hoffman, M.P. (2017). Exosomal MicroRNA Transport from Salivary Mesenchyme Regulates Epithelial Progenitor Expansion during Organogenesis. Dev Cell *40*, 95-103.

Hick, A.C., Delmarcelle, A.S., Bouquet, M., Klotz, S., Copetti, T., Forez, C., Van Der Smissen, P., Sonveaux, P., Collet, J.F., Feron, O.*, et al.* (2013). Reciprocal

epithelial:endothelial paracrine interactions during thyroid development govern follicular organization and C-cells differentiation. Developmental biology *381*, 227-240.

Hood, J.L. (2016). Post isolation modification of exosomes for nanomedicine applications. Nanomedicine (London, England) *11*, 1745-1756.

Hoshino, A., Costa-Silva, B., Shen, T.L., Rodrigues, G., Hashimoto, A., Tesic Mark, M., Molina, H., Kohsaka, S., Di Giannatale, A., Ceder, S*., et al.* (2015). Tumour exosome integrins determine organotropic metastasis. Nature *527*, 329-335.

Hoshino, D., Kirkbride, Kellye C., Costello, K., Clark, Emily S., Sinha, S., Grega-Larson, N., Tyska, Matthew J., and Weaver, Alissa M. (2013). Exosome Secretion Is Enhanced by Invadopodia and Drives Invasive Behavior. Cell Reports *5*, 1159-1168.

Hristov, M., Erl, W., Linder, S., and Weber, P.C. (2004). Apoptotic bodies from endothelial cells enhance the number and initiate the differentiation of human endothelial progenitor cells in vitro. Blood *104*, 2761-2766.

Irion, U., and St Johnston, D. (2007). bicoid RNA localization requires specific binding of an endosomal sorting complex. Nature *445*, 554-558.

Jang, S.C., Kim, O.Y., Yoon, C.M., Choi, D.S., Roh, T.Y., Park, J., Nilsson, J., Lotvall, J., Kim, Y.K., and Gho, Y.S. (2013). Bioinspired exosome-mimetic nanovesicles for targeted delivery of chemotherapeutics to malignant tumors. ACS nano *7*, 7698-7710.

Kalra, H., Drummen, G.P., and Mathivanan, S. (2016). Focus on Extracellular Vesicles: Introducing the Next Small Big Thing. Int J Mol Sci *17*, 170.

Kidd, S., and Lieber, T. (2016). Mechanism of Notch Pathway Activation and Its Role in the Regulation of Olfactory Plasticity in Drosophila melanogaster. PLoS One *11*, e0151279.

Kikuchi, A. (2000). Regulation of beta-catenin signaling in the Wnt pathway. Biochemical and biophysical research communications *268*, 243-248.

Kimura, E.T., Nikiforova, M.N., Zhu, Z., Knauf, J.A., Nikiforov, Y.E., and Fagin, J.A. (2003). High prevalence of BRAF mutations in thyroid cancer: genetic evidence for

constitutive activation of the RET/PTC-RAS-BRAF signaling pathway in papillary thyroid carcinoma. Cancer Res *63*, 1454-1457.

Kitahara, C.M., and Sosa, J.A. (2016). The changing incidence of thyroid cancer. Nature reviews Endocrinology *12*, 646-653.

Kleinau, G., Neumann, S., Gruters, A., Krude, H., and Biebermann, H. (2013). Novel insights on thyroid-stimulating hormone receptor signal transduction. Endocrine reviews *34*, 691-724.

Klumperman, J., and Raposo, G. (2014). The complex ultrastructure of the endolysosomal system. Cold Spring Harbor perspectives in biology *6*, a016857.

Knobel, M., and Medeiros-Neto, G. (2003). An outline of inherited disorders of the thyroid hormone generating system. Thyroid : official journal of the American Thyroid Association *13*, 771-801.

Koch, S., Tugues, S., Li, X., Gualandi, L., and Claesson-Welsh, L. (2011). Signal transduction by vascular endothelial growth factor receptors. The Biochemical journal *437*, 169-183.

Koumarianou, P., Gomez-Lopez, G., and Santisteban, P. (2017). Pax8 controls thyroid follicular polarity through cadherin-16. Journal of cell science *130*, 219-231.

Kourembanas, S. (2015). Exosomes: vehicles of intercellular signaling, biomarkers, and vectors of cell therapy. Annu Rev Physiol *77*, 13-27.

Kowal, J., Arras, G., Colombo, M., Jouve, M., Morath, J.P., Primdal-Bengtson, B., Dingli, F., Loew, D., Tkach, M., and Thery, C. (2016). Proteomic comparison defines novel markers to characterize heterogeneous populations of extracellular vesicle subtypes. Proc Natl Acad Sci U S A *113*, E968-977.

Kowal, J., Tkach, M., and Thery, C. (2014). Biogenesis and secretion of exosomes. Current opinion in cell biology *29*, 116-125.

Krause, M., Rak-Raszewska, A., Naillat, F., Saarela, U., Schmidt, C., Ronkainen, V.P., Bart, G., Yla-Herttuala, S., and Vainio, S.J. (2018). Exosomes as secondary inductive signals involved in kidney organogenesis. Journal of extracellular vesicles *7*, 1422675.

Kusakabe, T., Hoshi, N., and Kimura, S. (2006). Origin of the ultimobranchial body cyst: T/ebp/Nkx2.1 expression is required for development and fusion of the ultimobranchial body to the thyroid. Developmental dynamics : an official publication of the American Association of Anatomists *235*, 1300-1309.

Lakkaraju, A., and Rodriguez-Boulan, E. (2008). Itinerant exosomes: emerging roles in cell and tissue polarity. Trends Cell Biol *18*, 199-209.

Lania, G., Zhang, Z., Huynh, T., Caprio, C., Moon, A.M., Vitelli, F., and Baldini, A. (2009). Early thyroid development requires a Tbx1-Fgf8 pathway. Developmental biology *328*, 109-117.

Lasser, C., Eldh, M., and Lotvall, J. (2012). Isolation and characterization of RNA-containing exosomes. Journal of visualized experiments : JoVE, e3037.

Lasser, C., O'Neil, S.E., Shelke, G.V., Sihlbom, C., Hansson, S.F., Gho, Y.S., Lundback, B., and Lotvall, J. (2016). Exosomes in the nose induce immune cell trafficking and harbour an altered protein cargo in chronic airway inflammation. Journal of translational medicine *14*, 181.

Lee, J.C., Zhao, J.T., Gundara, J., Serpell, J., Bach, L.A., and Sidhu, S. (2015). Papillary thyroid cancer-derived exosomes contain miRNA-146b and miRNA-222. The Journal of surgical research *196*, 39-48.

Lener, T., Gimona, M., Aigner, L., Borger, V., Buzas, E., Camussi, G., Chaput, N., Chatterjee, D., Court, F.A., Del Portillo, H.A*., et al.* (2015). Applying extracellular vesicles based therapeutics in clinical trials - an ISEV position paper. Journal of extracellular vesicles *4*, 30087.

Li, B., Antonyak, M.A., Zhang, J., and Cerione, R.A. (2012). RhoA triggers a specific signaling pathway that generates transforming microvesicles in cancer cells. Oncogene *31*, 4740.

Li, X., Chen, C., Wei, L., Li, Q., Niu, X., Xu, Y., Wang, Y., and Zhao, J. (2016). Exosomes derived from endothelial progenitor cells attenuate vascular repair and accelerate reendothelialization by enhancing endothelial function. Cytotherapy *18*, 253-262.

Liang, S., Johansson, E., Barila, G., Altschuler, D.L., Fagman, H., and Nilsson, M. (2018). A branching morphogenesis program governs embryonic growth of the thyroid gland. Development *145*.

Lim, J., Yeap, S.P., Che, H.X., and Low, S.C. (2013). Characterization of magnetic nanoparticle by dynamic light scattering. Nanoscale Research Letters *8*, 381.

Longmire, T.A., Ikonomou, L., Hawkins, F., Christodoulou, C., Cao, Y., Jean, J.C., Kwok, L.W., Mou, H., Rajagopal, J., Shen, S.S*., et al.* (2012). Efficient derivation of purified lung and thyroid progenitors from embryonic stem cells. Cell stem cell *10*, 398-411.

Lotvall, J., Hill, A.F., Hochberg, F., Buzas, E.I., Di Vizio, D., Gardiner, C., Gho, Y.S., Kurochkin, I.V., Mathivanan, S., Quesenberry, P*., et al.* (2014). Minimal experimental requirements for definition of extracellular vesicles and their functions: a position statement from the International Society for Extracellular Vesicles. Journal of extracellular vesicles *3*, 26913.

Lunavat, T.R., Cheng, L., Einarsdottir, B.O., Olofsson Bagge, R., Veppil Muralidharan, S., Sharples, R.A., Lasser, C., Gho, Y.S., Hill, A.F., Nilsson, J.A*., et al.* (2017). BRAF(V600) inhibition alters the microRNA cargo in the vesicular secretome of malignant melanoma cells. Proc Natl Acad Sci U S A *114*, E5930-e5939.

Lunavat, T.R., Jang, S.C., Nilsson, L., Park, H.T., Repiska, G., Lasser, C., Nilsson, J.A., Gho, Y.S., and Lotvall, J. (2016). RNAi delivery by exosome-mimetic nanovesicles - Implications for targeting c-Myc in cancer. Biomaterials *102*, 231-238.

MacDonald, C., Payne, J.A., Aboian, M., Smith, W., Katzmann, D.J., and Piper, R.C. (2015). A family of tetraspans organizes cargo for sorting into multivesicular bodies. Dev Cell *33*, 328-342.

Maeda, O., Usami, N., Kondo, M., Takahashi, M., Goto, H., Shimokata, K., Kusugami, K., and Sekido, Y. (2004). Plakoglobin (gamma-catenin) has TCF/LEF family-dependent transcriptional activity in beta-catenin-deficient cell line. Oncogene *23*, 964-972.

Maenhaut, C., Christophe, D., Vassart, G., Dumont, J., Roger, P.P., and Opitz, R. (2015). Ontogeny, Anatomy, Metabolism and Physiology of the Thyroid. In

Endotext, L.J. De Groot, G. Chrousos, K. Dungan, K.R. Feingold, A. Grossman, J.M. Hershman, C. Koch, M. Korbonits, R. McLachlan, M. New*, et al.*, eds. (South Dartmouth (MA): MDText.com, Inc.).

Maheshwari, R., and Weis, E. (2012). Thyroid associated orbitopathy. Indian journal of ophthalmology *60*, 87-93.

Martin, T.A., Mason, M.D., and Jiang, W.G. (2011). Tight junctions in cancer metastasis. Frontiers in bioscience (Landmark edition) *16*, 898-936.

Matter, K., Aijaz, S., Tsapara, A., and Balda, M.S. (2005). Mammalian tight junctions in the regulation of epithelial differentiation and proliferation. Current opinion in cell biology *17*, 453-458.

Matusek, T., Wendler, F., Poles, S., Pizette, S., D'Angelo, G., Furthauer, M., and Therond, P.P. (2014). The ESCRT machinery regulates the secretion and long-range activity of Hedgehog. Nature *516*, 99-103.

Mauchamp, J., Mirrione, A., Alquier, C., and Andre, F. (1998). Follicle-like structure and polarized monolayer: role of the extracellular matrix on thyroid cell organization in primary culture. Biology of the cell *90*, 369-380.

McConnell, R.E., Higginbotham, J.N., Shifrin, D.A., Jr., Tabb, D.L., Coffey, R.J., and Tyska, M.J. (2009). The enterocyte microvillus is a vesicle-generating organelle. J Cell Biol *185*, 1285-1298.

McGrogan, A., Seaman, H.E., Wright, J.W., and de Vries, C.S. (2008). The incidence of autoimmune thyroid disease: a systematic review of the literature. Clinical endocrinology *69*, 687-696.

Meehan, B., Rak, J., and Di Vizio, D. (2016). Oncosomes - large and small: what are they, where they came from? Journal of extracellular vesicles *5*, 33109.

Minciacchi, V.R., Freeman, M.R., and Di Vizio, D. (2015). Extracellular vesicles in cancer: exosomes, microvesicles and the emerging role of large oncosomes. Seminars in cell & developmental biology *40*, 41-51.

Minoo, P., Su, G., Drum, H., Bringas, P., and Kimura, S. (1999). Defects in tracheoesophageal and lung morphogenesis in Nkx2.1(-/-) mouse embryos. Developmental biology *209*, 60-71.

Morin, P.J. (1999). beta-catenin signaling and cancer. BioEssays : news and reviews in molecular, cellular and developmental biology *21*, 1021-1030.

Mulcahy, L.A., Pink, R.C., and Carter, D.R. (2014). Routes and mechanisms of extracellular vesicle uptake. Journal of extracellular vesicles *3*.

Munari-Silem, Y., Audebet, C., and Rousset, B. (1991). Hormonal control of cell to cell communication: regulation by thyrotropin of the gap junction-mediated dye transfer between thyroid cells. Endocrinology *128*, 3299-3309.

Munari-Silem, Y., Guerrier, A., Fromaget, C., Rabilloud, R., Gros, D., and Rousset, B. (1994). Differential control of connexin-32 and connexin-43 expression in thyroid epithelial cells: evidence for a direct relationship between connexin-32 expression and histiotypic morphogenesis. Endocrinology *135*, 724-734.

Muralidharan-Chari, V., Clancy, J., Plou, C., Romao, M., Chavrier, P., Raposo, G., and D'Souza-Schorey, C. (2009). ARF6-regulated shedding of tumor cell-derived plasma membrane microvesicles. Current biology : CB *19*, 1875-1885.

Muralidharan-Chari, V., Clancy, J.W., Sedgwick, A., and D'Souza-Schorey, C. (2010). Microvesicles: mediators of extracellular communication during cancer progression. Journal of cell science *123*, 1603-1611.

Naphade, S., Sharma, J., Gaide Chevronnay, H.P., Shook, M.A., Yeagy, B.A., Rocca, C.J., Ur, S.N., Lau, A.J., Courtoy, P.J., and Cherqui, S. (2015). Brief reports: Lysosomal cross-correction by hematopoietic stem cell-derived macrophages via tunneling nanotubes. Stem cells (Dayton, Ohio) *33*, 301-309.

Nilsson, M., and Fagman, H. (2013). Mechanisms of thyroid development and dysgenesis: an analysis based on developmental stages and concurrent embryonic anatomy. Curr Top Dev Biol *106*, 123-170.

Nilsson, M., and Fagman, H. (2017). Development of the thyroid gland. Development *144*, 2123-2140.

O'Brien, L.E., Jou, T.S., Pollack, A.L., Zhang, Q., Hansen, S.H., Yurchenco, P., and Mostov, K.E. (2001). Rac1 orientates epithelial apical polarity through effects on basolateral laminin assembly. Nat Cell Biol *3*, 831-838.

Opitz, R., Maquet, E., Huisken, J., Antonica, F., Trubiroha, A., Pottier, G., Janssens, V., and Costagliola, S. (2012). Transgenic zebrafish illuminate the dynamics of thyroid morphogenesis and its relationship to cardiovascular development. Developmental biology *372*, 203-216.

Ostrowski, M., Carmo, N.B., Krumeich, S., Fanget, I., Raposo, G., Savina, A., Moita, C.F., Schauer, K., Hume, A.N., Freitas, R.P*., et al.* (2010). Rab27a and Rab27b control different steps of the exosome secretion pathway. Nat Cell Biol *12*, 19-30; sup pp 11-13.

Pan, B.T., and Johnstone, R.M. (1983). Fate of the transferrin receptor during maturation of sheep reticulocytes in vitro: selective externalization of the receptor. Cell *33*, 967-978.

Panakova, D., Sprong, H., Marois, E., Thiele, C., and Eaton, S. (2005). Lipoprotein particles are required for Hedgehog and Wingless signalling. Nature *435*, 58-65.

Parlato, R., Rosica, A., Rodriguez-Mallon, A., Affuso, A., Postiglione, M.P., Arra, C., Mansouri, A., Kimura, S., Di Lauro, R., and De Felice, M. (2004). An integrated regulatory network controlling survival and migration in thyroid organogenesis. Developmental biology *276*, 464-475.

Porreca, I., De Felice, E., Fagman, H., Di Lauro, R., and Sordino, P. (2012). Zebrafish bcl2l is a survival factor in thyroid development. Developmental biology *366*, 142-152.

Raposo, G., Nijman, H.W., Stoorvogel, W., Liejendekker, R., Harding, C.V., Melief, C.J., and Geuze, H.J. (1996). B lymphocytes secrete antigen-presenting vesicles. The Journal of experimental medicine *183*, 1161-1172.

Raposo, G., and Stoorvogel, W. (2013). Extracellular vesicles: exosomes, microvesicles, and friends. J Cell Biol *200*, 373-383.

Record, M., Carayon, K., Poirot, M., and Silvente-Poirot, S. (2014). Exosomes as new vesicular lipid transporters involved in cell-cell communication and various pathophysiologies. Biochimica et biophysica acta *1841*, 108-120.

Roset, R., Ortet, L., and Gil-Gomez, G. (2007). Role of Bcl-2 family members on apoptosis: what we have learned from knock-out mice. Frontiers in bioscience : a journal and virtual library *12*, 4722-4730.

Rousset, B., Dupuy, C., Miot, F., and Dumont, J. (2015). Chapter 2 Thyroid Hormone Synthesis And Secretion. In Endotext, L.J. De Groot, G. Chrousos, K. Dungan, K.R. Feingold, A. Grossman, J.M. Hershman, C. Koch, M. Korbonits, R. McLachlan, M. New*, et al.*, eds. (South Dartmouth (MA): MDText.com, Inc.).

Samsonov, R., Burdakov, V., Shtam, T., Radzhabovsmall a, C.Z., Vasilyev, D., Tsyrlina, E., Titov, S., Ivanov, M., Berstein, L., Filatov, M*., et al.* (2016). Plasma exosomal miR-21 and miR-181a differentiates follicular from papillary thyroid cancer. Tumour biology : the journal of the International Society for Oncodevelopmental Biology and Medicine *37*, 12011-12021.

Silberschmidt, D., Rodriguez-Mallon, A., Mithboakar, P., Cali, G., Amendola, E., Sanges, R., Zannini, M., Scarfo, M., De Luca, P., Nitsch, L*., et al.* (2011). In vivo role of different domains and of phosphorylation in the transcription factor Nkx2-1. BMC developmental biology *11*, 9.

Smyth, T., Kullberg, M., Malik, N., Smith-Jones, P., Graner, M.W., and Anchordoquy, T.J. (2015). Biodistribution and delivery efficiency of unmodified tumor-derived exosomes. Journal of controlled release : official journal of the Controlled Release Society *199*, 145-155.

Steed, E., Balda, M.S., and Matter, K. (2010). Dynamics and functions of tight junctions. Trends Cell Biol *20*, 142-149.

Studer, H., Peter, H.J., and Gerber, H. (1989). Natural heterogeneity of thyroid cells: the basis for understanding thyroid function and nodular goiter growth. Endocrine reviews *10*, 125-135.

Takahashi, Y., Nishikawa, M., Shinotsuka, H., Matsui, Y., Ohara, S., Imai, T., and Takakura, Y. (2013). Visualization and in vivo tracking of the exosomes of murine

melanoma B16-BL6 cells in mice after intravenous injection. Journal of Biotechnology *165*, 77-84.

Takov, K., Yellon, D.M., and Davidson, S.M. (2017). Confounding factors in vesicle uptake studies using fluorescent lipophilic membrane dyes. Journal of extracellular vesicles *6*, 1388731.

Taverna, S., Ghersi, G., Ginestra, A., Rigogliuso, S., Pecorella, S., Alaimo, G., Saladino, F., Dolo, V., Dell'Era, P., Pavan, A.*, et al.* (2003). Shedding of membrane vesicles mediates fibroblast growth factor-2 release from cells. J Biol Chem *278*, 51911-51919.

Teshima, T.H., Lourenco, S.V., and Tucker, A.S. (2016). Multiple Cranial Organ Defects after Conditionally Knocking Out Fgf10 in the Neural Crest. Frontiers in physiology *7*, 488.

Thery, C., Amigorena, S., Raposo, G., and Clayton, A. (2006). Isolation and characterization of exosomes from cell culture supernatants and biological fluids. Current protocols in cell biology *Chapter 3*, Unit 3.22.

Thi, M.M., Islam, S., Suadicani, S.O., and Spray, D.C. (2012). Connexin43 and pannexin1 channels in osteoblasts: who is the "hemichannel"? The Journal of membrane biology *245*, 401-409.

Thoene, J., Goss, T., Witcher, M., Mullet, J., N'Kuli, F., Van Der Smissen, P., Courtoy, P., and Hahn, S.H. (2013). In vitro correction of disorders of lysosomal transport by microvesicles derived from baculovirus-infected Spodoptera cells. Molecular genetics and metabolism *109*, 77-85.

Thomason, H.A., Scothern, A., McHarg, S., and Garrod, D.R. (2010). Desmosomes: adhesive strength and signalling in health and disease. The Biochemical journal *429*, 419-433.

Tkach, M., and Thery, C. (2016). Communication by Extracellular Vesicles: Where We Are and Where We Need to Go. Cell *164*, 1226-1232.

Toda, S., Aoki, S., Uchihashi, K., Matsunobu, A., Yamamoto, M., Ootani, A., Yamasaki, F., Koike, E., and Sugihara, H. (2011). Culture models for studying thyroid biology and disorders. ISRN endocrinology *2011*, 275782.

Trajkovic, K., Hsu, C., Chiantia, S., Rajendran, L., Wenzel, D., Wieland, F., Schwille, P., Brugger, B., and Simons, M. (2008). Ceramide triggers budding of exosome vesicles into multivesicular endosomes. Science (New York, NY) *319*, 1244-1247.

Twyffels, L., Strickaert, A., Virreira, M., Massart, C., Van Sande, J., Wauquier, C., Beauwens, R., Dumont, J.E., Galietta, L.J., Boom, A.*, et al.* (2014). Anoctamin-1/TMEM16A is the major apical iodide channel of the thyrocyte. American journal of physiology Cell physiology *307*, C1102-1112.

Ulrich, H., do Nascimento, I.C., Bocsi, J., and Tarnok, A. (2015). Immunomodulation in stem cell differentiation into neurons and brain repair. Stem cell reviews *11*, 474-486.

Valadi, H., Ekstrom, K., Bossios, A., Sjostrand, M., Lee, J.J., and Lotvall, J.O. (2007). Exosome-mediated transfer of mRNAs and microRNAs is a novel mechanism of genetic exchange between cells. Nat Cell Biol *9*, 654-659.

van Balkom, B.W., de Jong, O.G., Smits, M., Brummelman, J., den Ouden, K., de Bree, P.M., van Eijndhoven, M.A., Pegtel, D.M., Stoorvogel, W., Wurdinger, T.*, et al.* (2013). Endothelial cells require miR-214 to secrete exosomes that suppress senescence and induce angiogenesis in human and mouse endothelial cells. Blood *121*, 3997-4006, S3991-3915.

Van Deun, J., Mestdagh, P., Agostinis, P., Akay, O., Anand, S., Anckaert, J., Martinez, Z.A., Baetens, T., Beghein, E., Bertier, L.*, et al.* (2017). EV-TRACK: transparent reporting and centralizing knowledge in extracellular vesicle research. Nature methods *14*, 228-232.

van Niel, G., Charrin, S., Simoes, S., Romao, M., Rochin, L., Saftig, P., Marks, M.S., Rubinstein, E., and Raposo, G. (2011). The tetraspanin CD63 regulates ESCRT-independent and -dependent endosomal sorting during melanogenesis. Dev Cell *21*, 708-721.

van Niel, G., D'Angelo, G., and Raposo, G. (2018). Shedding light on the cell biology of extracellular vesicles. Nature reviews Molecular cell biology.

Villacorte, M., Delmarcelle, A.S., Lernoux, M., Bouquet, M., Lemoine, P., Bolsee, J., Umans, L., de Sousa Lopes, S.C., Van Der Smissen, P., Sasaki, T.*, et al.* (2016). Thyroid

follicle development requires Smad1/5- and endothelial cell-dependent basement membrane assembly. Development *143*, 1958-1970.

Villarroya-Beltri, C., Gutierrez-Vazquez, C., Sanchez-Cabo, F., Perez-Hernandez, D., Vazquez, J., Martin-Cofreces, N., Martinez-Herrera, D.J., Pascual-Montano, A., Mittelbrunn, M., and Sanchez-Madrid, F. (2013). Sumoylated hnRNPA2B1 controls the sorting of miRNAs into exosomes through binding to specific motifs. Nat Commun *4*, 2980.

Welman, A., Barraclough, J., and Dive, C. (2007). Tetracycline regulated systems in functional oncogenomics. Translational oncogenomics *2*, 17-33.

Wendl, T., Adzic, D., Schoenebeck, J.J., Scholpp, S., Brand, M., Yelon, D., and Rohr, K.B. (2007). Early developmental specification of the thyroid gland depends on han-expressing surrounding tissue and on FGF signals. Development *134*, 2871-2879.

Willms, E., Johansson, H.J., Mager, I., Lee, Y., Blomberg, K.E., Sadik, M., Alaarg, A., Smith, C.I., Lehtio, J., El Andaloussi, S*., et al.* (2016). Cells release subpopulations of exosomes with distinct molecular and biological properties. Sci Rep *6*, 22519.

Witwer, K.W., Buzas, E.I., Bemis, L.T., Bora, A., Lasser, C., Lotvall, J., Nolte-'t Hoen, E.N., Piper, M.G., Sivaraman, S., Skog, J*., et al.* (2013). Standardization of sample collection, isolation and analysis methods in extracellular vesicle research. Journal of extracellular vesicles *2*.

Witwer, K.W., Soekmadji, C., Hill, A.F., Wauben, M.H., Buzas, E.I., Di Vizio, D., Falcon-Perez, J.M., Gardiner, C., Hochberg, F., Kurochkin, I.V*., et al.* (2017). Updating the MISEV minimal requirements for extracellular vesicle studies: building bridges to reproducibility. Journal of extracellular vesicles *6*, 1396823.

Wolf, P. (1967). The nature and significance of platelet products in human plasma. British journal of haematology *13*, 269-288.

Worsdorfer, P., Bosen, F., Gebhardt, M., Russ, N., Zimmermann, K., Komla Kessie, D., Sekaran, T., Egert, A., Ergun, S., Schorle, H*., et al.* (2017). Abrogation of Gap Junctional Communication in ES Cells Results in a Disruption of Primitive Endoderm Formation in Embryoid Bodies. Stem cells (Dayton, Ohio) *35*, 859-871.

Yamada, S., Pokutta, S., Drees, F., Weis, W.I., and Nelson, W.J. (2005). Deconstructing the cadherin-catenin-actin complex. Cell *123*, 889-901.

Yanez-Mo, M., Siljander, P.R., Andreu, Z., Zavec, A.B., Borras, F.E., Buzas, E.I., Buzas, K., Casal, E., Cappello, F., Carvalho, J.*, et al.* (2015). Biological properties of extracellular vesicles and their physiological functions. Journal of extracellular vesicles *4*, 27066.

Yim, N., Ryu, S.W., Choi, K., Lee, K.R., Lee, S., Choi, H., Kim, J., Shaker, M.R., Sun, W., Park, J.H.*, et al.* (2016). Exosome engineering for efficient intracellular delivery of soluble proteins using optically reversible protein-protein interaction module. Nat Commun *7*, 12277.

Yue, S., Mu, W., Erb, U., and Zoller, M. (2015). The tetraspanins CD151 and Tspan8 are essential exosome components for the crosstalk between cancer initiating cells and their surrounding. Oncotarget *6*, 2366-2384.

Zabeo, D., Cvjetkovic, A., Lasser, C., Schorb, M., Lotvall, J., and Hoog, J.L. (2017). Exosomes purified from a single cell type have diverse morphology. Journal of extracellular vesicles *6*, 1329476.

Zhang, B., Yeo, R.W., Tan, K.H., and Lim, S.K. (2016a). Focus on Extracellular Vesicles: Therapeutic Potential of Stem Cell-Derived Extracellular Vesicles. Int J Mol Sci *17*, 174.

Zhang, J., Chen, C., Hu, B., Niu, X., Liu, X., Zhang, G., Zhang, C., Li, Q., and Wang, Y. (2016b). Exosomes Derived from Human Endothelial Progenitor Cells Accelerate Cutaneous Wound Healing by Promoting Angiogenesis Through Erk1/2 Signaling. International journal of biological sciences *12*, 1472-1487.

Zhao, H., Yang, L., Baddour, J., Achreja, A., Bernard, V., Moss, T., Marini, J.C., Tudawe, T., Seviour, E.G., San Lucas, F.A.*, et al.* (2016). Tumor microenvironment derived exosomes pleiotropically modulate cancer cell metabolism. eLife *5*, e10250.

Zimmerman, B., Kelly, B., McMillan, B.J., Seegar, T.C.M., Dror, R.O., Kruse, A.C., and Blacklow, S.C. (2016). Crystal Structure of a Full-Length Human Tetraspanin Reveals a Cholesterol-Binding Pocket. Cell *167*, 1041-1051.e1011.

Zitvogel, L., Regnault, A., Lozier, A., Wolfers, J., Flament, C., Tenza, D., Ricciardi-Castagnoli, P., Raposo, G., and Amigorena, S. (1998). Eradication of established murine tumors using a novel cell-free vaccine: dendritic cell-derived exosomes. Nature medicine *4*, 594-600.

Zomer, A., Maynard, C., Verweij, F.J., Kamermans, A., Schafer, R., Beerling, E., Schiffelers, R.M., de Wit, E., Berenguer, J., Ellenbroek, S.I.J.*, et al.* (2015). In Vivo imaging reveals extracellular vesicle-mediated phenocopying of metastatic behavior. Cell *161*, 1046-1057.